FINAL REPORT

EFFECT OF CONFINEMENT IN TRANSFER REGION ON THE INTERACTION BETWEEN BOND AND SHEAR FORCES IN PRESTRESSED CONCRETE GIRDERS

SPONSORED BY

FLORIDA DEPARTMENT OF TRANSPORTATION

State Job No.: 99700-7578-119
UF Project No.: 4910450437512
WPI No.: 0510613
Contract No.: C-4109
HPR No.: 0613

December 1995

Principal Investigators: Fernando E. Fagundo, PhD
John M. Lybas, PhD

Graduate Research Assistant: Anindya Basu

Department of Civil Engineering
University of Florida
Gainesville, Florida 32611

Engineering & Industrial Experiment Station

Technical Report Documentation Page

1. Report No.	2. Government Accession No.	3. Recipient's Catalog No.
FL/DOT/RMC/613-4109		

4. Title and Subtitle	5. Report Date
Effect of Confinement in Transfer Region on the Interaction Between Bond and Shear Forces in Prestressed Concrete Girders	December 1995
	6. Performing Organization Code
	8. Performing Organization Report No.
7. Author(s)	4910450437512
F.E. Fagundo, J.M. Lybas, A. Basu, T.J. Shaw, D. White	
9. Performing Organization Name and Address	10. Work Unit No. (TRAIS)
University of Florida Department of Civil Engineering 345 Weil Hall / P. O. Box 116580 Gainesville, FL 32611-6580	11. Contract or Grant No. HPR 0613
12. Sponsoring Agency Name and Address	13. Type of Report and Period Covered
Florida Department of Transportation Research Management Center 605 Suwannee Street, MS 30 Tallahassee, FL 32301-8064	Final Report November 1, 1991 - June 30, 1993
	14. Sponsoring Agency Code 99700-7578-119

15. Supplementary Notes

Prepared in cooperation with the Federal Highway Administration

16. Abstract

The purpose of this report is to study the effects of the geometric ratio of shear span to depth and the moment to shear ratio on the interaction between bond and shear forces in prestressed concrete girders. Another aspect is to identify the parameters that will affect the transfer lengths of the prestressing strands and to evaluate the current code recommendations.

The project consisted of testing two identical sets of four simply supported beams, each with a length of 35 feet. The testing procedure began by testing the first beam in a set at its development length of 77 inches at one end and then at a distance of two times its effective depth at the other end. The order of testing was reversed and the span was reduced to eliminate the destroyed section of beam for the second test.

The beams that were tested at 2D tended to fail in a brittle manner. The failure of these beams was governed by a strut and tie action due to the presence of disturbed regions. The beams that were tested at LD tended to \fail in a more ductile manner than the beams tested at 2D. These beams had a shear span to depth ratios greater than 2.5. The modified compression field theory provided a rational and comprehensive method of analysis for prestressed concrete members with shear span to depth ratios greater than 2.5.

The presence of the shear cracks in these beams appeared to deteriorate the bond between the tendons and the surrounding concrete. As the shear cracks formed, there were sudden increases in tendon slip in every case. The shear and bond forces did appear to be related but any premature shear failures due to excessive loss of bond was not experienced.

The imposition of the upper bound in the simplified expression as recommended by the ACI code predicting the shear strength of a prestressed concrete beam appears to be overly conservative.

Based on these test results, the ACI equation for transfer length appears to be unconservative. The suggestion of using $f_{si}/3$ instead of $f_{se}/3$ appears to provide a closer comparison with the test results.

17. Key Words	18. Distribution Statement
Prestressed Concrete, Flexure, Transfer Length, Shear Strength	No restrictions. This document is available to the public through the National Technical Information Service, Springfield, VA, 22161

19. Security Classif. (of this report)	20. Security Classif. (of this page)	21. No. of Pages	22. Price
Unclassified	Unclassified	167	

SI* (MODERN METRIC) CONVERSION FACTORS

APPROXIMATE CONVERSIONS TO SI UNITS

Symbol	When You Know	Multiply By	To Find	Symbol
	LENGTH			
in	inches	25.4	millimeters	mm
ft	feet	0.305	meters	m
yd	yards	0.914	meters	m
mi	miles	1.61	kilometers	km
	AREA			
in^2	square inches	645.2	square millimeters	mm^2
ft^2	square feet	0.093	square meters	m^2
yd^2	square yards	0.836	square meters	m^2
ac	acres	0.405	hectares	ha
mi^2	square miles	2.59	square kilometers	km^2
	VOLUME			
fl oz	fluid ounces	29.57	milliliters	ml
gal	gallons	3.785	liters	l
ft^3	cubic feet	0.028	cubic meters	m^3
yd^3	cubic yards	0.765	cubic meters	m^3
NOTE: Volumes greater than 1000 l shall be shown in m^3.				
	MASS			
oz	ounces	28.35	grams	g
lb	pounds	0.454	kilograms	kg
T	short tons (2000 lb)	0.907	megagrams	Mg
	TEMPERATURE (exact)			
°F	Fahrenheit temperature	5(F-32)/9 or (F-32)/1.8	Celcius temperature	°C
	ILLUMINATION			
fc	foot-candles	10.76	lux	l
fl	foot-Lamberts	3.426	candela/m^2	cd/m^2
	FORCE and PRESSURE or STRESS			
lbf	poundforce	4.45	newtons	N
psi	poundforce per square inch	6.89	kilopascals	kPa

APPROXIMATE CONVERSIONS FROM SI UNITS

Symbol	When You Know	Multiply By	To Find	Symbol
	LENGTH			
mm	millimeters	0.039	inches	in
m	meters	3.28	feet	ft
m	meters	1.09	yards	yd
km	kilometers	0.621	miles	mi
	AREA			
mm^2	square millimeters	0.0016	square inches	in^2
m^2	square meters	10.764	square feet	ft^2
m^2	square meters	1.195	square yards	ac
ha	hectares	2.47	acres	mi^2
km^2	square kilometers	0.386	square miles	
	VOLUME			
ml	milliliters	0.034	fluid ounces	fl oz
l	liters	0.264	gallons	gal
m^3	cubic meters	35.71	cubic feet	ft^3
m^3	cubic meters	1.307	cubic yards	yd^3
	MASS			
g	grams	0.035	ounces	oz
kg	kilograms	2.202	pounds	lb
Mg	megagrams	1.103	short tons (2000 lb)	T
	TEMPERATURE (exact)			
°C	Celcius temperature	1.8C + 32	Fahrenheit temperature	°F
	ILLUMINATION			
lx	lux	0.0929	foot-candles	fc
cd/m^2	candela/m^2	0.2919	foot-Lamberts	fl
	FORCE and PRESSURE or STRESS			
N	newtons	0.225	poundforce	lbf
kPa	kilopascals	0.145	poundforce per square inch	psi

* SI is the symbol for the International System of Units. Appropriate rounding should be made to comply with Section 4 of ASTM E380.

(Revised August 1992)

FINAL REPORT

EFFECT OF CONFINEMENT IN TRANSFER REGION ON THE INTERACTION BETWEEN BOND AND SHEAR FORCES IN PRESTRESSED CONCRETE GIRDERS

SPONSORED BY

FLORIDA DEPARTMENT OF TRANSPORTATION

State Job No.: 99700-7578-119
UF Project No.: 4910450437512
WPI No.: 0510613
Contract No.: C-4109
HPR No.: 0613

December 1995

Principal Investigators: Fernando E. Fagundo, PhD
John M. Lybas, PhD

Graduate Research Assistant: Anindya Basu

Department of Civil Engineering
University of Florida
Gainesville, Florida 32611

Engineering & Industrial Experiment Station

DISCLAIMER

"The opinions, findings and conclusions expressed in this publication are those of the authors and-not necessarily those of the Florida Department of Transportation or the U.S. Department of Transportation.

Prepared in cooperation with the State of Florida Department of Transportation and the U.S. Department of Transportation."

EFFECT OF CONFINEMENT IN TRANSFER REGION ON THE INTERACTION BETWEEN BOND AND SHEAR FORCES IN PRESTRESSED CONCRETE GIRDERS

By

Fernando E. Fagundo

John M. Lybas

Anindya Basu

Thomas J. Shaw

David White

UNIVERSITY OF FLORIDA

1995

TABLE OF CONTENTS

LIST OF TABLES

LIST OF FIGURES

EFFECT OF CONFINEMENT IN TRANSFER REGION
ON THE INTERACTION BETWEEN BOND AND SHEAR FORCES IN
PRESTRESSED CONCRETE GIRDERS

SUMMARY

The purpose of this research is to study the effects of the geometric ratio of shear span to depth and the moment to shear ratio on the interaction between bond and shear forces in prestressed concrete girders. Another aspect of this research is to identify the parameters that will affect the transfer lengths of the prestressing strands and to evaluate the current code recommendations.

The project consisted of testing two identical sets of four simply supported beams each with a length of 35 feet. The testing procedure began by testing the first beam in a set at its development length of 77 inches at one end and then at a distance of two times its effective depth at the other end. The order of testing was reversed and the span was reduced to eliminate the destroyed section of beam for the second test.

The beams that were tested at 2D tended to fail in a brittle manner. The failure of these beams was governed by a strut and tie action due to the presence of disturbed regions. The beams that were tested at LD tended to fail in a more ductile manner than the beams tested at 2D. These beams had a shear span to depth ratios greater than 2.5. The modified compression field theory provided a rational and comprehensive method of analysis for prestressed concrete members with shear span to depth ratios greater than 2.5.

The presence of the shear cracks in these beams appeared to deteriorate the bond between the tendons and the surrounding concrete. As the shear cracks formed there were sudden increases in tendon slip in every case. The shear and bond forces did appear to be related but any premature shear failures due to excessive loss of bond was not experienced.

The imposition of the upper bound in the simplified expression as recommended by the ACI code predicting the shear strength of a prestressed concrete beam appears to be overly conservative.

Based on these test results, the ACI equation for transfer length appears to be unconservative. The suggestion of using $f_{si}/3$;instead of $f_{se}/3$ appears to provide a closer comparison with the test results.

CHAPTER 1
INTRODUCTION

1.1 General Information

Since its development in the late 1920s, prestressed concrete has grown to be a dominant component of the construction industry in North America. Prestressed concrete has proved to be technically advantageous, economically competitive, and aesthetically' superior for modern structures and particularly in bridge design. Prestressed concrete bridge girders constitute the dominant structural component in the highway system for the State of Florida. Through improved serviceability and crack and deflection control at service-loads, prestressing allows for the efficient utilization of high-strength materials. Thus, smaller and more economical members may be designed, and the range of use for structural concrete is greatly expanded.

1.2 Problem Statement

Previous studies have raised serious questions about the adequacy of current design requirements for bond and shear in prestressed flexural members. The effect of prestressing on shear requirements and the interaction between bond and shear seem to be considerably underestimated. The underestimation of the effect of prestressing on shear strength leads to a conservative design, but the effect of the shear-bond interaction could lead to unsafe circumstances.

Present design recommendations for prestressed concrete beams follows an essentially empirical procedure where each internal force component of flexure, shear, bond, axial force and torsion is accounted for independently from each other. While present design procedures are based on this assumption, it is generally accepted that flexure and shear as well as shear and bond forces interact to create a complex state of internal stresses. For beams that have relatively low shear span to depth ratio, where shear stresses become dominant, the initiation of shear cracks could lead to the deterioration of bond stresses and result in insufficient development length. This becomes particularly important in prestressed concrete members if a reduction in bond strength could lead to a reduction in shear capacity which could ultimately lead to a sudden and catastrophic collapse.

1.3 Scope and Objectives

1.3.1 Scone

This research will examine current design recommendations for bond and shear in prestressed concrete flexural members. These will be evaluated in light of available information in the published literature. The analytical phase of this project consists of analyzing each beam according to current ACI code (Ref. 1) requirements and comparing these results to various analytical models and to the experimental results. The test phase consists of conducting shear tests on two identical sets of four simply supported beams 35 feet in length. The beams to be tested have a 12-inch width and heights of 30, 36, 42, and 48 inches. All of the beams are designed for a full AASHTO HS 15 truck loading and each beam will have approximately the same ultimate flexural strength. The beams were also

designed to have the same tensile stress at midspan under full service load conditions of 50 psi. The 48-inch beam was designed for minimum shear reinforcement for the entire span length as suggested by the ACI code (Ref. 1). The same size and spacing of stirrups was provided for every beam in order to keep the amount of shear reinforcement constant.

1.3.2 Objectives

The primary objectives for this project are as follows:

(1) Investigate to what extent the shear strength of a section located within the transfer length region of strands differs from that of a section loaded outside of the anchorage zone.

(2) Identify the parameters that will affect the transfer length of prestressing strands and evaluate current recommendations as well as propose new recommendations.

1.4 Summary

The purpose of this project is to study the effects of the geometric ratio of shear span to depth and the moment to shear ratio on the interaction between bond and shear forces in prestressed concrete beams. A literature survey was conducted in order to determine the existing information and research in the area of bond and shear in prestressed concrete members. An overview of the background information on these findings can be found in Chapter 2.

This project consisted of the testing of two identical sets of four simply supported beams each with a clear span of 35 feet. The beams all had a width of 12 inches and height of 30, 36, 42 and 48 inches. The testing procedure began by loading the first beam

in a set at its development length of 77 inches at one end and then at a distance of two times its effective depth at the other end. The order of testing was reversed and the span was reduced to eliminate the destroyed section of beam for the second test.

The test data was presented in graphical form of load versus displacement and load versus strain. The complete summary of all of the test results can be found in Chapter 4. The test data was compared to several analytical models which are presented in Chapter 5 The two primary ones being the strut and tie model and the modified compression field theory.

The discussion and comparison of the results to the predicted values is presented in Chapter 5. The summary, conclusions and suggested design recommendations and recommendations for further research are presented in Chapter 6.

CHAPTER 2
BACKGROUND

2.1 Transfer Length

2.1.1 General Information .

In pretensioned prestressed concrete members, the total force of prestressing must be transferred to the concrete entirely by the bonding of the prestressing strand to the concrete surrounding it. This differs from post-tensioned construction, where the full compressive force is transferred to the concrete section by means of special end anchorages and end plates.

When the external jacking force is released in pretensioned beams, the prestressing force is effectively transmitted to the concrete near the ends of the member over a distance that is known as the transfer length. In the transfer zone, reduction in the tensile strain of the steel does not equal the compressive strain in the concrete at the same point. There is relative movement of the steel and concrete, and accordingly adhesion does not have a significant effect on prestress transfer. The mechanism that provides this transfer is primarily due to friction combined with the Poisson effect or lateral swelling of the steel in the transfer zone. When the strand is stressed in tension there is a slight reduction in diameter. For a pretensioned tendon, the diameter reduction has already taken place when the concrete is poured. After the initial prestress force is released, the tension at the ends of the member is greatly reduced. This reduction in longitudinal stress is accompanied by a slight

increase in the diameter of the steel which causes radial compression across the concrete steel interface. The "swelling" of the tendon tends to enhance the frictional resistance to pullout. This improvement in bond caused by lateral expansion of the released tendon is sometimes referred to as the Hoyer effect (Ref. 2).

When a member is subjected to bending due to externally applied loads, another type of bond mechanism termed flexural bond is mobilized. As these loads are increased, the stress in the strand also increases. The additional length over which the increase in strand force is transmitted to the concrete is known as the flexural bond length. As the ultimate capacity of the member is approached, the total of the transfer length and the flexural bond length is known as the development length.

The determination of the development length in pretensioned beams is of particular importance because the transverse stresses due to shear are usually a maximum within this region. These stresses can be considerable and a knowledge of the transmission length is necessary to ensure that sufficient build-up of horizontal stress has taken place to develop the strands. The total development length must be sufficient to prevent the overlapping of the transfer bond region and the flexural bond region. If inadequate development is provided, ultimate strength is governed by bond rather than flexure. Bond slippage of the strands generally occurs in three stages:

(1) Progressive bond slip begins at flexural cracks.
(2) General bond slip is initiated along the entire development length.
(3) Mechanical interlock between the helical strand surface and the concrete is destroyed.

Even though excessive slip has occurred, the mechanical interlock is generally sufficient enough to maintain considerable strand stress. In many cases the strand stress

after general bond slip is reduced to the stress developed from initial prestressing force only and not to zero as might be expected. Thus, the final effect of inadequate development length may be a premature flexural failure at a reduced strand stress, corresponding to a final bending moment less than the computed design strength in flexure.

2.1.2 Bond Parameters

It is generally accepted that the most significant parameters affecting transfer length of prestressing steel are:

- type of steel (e.g., wire, strand), steel size (e.g., diameter)
- steel tensile stress level
- condition of the steel (e.g., clean, oiled, rusted)
- type of loading (e.g., static, repeated, impact)
- technology used to release prestressing (e.g., gradual or sudden by flame cutting or sawing)
- shape of shear reinforcement around prestressing steel (e.g., helix or stirrups)
- time-dependent effects
- consolidation and consistency of concrete around steel
- amount of concrete cover

It is also generally agreed that transfer length is greater for larger steel sizes, higher prestress levels and lower concrete strengths. The effect of sudden release may be minimized by gradual heating of the strand in a sufficient length before cutting. Strands develop some mechanical bond with concrete in addition to friction; thus the transfer lengths of strands are shorter than those of smooth wires of comparable diameter.

2.1.3 Current ACI/AASHTO Provisions

Current ACI code (Ref. 1) and AASHTO (Ref. 3) requirements for bond and anchorage are essentially the same. Therefore, for discussion purposes, the transfer and development length provisions of both codes can be considered identical.

The current ACI provisions for development length of prestressing strand are contained in Section 12.9 of ACI 318-89 (Ref. 1). The provisions are as follows:

Section 12.9.1: Three- or seven-wire pretensioning strand; shall be bonded beyond the critical section for development length, in inches, not less than:

$$l_d = (f_{ps} - 2/3 f_{se})\, d_b \qquad \text{Eq. 2-1}$$

where, f_{ps} = stress in prestressing reinforcement at nominal strength, ksi,

f_{se} = effective stress in prestressed reinforcement after all losses, ksi.

d_b = nominal strand diameter, in.

Section 12.9.2: Investigation maybe limited to cross-sections nearest to each end of the member that are required to develop full design strength under specified factored loads. The above equation can be rewritten as follows:

$$l_d = (f_{se}/3)\, d_b + (f_{ps} - f_{se})\, d_b \qquad \text{Eq. 2-2}$$

The variation of the strand stress along the development length of the strand is shown in Figure 2-1. The first term in Equation 2-2 represents the "transfer length" and the second term represents the “flexural bond length.”

The effective steel stress, f_{se}, depends on the initial prestress, f_{si}, and the amount of prestress loss. Zia and Mostafa (Ref. 4) have pointed out that the denominator "3" in the

expression for transfer length represents a conservative average concrete strength at the time of transfer in ksi. Similarly, the expression for flexural bond length implies a value of 1 ksi in- the denominator. ACI Code assumes a bond strength of 750 psi within the transfer length and then 256 psi for the interior portion of the strand where the bond, stress is calculated on the basis of the nominal circumference of the strand (i.e., π, d_b).

In a comprehensive study Zia and Mostafa proposed, the following equation for development length:

$$l_t = (1.5\ f_{si}\ d_b)/\ f'_{ci} - 4.6 \qquad \text{Eq. 2-3}$$

$$l_b = 1.25\ (f_{ps} - f_{se})\ d_b \qquad \text{Eq. 2-4}$$

$$l_d = l_t + l_b \qquad \text{Eq. 2-5}$$

where, f_{si} = stress in prestressing steel at transfer, ksi.

f'_{ci} = compressive strength of concrete at transfer, ksi.

l_t = transfer length of prestressing strand, inches.

l_b = flexural bond development length of prestressing strand, inches.

The expression for l_b is based on the theoretically derived expression:

$$l_b = (f_{ps} - f_{se})\ d_b/4u_{avg} \qquad \text{Eq. 2-6}$$

where u_{avg} is the average bond stress within l_b. The ACI code assumes this stress to be 250 psi while Zia and Mostafa use a value of 200 psi. This equation for transfer length is applicable for concrete strengths ranging from 2-8 ksi and takes into account the effects of strand size, initial prestress and the concrete stress at transfer.

It has also been suggested by Shahawy (Ref. 5) that the ACI equation for transfer length ($f_{se}/3$) appears to be inadequate. Through a series of tests on: shielded and unshielded systems; he suggests that the stress in the prestressing strand at transfer, f_{si}, be used instead of f_{se}.

2.2 Shear in Prestressed Concrete Members

2.2.1 General Information

Prestressed concrete beams are usually designed for flexure first which leads to the size of the section and the arrangement of the longitudinal steel to provide the necessary moment resistance. The beam is subsequently designed to account for the effect of shear forces. The flexural strength of a prestressed concrete beam can be predicted fairly accurately and a flexural failure is usually preceded by obvious cracking and large deflections. It is more difficult to accurately predict the shear strength.

The shear stresses that are produced in a prestressed concrete beam are usually much below the shear strength of the: concrete. The primary concern is with the principal diagonal tensile stress in the concrete that is produced by the shear stresses, either acting alone or in combination with longitudinal normal stress. As a result of it, failure may take place suddenly and without warning if the member is overloaded.

2.2.2 Beam and Arch Action

The average value of shear stress in concrete beams can be calculated as follows:

$$v = \frac{V}{b_w jd} \qquad \text{Eq. 2-7}$$

where jd $\approx$ 0.875d and b_w is the thickness of the web. This equation assumes that the beam is prismatic and that the lever arm jd is constant. The relationship between shear force and the force in the tendons can be written as follows:

$$V = \frac{d}{dx}(Tjd) \qquad \text{Eq. 2-8}$$

which can be expanded as

$$V = \frac{d(T)}{dx} jd + \frac{d(jd)}{dx} T \qquad \text{Eq. 2-9}$$

Normal elastic beam theory assumes that the lever arm jd remains constant, therefore:

$$\frac{d(jd)}{dx} = 0 \qquad \Rightarrow V = \frac{d(T)}{dx} jd \qquad \text{Eq. 2-10}$$

where d(T)/dx is the shear flow across any horizontal plane between the reinforcement and the compression zone. This shear flow must be present in order for a specimen to exhibit "beam" action. If the shear flow is equal to zero then

$$V = T\frac{d(jd)}{dx} \qquad \text{Eq. 2-11}$$

This may occur if the shear flow can not be transmitted due to debonding of the steel or if an inclined crack is extending from the load to the reactions. When this is the case, the shear is transferred by "arch" action rather than beam action. The shear resisting mechanisms are very different for regions displaying beam action, referred to as B-regions, and those displaying arch action, referred to as D-regions. The D refers to a discontinuity or disturbance which results in load transfer by in-plane forces such as arch action.

D-regions extend about one member depth in each direction from concentrated loads, reactions, and abrupt changes in section. The regions between these D-regions may be treated as B-regions. The general behavioral trend is that, arch action tends to increase the. strength of the section while the corresponding B-regions tend to be weaker.

The behavior of beams that exhibit shear failures is extremely variable depending on the relative contributions of beam action and arch action. Therefore, beams can be divided into four general types based on their shear spans: very short, short, slender, and very slender. These divisions have a shear span to depth ratio, a/d, of < 1, 10 to 2.5, 2.5 to 6.5, > 6.5 respectively. The term deep beam is used to describe beams with very short and short shear spans. Deep beams with a/d less than 1 tend to develop inclined cracks that join the load and the support which, in effect, destroy the horizontal shear flow from the longitudinal steel to the compression zone. Thus, the behavior changes from beam to arch action. In this type of beam the most common mode of failure is an anchorage failure at the ends of the reinforcement.

When beams with short shear spans develop inclined cracks they tend to redistribute the internal forces allowing for additional load to be carried in part by arch action.

The final failure of such beams will be caused by a bond failure, a splitting failure, a dowel failure along the tension reinforcement, or by crushing of the compression zone over the crack. Beams that are slender and very slender usually fait in flexure before inclined cracking occurs.

2.2.3 Truss Analogy

Early design procedures for reinforced concrete design in shear were based on the "truss analogy" developed at the turn of the century by Ritter and Morsch (Ref. 6). The truss analogy, which assumes concrete does not resist tension, models a reinforced concrete beam as a truss with parallel longitudinal chords and a web composed of diagonal concrete struts and transverse steel ties as shown in Figure 2-2. When a load is applied to this truss, the diagonal struts and the top chord go into compression while tension is developed in the transverse ties and the longitudinal chords. The force components in each can be determined by static. It was later made clear by Mitchell and Collins (Ref. 7) that rather than having discrete diagonal compressive struts there was a continuous field of diagonal. compression resisting the shear. The equilibrium conditions of the 45-degree truss model are shown in Figure 2-3. The magnitude of the principal compressive stress in Figure 2-3 can be calculated by the following expression,

$$f_2 = 2\frac{V}{b_w jd} \qquad \text{Eq. 2-12}$$

The longitudinal component of the diagonal compressive force, V, must be counteracted by an equal tensile force, N_v, in the longitudinal reinforcement. From the free-body diagram in Figures 2-3(b) and 2-3(c), it can be seen that the diagonal compressive stress, f_2, must be balanced by the tensile force in the stirrups, A_v, f_v. Therefore, the following equation is developed:

$$\frac{A_v f_v}{s} = \frac{V}{jd} \qquad \text{Eq. 2-13}$$

where A_v = the cross-sectional area of the stirrups

s = the stirrup spacing

f_v = the tensile stress in the stirrups

The equilibrium conditions alone are not sufficient to find the stresses in the beam resulting from a given shear. There are four unknowns (i.e., the principal compressive stress, the tensile force in the longitudinal reinforcement, the stress in the stirrups, and the inclination, θ, of the principal compressive stresses), but there are only three equilibrium conditions. Therefore, Morsch concluded that it was mathematically impossible to determine the slope of the diagonal compression struts but that 45 degrees was a conservative assumption.

Provided that the beam is designed as an under-reinforced section, the capacity of the beam will be governed by the yielding of the longitudinal and web reinforcement. Any contribution of the concrete to the shear capacity of the beam is neglected. This is a very conservative assumption, especially for beams designed with little or no web reinforcement. The 45-degree truss model would predict the shear strength of abeam without shear reinforcement to be zero, but in fact the beam will not fail in shear until diagonal cracks have formed. This excessive conservatism made it necessary to develop some rational method of: accounting for the shear strength provided by the concrete.

2.2.4 Modified Truss Approach

After extensive testing, the conservatism existing in the truss model was corrected by the development of the modified truss model. This was done with the addition of an empirical term called the "concrete contribution" factor, V_c, and accounting for the fact that 8 is typically less than 45 degrees. This empirical term, V_c, is the sum resistance offered to shear by aggregate interlock, dowel action, and the untracked portion of the concrete. The Modified Truss Approach incorporates a combination of the truss model and the supplementary concrete contribution. Figure 2-4(a) shows an example of a variable angle truss model for a beam under a symmetric two point loading. From the geometry in Figure 2-4(b) of the crack at ultimate, the number of stirrups at a constant spacing, s, crossing the crack is:

$$n = \frac{z}{s(\tan\theta)} = \frac{z}{s}\cot\theta \qquad \text{Eq. 2-14}$$

The stirrups are assumed to be at yield hence V_s is calculated as:

$$V_s = A_v f_y n = A_v f_y \frac{z}{s}\cot\theta \qquad \text{Eq. 2-15}$$

where, A_v = area of web reinforcement within spacing, s

f_y = yield strength of web reinforcement

z = depth of truss model

s = stirrup spacing

θ = inclination at failure of the diagonal compression struts in the truss model

The proposed concrete contribution factor behaves elastically prior to initial cracking and then decreases linearly. This reduction of the concrete contribution is a function of the nominal shear stress across the section:

$$v_u = \frac{V_u}{b_w d} \qquad \text{Eq. 2-16}$$

As the nominal shear stress increases, the concrete contribution approaches zero and full truss action is considered to model the ultimate behavior of the beam. When this point is reached the capacity of the truss is that provided by the web reinforcement. Figure 2-5 shows a plot of the three possible stages of concrete contribution: uncracked, transition and full truss action.

The concrete contribution in the uncracked stage is the diagonal tension cracking strength in terms of shear stress, v_{cr}, times K. The v_{cr} factor is the nominal shear stress required to crack a non-prestressed concrete beam. The recommended value for v_{cr} is:

$$v_{cr} = 2\sqrt{f'_c} \qquad \text{Eq. 2-17}$$

The constant K, accounts for the increased shear force required to reach the tensile strength of the concrete.

The beneficial influence of prestressing in reducing diagonal tension in concrete becomes evident when using Mohes circle to compare a non-prestressed beam, Figure 2-6(a) and a prestressed beam, Figure 2-6(e). A small element "a" is located at the neutral axis of the reinforced concrete beam and is subjected to positive shear stress v acting on the vertical faces, and negative shears of the same magnitude on the horizontal faces Figure 2-6(b). Making use of Mohr's circle, it is found that the principal tension stress f_1

is equal (in absolute value) to the shear stress and acts at 45 degrees to the horizontal axis of the member Figure 2-6(g). Thus the value of K is 1.

The corresponding element "b" in the prestressed beam is subjected to identical shearing stresses Figure 2-6(f) and is also subjected to horizontal compressive stress f due to the presence of prestressing. Again using Mohr's circle Figure 2-6(g), the principal tension is reduced to a much lower value and acts at a considerably greater angle with the horizontal beam axis Figure 2-6(e). Therefore, an increase in the shear stress is required to exceed the tensile strength of the concrete and the value of K is calculated as:

$$K = \left[1 + \frac{f_{pc}}{f'_t}\right]^{0.5} \qquad \text{Eq. 2-18}$$

where, f_{pc} = compressive stress due to prestressing

f'_t = tensile strength of concrete

The maximum value of K is limited to 2. The Value of K is set at 1 when the flexural stresses exceed the cracking capacity of the beam at ultimate strength. This limitation is similar to the ACI and AASHTO specification which limits the concrete contribution to the lesser of V_{cw} and V_{ci}.

The concrete contribution in the transition stage is calculated as follows:

$$V_c = \frac{K}{2}[(K+2)v_{cr} - v_u]b_w z \qquad \text{Eq. 2-19}$$

where, K =constant which accounts for the increased shear force required to reach the tensile strength of the concrete.

v_{cr} = shear stress of concrete at diagonal cracking

v_u = shear stress of concrete at ultimate failure

b_w = width of the web

Z = effective shear depth.

Limits are placed on the orientation of the diagonal compression struts and the compressive stresses allowed in these members. The limits for the orientation of the truss diagonals and the compressive stresses in the struts have been proposed' by James G. MacGregor (Ref. 8) as $25° < \theta < 65°$ and $0.5\ f'_c$, respectively.

The main advantage of the truss model approach is that it allows a clear visualization of the internal shear carrying mechanisms of beams, thus aiding in the proper detailing of the reinforcement.

2.2.5 Deep Beams/Strut and Tie Model

Deep beam behavior becomes dominant in beams with shear span to depth ratios less than 2.5. In general, a deep beam is a beam in which a significant amount of the load is carried to the supports by a compression thrust joining the load and the reaction. Elastic analysis of deep beams is only meaningful prior to cracking. Afterwards, it cannot accurately predict the redistribution of stresses that will occur after cracking of the concrete. The primary interest in the elastic analysis of a deep beam is that it shows the distribution of the stresses which cause cracking and hence gives guidance as to the direction. of cracking and the flow of forces after cracking.

Considerable insight into the flow of forces in these disturbed or D-regions can be gained by the use of a simple strut and tie model. After significant cracking has occurred, the principal compressive stress trajectories in the concrete tend to be straight lines and can be approximated as straight compressive struts in uniaxial compression. The principal

reinforcement is modeled as a tension tie that joins the compression strut at a nodal zone which is subject to multidirectional stresses.

Recent studies by Marti (Ref. 9) of elastic stress fields in D-regions has pointed out the importance of considering the actual dimensions of the compressive struts and the tension ties in formulating the strut and tie model. This also implies that the truss joint or nodal zone is a member with finite dimensions. In developing a strut and tie model the first step is to sketch the flow of forces and to locate the nodal zones The nodal zones must have sufficient size to ensure that the compressive stresses remain below permissible limits. These limits are presented in the context of ACI (Ref. 1) load and factors. Concrete compressive stresses should not exceed $0.85\Phi f'_c$ in nodal zones bounded by compressive struts and bearing areas, $0.75\Phi f'_c$ in nodal zones anchoring one tension tie, and $0.60\Phi f'_c$ in nodal zones anchoring tension ties in more than one direction. The strength reduction factor, Φ, is assumed as that forbearing on concrete (Φ = 0.70). The nodes are located at the intersection of the forces which meet at the nodal zones. After the geometry of the truss has been determined the forces in the struts and ties due to factored loads can be found with the use of simple static.

Once the forces in the truss have been determined, the required area of tension tie reinforcement is calculated. The strength reduction factor for axial tension (Φ = 0.90) is used. In order to resist tension due to factored loads, the area of reinforcement in the tension tie must satisfy

$$\phi\left(A_s f_y + A_{ps} f_{ps}\right) \geq N_u \qquad \text{Eq. 2-20}$$

The dimensions of the strut must be large enough to ensure that

$$\phi A_c f_{2\max} \geq N_u \qquad \text{Eq. 2-21}$$

where, N_u = axial compression in strut due to factored loads

Φ = strength reduction factor for axial compression,($\Phi = 0.70$)

A_c = effective cross-sectional area of the strut

$f_{2\max}$ = effective compressive strength of concrete

The effective cross-sectional area of the strut is determined using the available concrete area and the bearing and loading conditions at both ends of the strut. The size of the bearing plate that the beam rests on and the plate that is used to transfer the load are both used to determine the size of the strut. The concrete compressive, stress in the strut must not exceed the crushing strength of the cracked concrete, f_{2max}, where,

$$f_{2\max} = \frac{f'_c}{0.8 + 170 \in_1} \leq 0.85 f'_c \qquad \text{Eq. 2-22}$$

The value of the principal tensile strain, $\in_1$, is calculated considering the strain conditions in the concrete and the reinforcement in the area of the strut. If a tension tie crosses a compressive strut, the straining will reduce the capacity of the concrete, to resist compressive stresses. It is assumed that the tensile strain in the tie is $\in_s$, and that the principal compressive strain in the strut at failure is 0.002. It can be deduced from the principal tensile strain required by compatibility is

$$\in_1 = \in_s + (\in_s + 0.002) \cot^2 \alpha \qquad \text{Eq. 2-23}$$

where, α_s = the smallest angle between the tie and the strut

$\in_1$ = tensile strain in tension-tie reinforcement

The strut and tie model is valid for beams with a shear span to depth ratio less than approximately 2.5 as recommended by James G. MacGregor (Ref. 8). In this range the strength decreases rapidly as the shear span increases. Failure modes of beams in this range usually involve crushing of the concrete to some extent. Beams with shear span to depth ratio greater than 2.5 have failure mechanisms governed by conditions away from the disturbed regions near the supports and the load. The response of these beams can be more accurately predicted by sectional models such as the modified compression field theory. The strength of beams in this range is not influenced by details such as the size of the bearing plates and the strength decreases by only a small amount as the shear span increases.

2.2.6 ACI/AASHTO Design Provisions for Shear

The shear provisions in the ACI/AASHTO code are based on a member that is at a hypothetical overload, stage, with calculated dead loads and service loads multiplied by the usual overload factors. Part of the shear resistance of a beam is attributed to concrete in tension, the "concrete contribution," and the remainder to the web reinforcement, the "steel contribution." In the format of the ACI Code (Ref. 1), the design of across section subjected to shear is based on the following relation:

$$V_u \leq \phi V_n \qquad \text{Eq. 2-24}$$

where, V_u = shear force applied at factored loads

V_n = nominal shear strength of the section

Φ = strength reduction factor, 0.85 for shear

The nominal shear strength V_n is calculated from the following equation:

$$V_n = V_c + V_3 \qquad \text{Eq. 2-25}$$

where, V_c = nominal shear strength provided by the concrete

V_s = nominal shear strength provided by the steel

The shear strength provided by the concrete V is assumed to be equal to the shear causing significant inclined cracking. Extensive testing has shown that there are two types of diagonal cracking that occur in prestressed concrete beams: flexure-shear and web-shear cracking.

Flexure-shear cracks occur after flexural cracks that extend vertically into the beam from the tension face have already formed. When a critical combination of flexural and shear stresses have formed at the head of the flexural crack, that crack propagates at an inclined direction. If inadequate web reinforcement is provided a flexural-shear crack may lead to a shear-compression failure. This is where the compression area of the concrete near the top of the beam is reduced by the diagonal cracking and is unable to resist the forces resulting from the flexure.

Flexure-shear cracks are the most common type of shear cracks, but web-shear cracks may also form, especially near the supports of heavily prestressed beams with relatively thin webs. Web-shear cracks initiate in the web without the formation of previous

flexural cracks. These cracks form when the principal tension in the concrete becomes equal to the tensile strength of the material. This type of distress leads to the formation of sudden inclined cracks which ultimately may lead to a rapid and catastrophic shear failure.

The value of V_c is assumed to be the smaller of V_{ci} and V_{cw} determined by flexure-shear cracking and web-shear cracking, respectively. V_{ci} is calculated as follows:

$$V_{ci} = 0.6\sqrt{f'_c}\,b_w d + V_o + \frac{V_i}{M_{\max}} M_{cr} \qquad \text{Eq. 2-26}$$

where, b_w = width of the web

d = depth from the compression face to the centroid of the prestressing steel, "d" is taken as the greater of d or 0.8h

V_i = the factored shear. due to the superimposed, dead load and live load

V_o = shear due to the self weight without load due to the superimposed dead

M_{max} = the factored moment due to the superimposed dead load and live load

M_{cr} = the moment causing flexural cracking due to superimposed dead load and live load

The cracking moment, M_{cr}, is the moment resulting from superimposed dead and live loads in addition to the moment due to the members self-weight. This value may be calculated based on the tensile concrete stress at the bottom face equal to the modulus of rupture of concrete which is conservatively assumed as $6\sqrt{f'_c}$.

$$M_{cr} = \frac{I_c}{c_2}\left(6\sqrt{f'_c} + f_{2p} - f_o\right) \qquad \text{Eq. 2-27}$$

where, f_{2p} = concrete compressive stress at the bottom face from axial and bending effects of eccentric prestress force, P_e

f_o = flexural stress at bottom face resulting from self weight

The self weight and the external loads are applied separately since the self weight is uniformly distributed and the external loads may have any distribution. The ACI code places a lower bound on V_{ci}

$$1.7\sqrt{f'_c}\, b_w d \qquad \text{Eq. 2-28}$$

The value for V_{cw} is computed from:

$$V_{cw} = (3.5\sqrt{f'_c} + 03\, f_{cc})\, b_w d + V_p \qquad \text{Eq. 2-29}$$

where, f_{cc} = compressive stress at the centroid of the member, due to the effective prestress.

V_P = the vertical component of the effective prestress

When shear reinforcement perpendicular to the axis of the member is used, its contribution to shear strength is:

$$V_s = \frac{A_v f_y d}{s} \qquad \text{Eq. 2-30}$$

The code also specifies a minimum amount of shear reinforcement to be provided in all prestressed concrete members. The minimum area of reinforcement is to be taken as the smaller of:

$$A_v = 50\frac{b_w s}{f_y} \qquad \text{Eq. 2-31}$$

and

$$A_v = \frac{A_p}{80}\frac{f_{pu}}{f_y}\frac{s}{d}\sqrt{\frac{d}{b_w}} \qquad \text{Eq. 2-32}$$

in which A_p is the cross-sectional area of the prestressing steel, f_y, is the yield stress of the stirrup steel, and f_{pu} is the ultimate tensile strength of the prestressing-steel. The maxi mum stirrup spacing is not to exceed the lesser of 0.75h or 24".

2.2.7 Compression Field Theory

Current design procedures for reinforced concrete beams in shear are largely based on the truss analogy developed by Ritter, and Morsch nearly a century ago. Recent years have seen a renewed interest concerning the behavior of reinforced concrete in shear. Much of the work has been directed toward formulating a more general model, free of empirical limitations.

Mitchell and Collins (Ref. 7) extended the truss analogy by realizing that the angle of inclination of the concrete struts was really only part of the strain compatibility require merits that must be satisfied together with the equilibrium requirements. This was done by introducing a compatibility condition for strains in the transverse and longitudinal reinforcement as well as the diagonal struts. It was assumed that after cracking, the concrete carries no tension and that the shear is carried by a field of diagonal compression. If strains in: three directions are known, the strains in any other direction can be found using geometry. The Mohr's circle of strains in Figure 2-7 is used to illustrate the transformations

involved. This resulted in the following expression for the angle on inclination of the diagonal compression:

$$\tan^2\theta = \frac{\in_x - \in_2}{\in_t - \in_2} \qquad \text{Eq. 2-33}$$

where, $\in_x$ = longitudinal strain of web, tension positive

$\in_t$ = transverse strain, tension positive

$\in_2$ = principal compressive strain, negative quantity

If the value of θ is known then the aforesaid equation can be regarded as a compatibility condition relating the three strains, $\in_x$, $\in_t$ and $\in_2$.

From Mohr's circle, the principal tensile strain in the web is

$$\in_1 = \in_x + \in_t - \in_2 \qquad \text{Eq. 2-34}$$

and the shear strain in the web is

$$\gamma_{xy} = 2\,(\in_x - \in_2)\cot\theta \qquad \text{Eq. 2-35}$$

For beams with low crack inclinations (low θ), the web reinforcement will be highly strained while for steep crack inclination (high θ), the longitudinal reinforcement will be highly strained.

When any typical prestressed concrete beam is subjected to shear, it can be shown that for any given level of shear, V, there are five unknowns: the stress in the longitudinal bars, f_x; the stress in the longitudinal-prestressing tendons, f_p, the stress in the stirrups, f_v; the diagonal compressive stress in the concrete, f_2; and the angle of inclination, θ; of these

diagonal compressive stresses. In order to solve for these five unknowns we must apply the three equilibrium equations, two compatibility equations, and the relationships for the materials that link the stresses and strains. The complete load-deformation response of a member subjected to shear can be determined by using equilibrium, compatibility and stress strain relationships. This approach has become known as the compression field theory.

The compressive stress-strain relationship for concrete is usually defined by the response of a standard concrete cylinder. That is the stress peaks at a stress of f'_c when he corresponding strain is $\in'_c$. The strain conditions in the cracked concrete in the web of a beam subjected to shear are quite different than those of a concrete cylinder test. The concrete in a cylinder test is subject to small tensile strains as a result of the Poisson effect. Whereas, the diagonally cracked concrete in the web of a beam is subjected to very substantial tensile strains. Additionally, the compressive stress may need to be transmitted across previously formed cracks. These factors cause the concrete in a diagonally cracked web to be weaker and softer than the concrete in a cylinder test.

Mitchell and Collins found that the principal compressive stress in concrete, f_2, is a function of the principal compressive Strain, $\in_2$ and the coexisting principal tensile strain, $\in_1$. They suggested the following stress-strain relationship:

$$f_2 = f_{2\max}\left[2\left(\frac{\in_2}{\in'_c}\right)-\left(\frac{\in_2}{\in'_c}\right)^2\right] \qquad \text{Eq. 2-36}$$

where,

$$\frac{f_{2\max}}{f'_c} = \frac{1}{0.8+170\in_1} \le 1.0 \qquad \text{Eq. 2-37}$$

The strength and the load-deformation response of members loaded in shear can be predicted fairly accurately using the compression. field theory. However, the exclusion of the tensile stress in the cracked concrete leads to conservative estimates of deformation and strength.

2.2.8 Modified Compression Field Theory

In an effort to reduce some of the conservatism that is inherent in the compression field theory, Mitchell and Collins developed the: modified compression field theory. This is an analytical model which predicts the behavior of reinforced concrete subjected to in-plane shear, axial and flexural stresses. The main difference is that the modified compression field theory accounts for the contribution of the tensile stresses that can exist in the concrete between the cracks. Although application of this method is too complex for use in everyday design, the procedure provides a rational method whenever a more thorough analysis is warranted.

The equilibrium equations for the modified compression field theory are best developed while investigating a beam section as shown in Figure 2.8. When a symmetrically reinforced member is subjected to pure shear, the shear force at a particular section must be resisted by the diagonal compressive stresses, f_2, together with the diagonal, tensile stresses, f_1. The diagonal tensile stresses in the cracked concrete vary from zero at the crack locations to a maximum between the cracks. Therefore, it is acceptable to use the average value of tensile strains when formulating these equilibrium expressions.

The principal tensile stress, f_1, is derived using Mohr's stress circle as follows:

$$f_1 = (\tan \theta + \cot \theta)\, v - f_2 \qquad \text{Eq. 2-38}$$

where,

$$v = \frac{V}{b_w jd} \qquad \text{Eq. 2-39}$$

where, b_w = width of the web

d = depth from the compression face to the centroid of the prestressing steel, "d" is taken as the greater of d or 0.8h

j = - 0.875

The diagonal compressive stresses tend to push the flanges of the beam apart while the tensile stresses tend to pull them together. The unbalanced component must be carried by tension in the web reinforcement. This equilibrium requirement can be expressed as follows:

$$A_v f_v = (f2 \sin^2 \theta - f_1 \cos^2 \theta)\, b_w s \qquad \text{Eq. 2-40}$$

where, f_v, is the average stress in the stirrups.

Substituting for f_2 from Equation 2-38 yields:

$$V = f_l b_w jd \cot \theta + \frac{A_v f_v}{s} jd \cot \theta \qquad \text{Eq. 2-41}$$

Equation 2-41 expresses the shear resistance of a member, as the sum of the concrete contribution and the steel contribution. The concrete contribution is dependent on the tensile stress of the concrete while the steel contribution is dependent of the tensile stress of the

steel. This is similar to the ACI shear equation of $V_c + V_s$. Vecchio and Collins (Ref. 10) tested several reinforced concrete panels in pure shear and recommended the following relationship for the average tensile stress versus average tensile strain:

if, $\in_1 \leq \in_{cr}$ then $f_1 = E_c \in_1$ Eq. 2-42

$\in_1 \geq \in_{cr}$ then $f_1 = \dfrac{\alpha_1 \alpha_2 f_{cr}}{1 + \sqrt{500 \in_1}}$ Eq. 2-43

where, α_l = factor accounting for bond characteristics of reinforcement

α_l = 1.0 for deformed reinforcing bars

a_l = 0.7 for plain bars, wires or bonded strands

α_1 = 0 for unbonded reinforcement

α_2 = factor accounting for sustained or repeated loading

α_2 = 1.0 for short-term monotonic loading

α_2 = 0.7 for sustained and/or repeated loads

Equation 2-43 was developed using average stresses and strains without dealing with local variations. At a crack the tensile stresses in the concrete are zero so the tensile stresses in the shear reinforcement become larger. Therefore, the shear capacity of a member may be limited by the ability of the member to transmit forces across the crack as shown in Figure 2-9.

Tension is transmitted across a crack by local increases in shear reinforcement stresses. As the shear force increases the transmission of tension across a crack will require local increases in shear stresses on the crack surface, v_{ci}. The limiting value of v_{ci} is suggested as:

$$v_{ci} = \frac{2.16\sqrt{f'_c}}{0.3 + \frac{24w}{a + 0.63}} \qquad \text{Eq. 2-44}$$

where, a = Maximum aggregate size

w = Width of the diagonal cracks

f'_c = Compressive strength of concrete

The ability of the crack interface to transmit these shear stresses depends on the crack width, w, which can be taken as the product of the principal tensile strain, $\in_1$, and the average spacing of the diagonal cracks. Thus,

$$w = \in_1 s_{m\theta} \qquad \text{Eq. 2-45}$$

The stresses shown in Figures 2-9(b) and 2-9(c) must be statically equivalent. Hence, the principal tensile stress, f_1, must be limited to

$$f_1 = v_{ci} \tan\theta + \frac{A_v}{sb_v}(f_{vy} - f_v) \qquad \text{Eq. 2-46}$$

where v_{ci} is given by Equation 2-44.

The spacing of the inclined cracks depends on the crack control characteristics of the longitudinal and the transverse reinforcement. This spacing is suggested as

$$s_{m\theta} = \frac{1}{\left(\frac{\sin\theta}{s_{mx}} + \frac{\cos\theta}{s_{mv}}\right)} \qquad \text{Eq. 2-47}$$

Where s_{mx} is the average crack spacing that would result if the member was subjected to longitudinal tension and s_{mv} is the average crack spacing that would result if the member

was subjected to a transverse tensile force. The following equations are used for uniform tensile straining:

$$s_{mx} = 2\left(c_x + \frac{s_x}{10}\right) + 0.25k_1\frac{d_{bx}}{\rho_x} \qquad \text{Eq. 2-48}$$

$$s_{mv} = 2\left(c_v + \frac{s}{10}\right) + 0.25k_1\frac{d_{bv}}{\rho_v} \qquad \text{Eq. 2-49}$$

In the previous equation $\rho_v = A_v/(b_w s)$, $\rho_x = (A_{sx} + A_{px})/A_c$ and k_1 is 0.4 for deformed bars and 0.8 for plain bars or bonded strand.

The previous formulations can be used in analyzing any reinforced or prestressed concrete beam by considering the beam to be composed of a series of concrete layers and longitudinal steel elements. This layered approach allows for the analysis of beams with unusual cross-sectional shapes or reinforcing details. Each concrete layer is defined by its individual width b, depth h, amount of transverse reinforcement ρ_y, and position relative to the top of the beam y. The longitudinal steel elements are defined by their crosssectional area A_s, initial prestrain $\Delta\in_p$, yield strength f_{yx}, and position relative to the top of the beam y, Properties common to the entire beam cross section can include the concrete cylinder strength f_c', concrete strain at peak stress $\in_c$', yield strength of the transverse reinforcement f_{yy}, and Young's modulus for steel E_s.

The concrete layers and the longitudinal steel elements are analyzed individually while conditions of equilibrium and compatibility must be satisfied for the section as a whole. The force equilibrium requirements are as follows: (1) balancing of the shear, moment and axial load acting on the section and (2) horizontal shear equilibrium. Uniform

stress conditions are assumed to exist in each layer and element. The only section compatibility requirement that is applied is that plane sections remain plane.

Mitchell and Collins (Ref. 7) have outlined a solution technique as follows:

Step 1: Choose a value of $\in_1$, at which to perform the calculations.

Step 2: Estimate θ.

Step 3: Calculate w from Eqs. (2-45), (2-47), (2-48), and (2-49).

Step 4: Estimate f_v.

Step 5: Calculate f_l from Eqs. (2-43 and 2-46).

Step 6: Calculate V from Eq. 2-41:

Step 7: Calculate f_2 from Eq. 2-38.

Step 8: Calculate f_2 from Eq. 2-37.

Step 9: Check that $f_2 \leq f_{2max}$

If $f_{2n} \geq f_{2max}$, solution is not possible. Return to step 1 and choose a smaller $\in_1$.

Step 10: Calculate $\in_2$.

$$\in_2 = \in'_c \left(1 - \sqrt{1 - f_2 / f_{2\max}}\right)$$

Step 11: Calculate $\in_x$ and $\in_t$ from Eqs. 2-33 and 2-34 as

$$\in_x = \frac{\in_1 \tan^2\theta + \in_2}{1 + \tan^2\theta}$$

$$\in_t = \frac{\in_1 + \in_2 \tan^2\theta}{1 + \tan^2\theta}$$

Step 12: Calculate $f_v = E_s \in_t \leq f_{vy}$.

Step 13: Check estimate of f_v. If necessary, revise estimate and return to step 5.

Step 14: Calculate $f_{sx} = E_s \in_x \leq f_y$ and $f_p = E_p(\in_x + \Delta\in_p) \leq f_{py}$.

Step 15: Calculate the axial force on the member.

$$N = A_{sx} f_{sx} + A_{px} f_p - \frac{V}{\tan\theta} + f_1 b_w jd - f_c \left(A_c - b_w jd\right)$$

where f_c is the axial compressive stress in the concrete areas outside the web. If $\in_x$ is tensile then $f_c = 0$, otherwise,

$$f_c = f'_c \left[2\left(\frac{\in_x}{\in'_c}\right) - \left(\frac{\in_x}{\in'_c}\right)^2 \right]$$

Step 16: Check the axial load. If N is not equal to the desired value (usually zero), make a new estimate of θ and return to step 2. Increasing θ increases N.

Step 17: Check that the longitudinal reinforcement can carry stresses across the crack. If this requirement is not satisfied, lower f_1 and return to step 6.

2.3 Summary

This chapter consists of three subchapters. The first subchapter has dealt with the basic definition and the theory of determining transfer length of a prestressed concrete member. The second subchapter has explained the theory involved with strut and tie model, compression field theory and modified compression field theory.

The theory presented in the first subchapter has been exactly followed to determine the transfer length. In the same manner the theory presented in the second subchapter has been followed to determine the shear strength of the test beams. Chapter 4 and Chapter 5 of this study present the comparisons of the test results and the theoretical results for transfer length and shear strength of the test beams.

Shear strength of the test beams have been estimated analytically by applying the theory associated with the strut and tie model and modified compression field theory. The summary of the comparison of the test results and the analytical results for shear strength of the test beams are presented in Chapter 6.

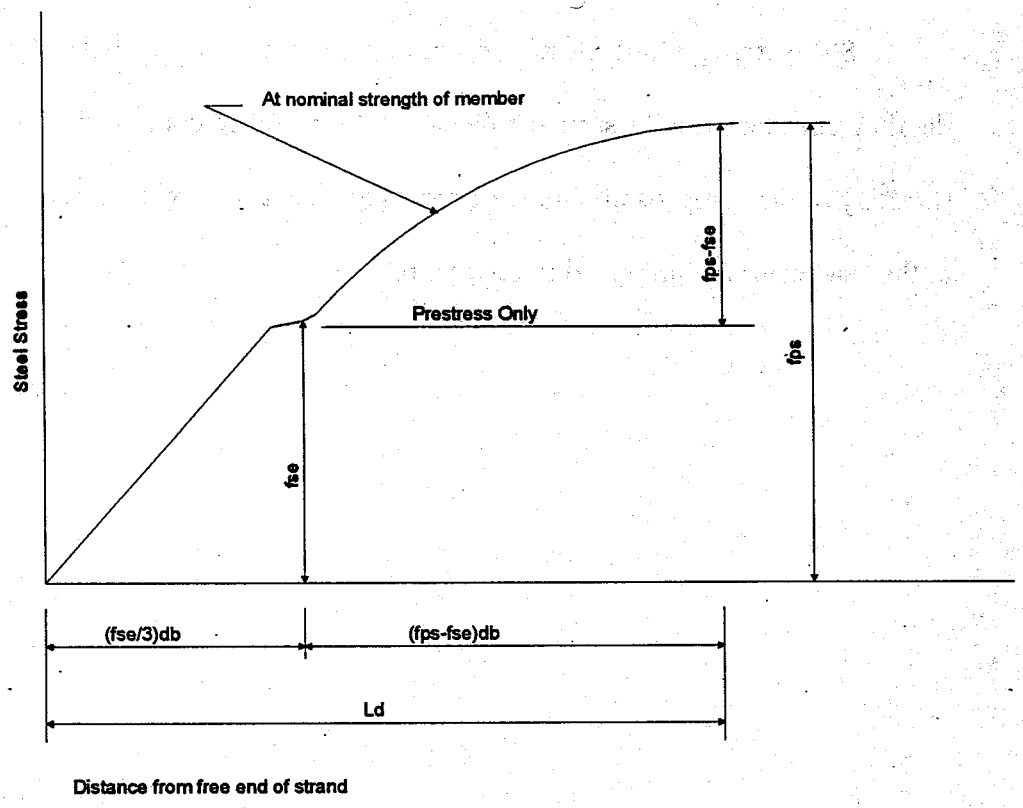

Figure 2-1. Variation of Steel Stress with Distance from Free End of Strand.

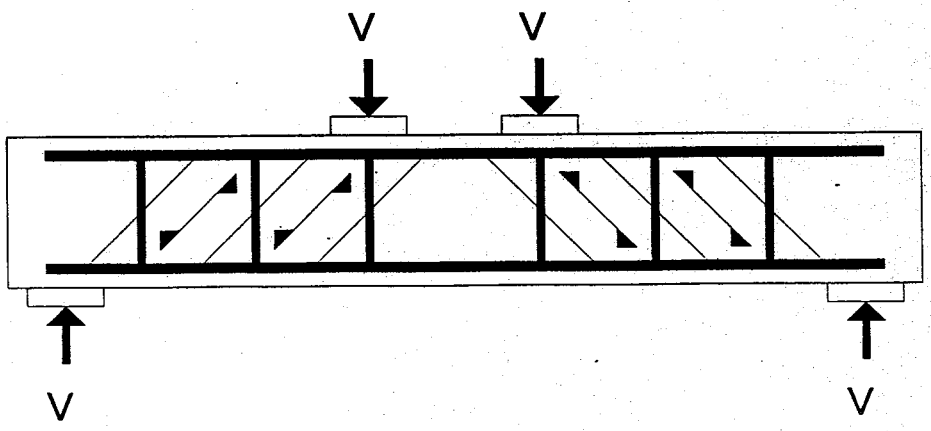

Figure 2-2. Truss Model.

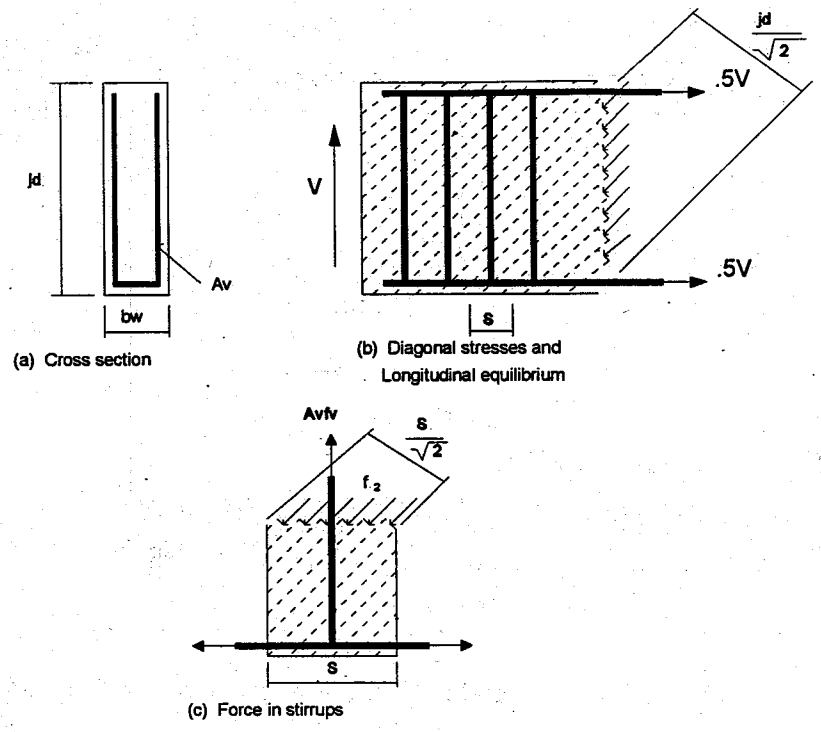

Figure 2-3. Equilibrium Conditions for 45° Truss Model.

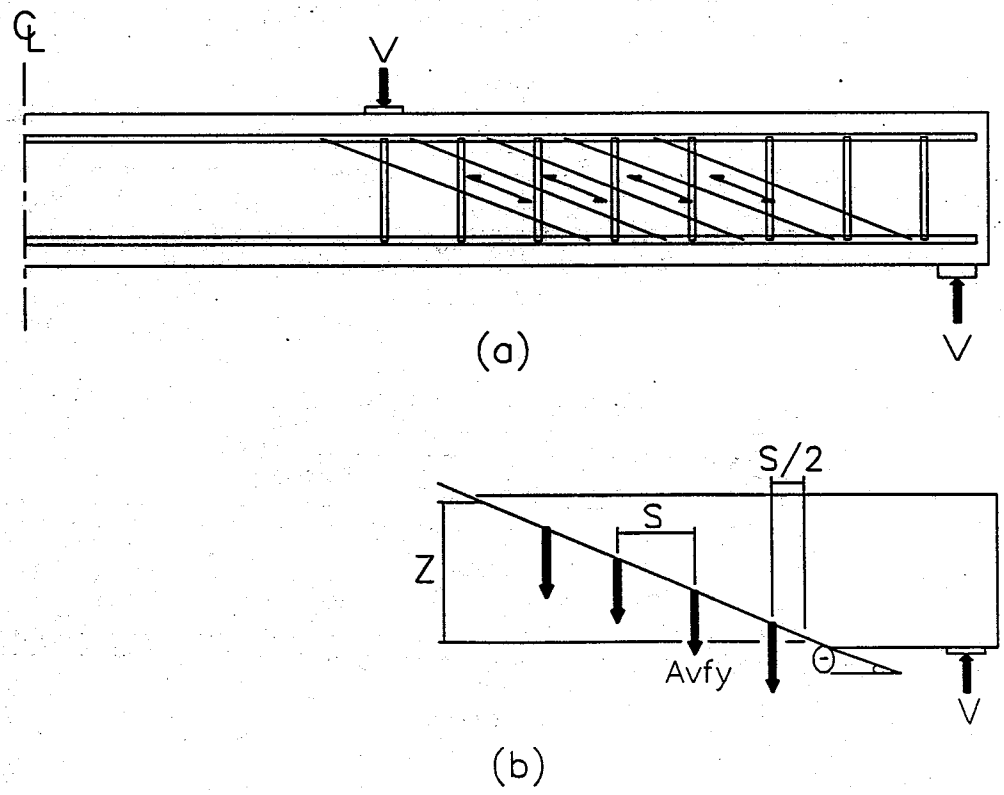

Figure 2-4. Variable Angle Truss Model.

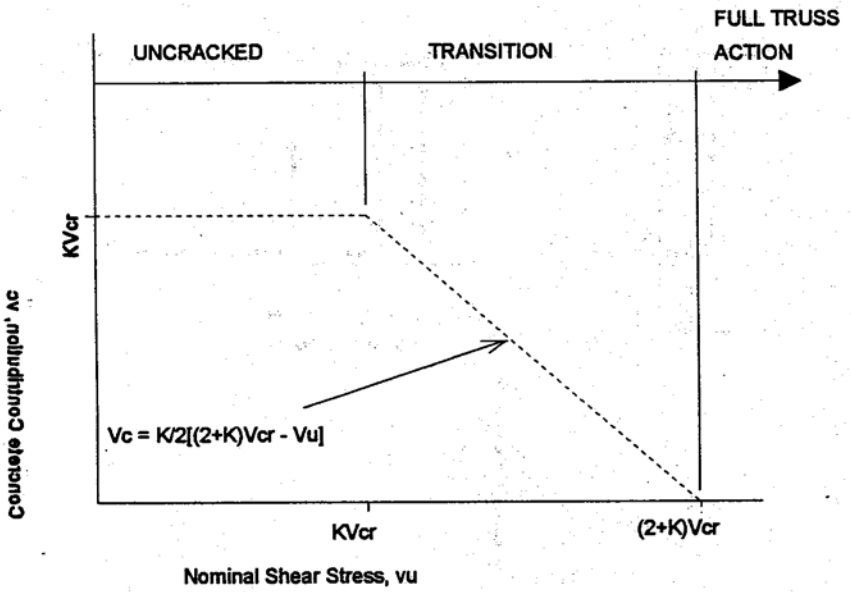

Figure 2-5. Concrete Contribution in Modified Truss Model.

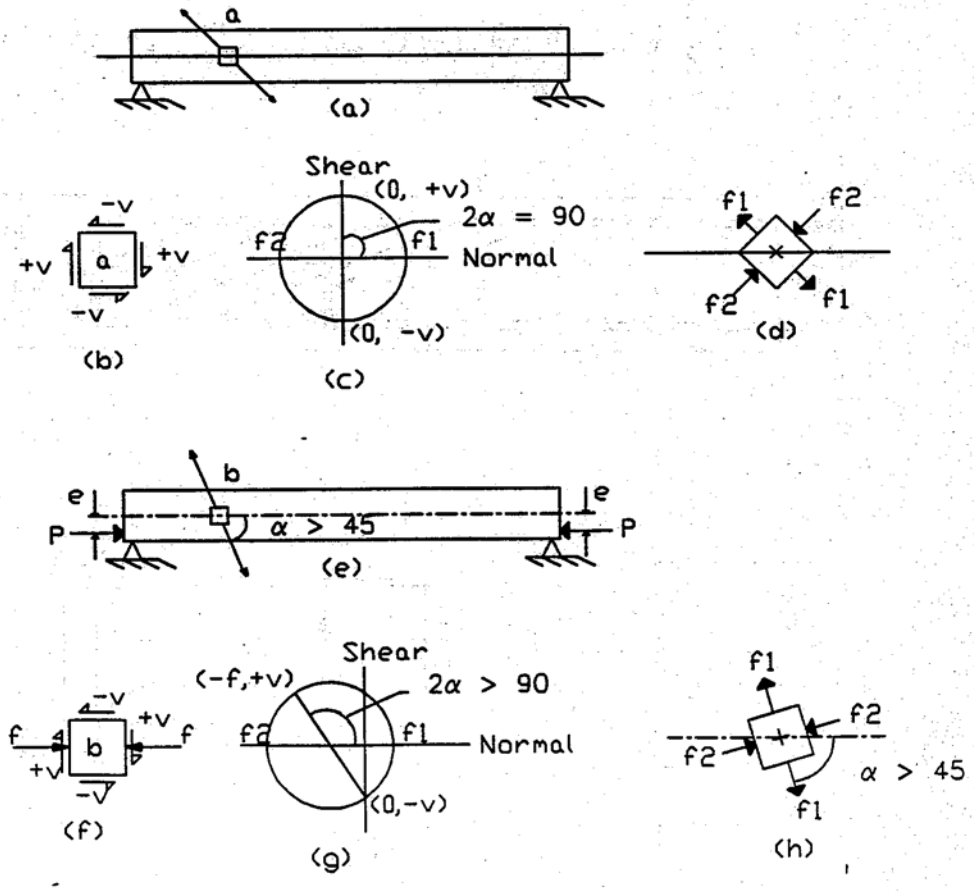

Figure 2-6. .K Factor, Modified Truss Model.

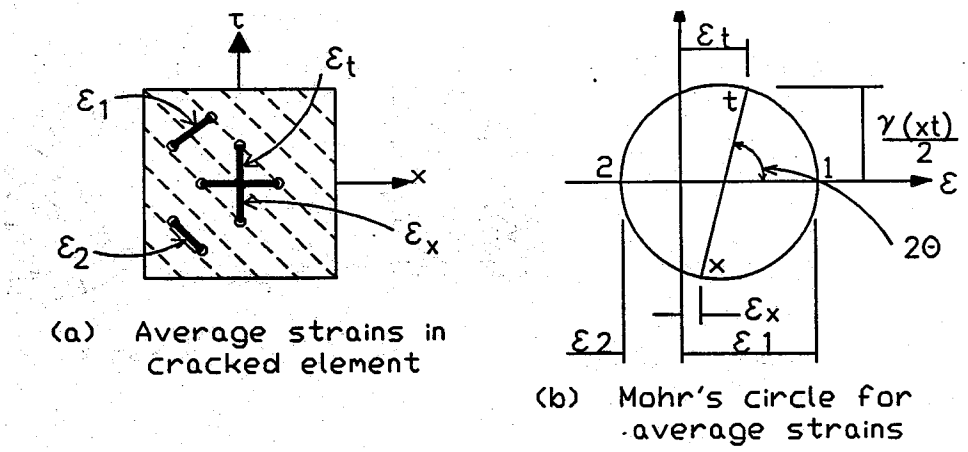

Figure 2-7. Compatibility Conditions for Cracked Web Element.

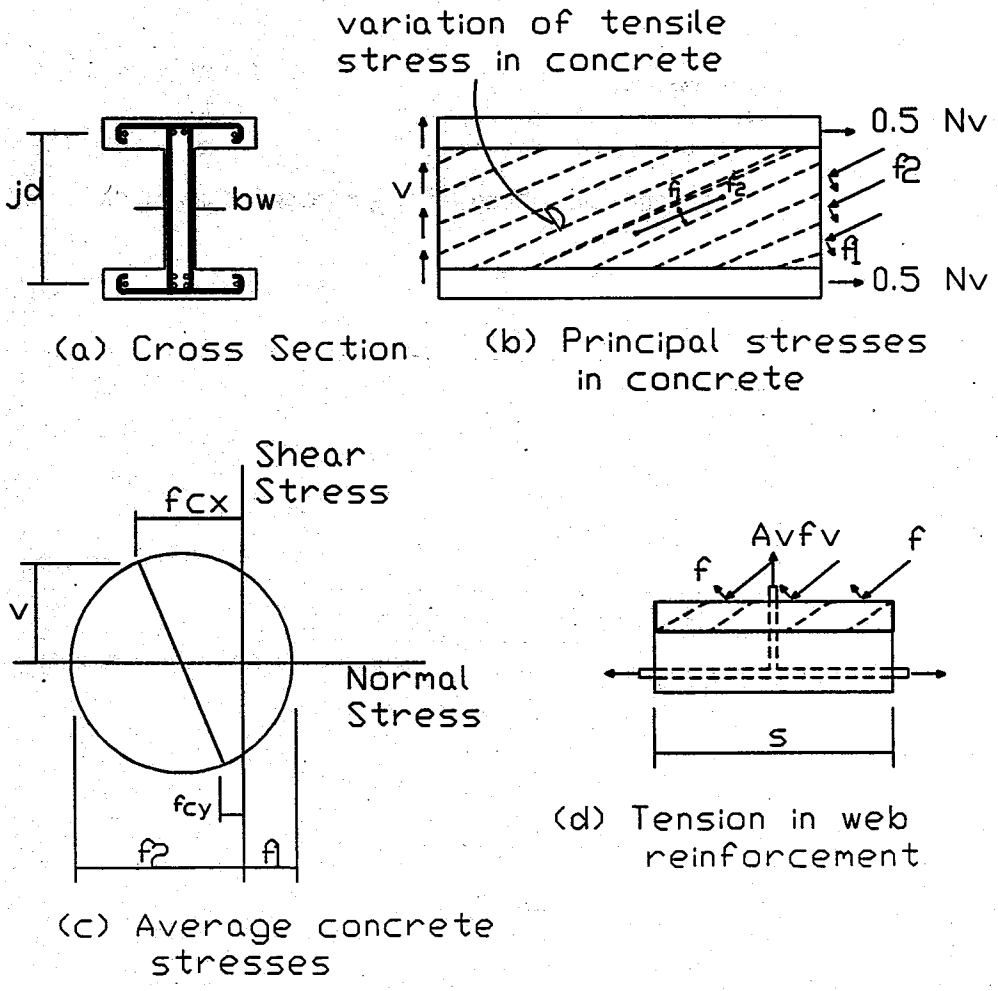

Figure 2-8. Equilibrium Conditions of MCFT.

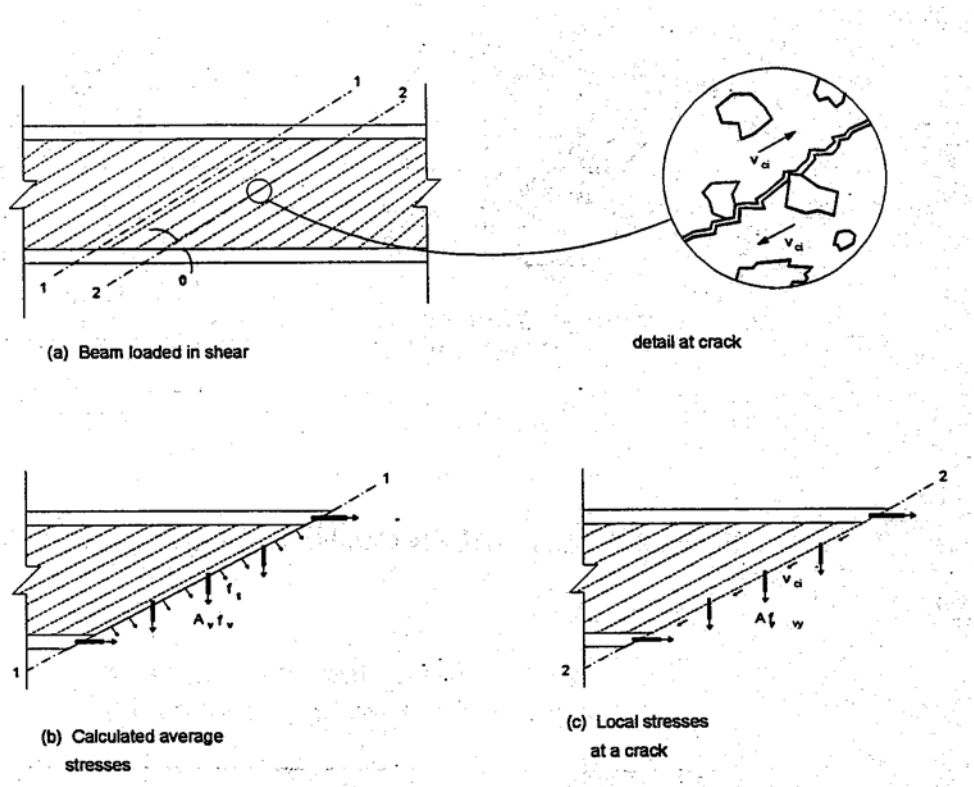

Figure 2-9. Transmitting Forces Across Cracks.

CHAPTER 3
TESTING AND INSTRUMENTATION

3.1 General

This chapter describes the variables that were considered during this study as well as a description of the test specimens, instrumentation, and the test sequence.

3.1.1 Beam Nomenclature

Each of eight beams were loaded at both ends for a total of 16 individual tests. The nomenclature used to identify the different tests consists of the following:

UF - identifies test series performed at the University of Florida;

1 or 2 - indicates the first or second beam in a series;

30, 36, 42, 48 - represents section height in inches; and

2D or Ld - identifies the loading point, either twice the effective depth (2D) or the development length (LD).

3.1.2 Description of Test Specimens

There are two identical sets of four simply supported beams 35 feet in length. The beams all have a width of 12 inches and heights of 30, 36, 42 and 48 inches and were reinforced with 1/2-inch grade 270 ksi Lolax strand. Figures 3-1 and 3-2 show an elevation view of the test beams and the different tendon layouts. All of the beams are designed for a full AASHTO HS 15 truck loading. The beams are also designed to have the same

tensile stress at midspan under full service load conditions of 50 psi. Another initial design requirement was that all of the test specimens have the same moment capacity, therefore the amount and location of the tendons varied for each set of beams. The shear reinforcement is provided by #3 bars spaced at 24 inches for the entire span length in all beams. Straight tendons were utilized for the prestressing force. Based on an assumed compress size concrete strength of 5,000 psi, and including a conservative factor of safety, the specimens were designed to ensure that they could be loaded to failure using equipment and facilities available in the structures testing laboratory at the University of Florida. The maximum capacity of the loading equipment was 200 kips.

Each specimen was tested twice; first loading one end of the specimen to failure under a concentrated load and then altering the test configuration to load the other end to failure. One end was tested with the load at twice the effective depth (2D) from the center line of the support while the other end was tested with the load at the development length (LD) from the center line of the support. To prevent damage in the first test from affecting the second test, the second test was performed at a reduced span, insuring that the cracks formed from the first test would not impinge on the test zone for the second. For the two replicate specimens of each design, the order of performing the 2D and LD test was reversed. Table 3-1 represents the number of tendons, effective depth, eccentricity of the tendons and loading position for each specimen.

The prestress jacking force, P_j, was measured by the elongation of the tendon and verified with a pressure gauge at the prestressing jack.

Table 3-1. Specimens and Loading Positions

Beam	Height	Number of Tendons	Eccn.	Effec. Depth	Loading Position
UF1-30-2D	30"	14	6.5"	21.5"	43"
UF1-30-LD	30"	14	6.5"	21.5"	77"
UF2-30-2D	30"	14	6.5"	21.5"	43"
UF2-30-LD	30"	14	6.5"	21.5"	77"
UF1-36-2D	36"	11	8.5"	26.5"	53"
UF1-36-LD	36"	11	8.5"	26.5"	77"
UF2-36-2D	36"	11	8.5"	26.5"	53"
UF2-36-LD	36"	11	8.5"	26.5"	77"
UF1-42-2D	42"	9	11"	32.0"	64"
UF1-42-LD	42"	9	11"	32.0"	77"
UF2-42-2D	42"	9	11"	32.0"	64"
UF2-42-LD	42"	9	11"	32.0"	77"
UF1-48-2D	48"	8	12.5"	36.5"	73"
UF1-48-LD	48"	8	12.5"	36.5"	77"
UF2-48-2D	48"	8	12.5"	36.5"	73"
UF2-48-LD	48"	8	12.5"	36.5"	77"

The losses for these test specimens were calculated in accordance with the requirements of AASHTO Section 9.16.2. The prestress jacking force, initial prestress force and effective prestress force for each beam are listed in Table 3-2. The sample calculations are presented in Appendix E .

It is also of interest to determine the strand stresses at the loading stages. The stresses present at the loading stages are presented in Table 3-3. The stress in the prestressing tendons at transfer, f_{si}, is determined as follows:

$$f_{si} = \frac{P_i}{A_p} \qquad \text{Eq. 3-1}$$

Table 3-2. Prestress Force Per Tendon (kips)

BEAM	P_j	P_i	P_e
UF1-30	21.0	19.9	16.7
UF2-30	21.0	19.9	16.7
UF1-36	21.9	20.2	17.4
UF2-36	21.9	20.2	17.4
UF1-42	22.2	21.7	19.1
UF2-42	22.2	21.7	19.1
UF1-48	22.6	21.9	19.6
UF2-48	22.6	21.9	19.6

Table 3-3. Steel Stress at Load Stages (ksi)

BEAM	f_{pi}	f_{pe}	f_{ps}
UF1-30	130	109	217.0
UF2-30	130	109	216.5
UF1-36	132	114	227.0
UF2-36	132	114	221.0
UF1-42	142	125	228.5
UF2-42	142	125	228.5
UF1-48	143	128	234.0
UF2-48	143	128	219.0

The stress in the prestressing tendons resulting from the application of the effective prestress force, P_c, acting alone and the associated strain are determined by:

$$f_{pe} = \frac{P_e}{A_p} \qquad \text{Eq. 3-2}$$

$$\epsilon_1 = \epsilon_{pe} = \frac{f_{pe}}{E_p} \qquad \text{Eq. 3-3}$$

The stress in the steel at transfer and after losses, can be found directly from Equations 3-1 and 3-2, whereas the steel stress at failure must be found from an iterative

approach. In order to do this it is necessary to determine the strain at an intermediate load stage between failure and transfer. At decompression the increase in strand stress is given by the following expression

$$\in_2 = \frac{P_e}{A_c E_c}\left(1 + \frac{e^2}{r^2}\right) \qquad \text{Eq. 3-4}$$

When the member is overloaded to the limit stage the neutral axis is at a distance c below the extreme compression fiber of the: beam and the increment of strain beyond decompression i s

$$\in_3 = \in_{cu}\left(\frac{d_p - c}{c}\right) \qquad \text{Eq. 3-5}$$

where, $\in_{cu}$ = 0.003, the ultimate strain-capacity of concrete

d = effective depth of the member.

The total steel strain at the limit stage, $\in_{ps}$, is the sum of the three components found from Equations 3-3, 3-4 and 3-5:

$$\in_{ps} = \in_1 + \in_2 + \in_3 \qquad \text{Eq. 3-6}$$

and the corresponding steel stress is obtained f r o m the stress-strain relationship for the strand.

The following procedure was used to determine the steel stress at failure, f_{ps}:

1. Assume a reasonable value of f_{ps} and note the corresponding value of $\in_{ps}$ from the steel stress-strain curve.
2. Determine the depth c to the neutral axis for that steel stress using the following equation.

$$c = \frac{A_{ps} f_{ps}}{0.85 \beta_1 f'_c b} \qquad \text{Eq. 3-7}$$

3. Calculate the incremental failure strain $\in_3$ (Eq. 3-5) and add this to $\in_1$ and $\in_2$ as indicated by Eq. 3-6.

4. If the failure strain $\in_{ps}$ differs significantly from that assumed in step (1), revise the assumption and repeat steps (1) through (3) until convergence is reached.

3.1.3 Fabrication of Formwork and Concrete

The beams were designed using- a standard 5000 psi mix. The mix design is presented in Appendix B. Steel forms were positioned along the length of the casting bed. They were then secured at the top to prevent separation due to the lateral pressure of the concrete. Form oil was sprayed on then sides of the forms to ensure easy separation after the concrete cured.

The concrete was poured in three layers according to ASTM specifications. Two identical beams were cast simultaneously end to end in a 550-foot prestressing bed. Care was taken to ensure that concrete was not: poured directly onto the instrumented stirrups. After each layer was poured, two vibrators were utilized to ensure adequate compaction. The concrete surface was then smoothed over and the beam designation sketched into the surface.

3.1.4 Material Properties

3.1.4.1 Concrete. The slump of the mix was measured prior to casting the specimen. For each beam, nine 4-inch by 8-inch test cylinders and two 6-inch by 12-inch test

cylinders were cast. The two 6-inch by 12-inch cylinders were tested for compressive strength at release of prestress. Three of the 4-inch by 86-inch cylinders were tested for compressive strength at 28, days after casting, while three were tested as split cylinders at the same age. If the slump did not meet the minimum specifications as, given in Appendix B, the batch was discarded and a new batch was tried. The specimens were allowed to cure for three days and the forms were then removed. The results of tests for the concrete strengths are given in Table 3-4.

Table 3-4. Summary of Concrete Strengths

BEAM	SLUMP (in)	fc' @ release (psi)	release date	fc'@ test (psi)	test date
UF1-48	2.5	6370	4/14	7374	7/21
UF2-48	4	5840	4/14	9353	7/24
UF1-42	3.25	6010	4/21	8367	7/17
UF2-42	4.25	4280	4/21	8356	7/20
UF1-36	3.25	4700	4/28	6800	7/1
UF2-36	2.25	4950	4/28	7633	6/18
UF1-30	3	6300	5/4	7182	6/29
UF2-30	5	4700	5/4	7348	6/24

3.1.4.2 Steel. The reinforcement consisted of 1/2-inch grade 270 ksi Lolax prestress concrete strand. Tests on the strand produced the following results:

Breaking Load	=	42,840 1bs
Guaranteed Ultimate Breaking Strength	=	41,300 lbs
Load @ 1% Elongation	=	40,200 lbs
Elongation @ 31,000 lbs	=	0.00718 in/in
Nominal Area	=	0.153 in^2
Modulus of Elasticity	=	28,200 ksi

3.2 Variables

The test beams have clear, spans ranging from 35 feet to 25 feet 6 inches and effective depths ranging from 21.5 to 36.5 inches. In each case there is a clear span to depth ratio, l_n/d, greater than 5.0 and according to ACI 11.8.1 (Ref. 1) these beams may be treated as slender members. However, the loading point of 2D with a single concentrated load causes the short shear span to act as a deep beam. Since the shear spans and the effective depths varied in our testing the same behavioral model may not be valid for every test situation. The test variables for each beam are listed in Table 3-5.

Table 3-5. Test Variables

BEAM	a/d	l_n (ft)	l_n/d	V_u/bdf_c'
UF1-30-2D	2.00	35.0	19.53	.089
UF1-30-LD	3.58	28.5	15.91	.053
UF2-30-2D	2.00	25.5	14.23	.083
UF2-30-LD	3.58	35.0	19.53	.053
UF1-36-2D	2.00	35.0	15.85	.055
UF1-36-LD	2.91	28.0	12.68	.047
UF2-36-2D	2.00	28.0	12.68	.069
UF2-36-LD	2.91	35.0	15.85	.054
UF1-42-2D	2.00	26.5	9.94	.044
UF1-42-LD	2.41	35.0	13.13	.040
UF2-42-2D	2.00	35.0	13.13	.042
UF2-42-LD	2.41	28.7	10.00	.038
UF1-48-2D	2.00	35.0	11.51	.029
UF1-48-LD	2.11	25.7	8.44	.028
UF2-48-2D	2.00	25.5	8.38	.038
UF2-48-LD	2.11	35.0	11.51	.037

The variables presented in Table 3-5 are as follows:

a/d = shear span to depth ratio

l_n = clear span

d = effective depth of the member

V = shear acting at the loading point

b = member width

f'_c = compressive strength of the concrete.

3.3 Instrumentation

3.3.1 Stirrup Instrumentation

Three stirrups at each end of the beam were instrumented with strain gauges located at the bottom of the stirrup, the tendon centroid, and the neutral axis of the beam as shown in Figure 3-3.

3.3.1.1 Surface preparation. The location of the strain gauges was ground flat to remove deformations and provide an adequate surface for instrumentation. The strain gauges were attached using a strain gauge welder and placing a series of spot welds along each edge of the gauge. After the gauges were welded in place, the lead wires were soldered to the tabs of the gauge and the gauges were insulated.

3 .3.1.2 Insulation and mechanical protection. Once the gauges were attached to the rebar a considerable amount of attention was given to mechanical protection. The first step was to apply several coats of an epoxy sealant over the entire gauge and the wire connections. Once this had dried a rubber pad was placed on top of the gauge and then wrapped with a. protective metallic tape. This was done in order to protect the gauge from the concrete in contact with the gauge region. This process was repeated for every internal

3.3.2 External Strain Gauge Instrumentation

Once the concrete had set and the forms were removed, the external strain gauges were applied. Since two beams were being cast simultaneously, the two adjacent ends were instrumented with strain gauges. These gauges were applied at 6-inch increments along the tendon centroid and in the form of a rectangular rosette along the diagonal compression strut. The location of these gauges was determined by drawing a horizontal line at the neutral axis and a line extending from the load to the support. The location of each group of strain gauges was taken as 6 inches to either side of the intersection of these two lines. Figure 3-3 shows the strain gauge locations for a typical, loading situation.

3.3.2.1 Surface preparation. Before the external strain gauges could be applied the concrete had to be ground smooth in order to remove any foreign material. The area that was ground smooth was then directly heated with heat lamps in order to remove any moisture from the immediate area. A very thin coat of epoxy was then applied to the smooth area. Once this had dried the area was wet with a mild acid and sanded smooth with a very fine sand paper. A neutralizer was applied and then the area was swabbed dry with gauze. Before the strain gauges were applied, a neutralizer was used to clean the strain gauge location. The strain gauges were then attached to the epoxy with super glue.

3.3.2.2 Insulation and protection. After the strain gauges were attached to the concrete the lead wires were then soldered to the tabs of the gauges and the entire gauge was coated with M-Coat A. As a final precaution, the gauges and the leads were coated with a layer of silicon to protect them from any adverse weather conditions.

3.3.3 Instrumentation for Measuring Displacements

Prior to testing the beams were instrumented with linear voltage differential transducers (LVDT) at one foot to either side of the load and at midspan in order to measure deflections during testing. LVDT's were also used to monitor the relative motion between the strand and the concrete at each end of the beam. The LVDT's were attached to a bracket that was then attached to the individual strands as shown in Figure 3-2. A strip of plastic was :glued to the surface of the beam in order for the end of the LVDT to bear on. This was necessary since the strands tend to rotate as they are slipping. The LVDT's that were used on the tendons, Schaevitz type GCD-121-250, had a maximum travel of 0.25 inches in either direction while the LVDT's that monitored deflections had a maximum travel of 1 inch in either direction.

The output for all of the strain gauges and the LVDT's was monitored and recorded with the use of a Hewlett-Packard 3497A Data Acquisition/Control unit together with a PC controller system.

3.3.4 Instrumentation for Strain Gauges Used for Rosettes

The principal stresses were measured at two positions. These position were located in the shear span and were found by the intersection of two lines. One line was marked off from the load to the center of the support. Another line was marked off along the section centroid. The rosettes were placed six inches to the left and right of this intersection.

Each rosette comprised of three strain gages. One strain gage was placed perpendicular to the centroidal axis and the other two were placed at 45-degree angles to the left and right of this gage. Figure 3-4 shows the position and orientation of the rosettes.

3.4 Test Procedure

The testing procedure can be divided in two categories; field tests and laboratory tests.

The following is a listing of the activities during the field testing operation:

1. Place and secure all instrumented stirrups after stressing the tendons.
2. Cast test cylinders for compressive strength tests.
3. Grind smooth and prepare strain gauge locations with a thin coat of epoxy.
4. Attach strain gauges, solder leads and protect the gauges with M-Coat A and silicon.
5. Attach all leads to data acquisition equipment.
6. Take an initial transfer length reading just prior to detensioning and then a final one after all of the prestress has been transferred to the concrete.

The following is a listing of the activities that went on once the beams were transported to the University of Florida in preparation for the laboratory testing operation:

1. Center loading point of specimen underneath the actuator that is attached to the load frame.
2. Once in position, place the specimen on a 6-inch wide steel plate with a 1-inch diameter bar welded to the bottom. This acts as a roller which is then placed on a 6-inch wide steel support.
3. Construct frame to support LVDT's that measure deflections, attach and zero LVDT.
4. Install and zero out LVDT's on strands.

5. Apply strain gauges in rectangular rosette form along compression strut.
6. Attach all leads to the data acquisition equipment.
7. Take initial readings and start loading in 10-kip increments up to first cracking and then continue in 5-kip increments until failure.
8. Break test cylinders after test has been performed.

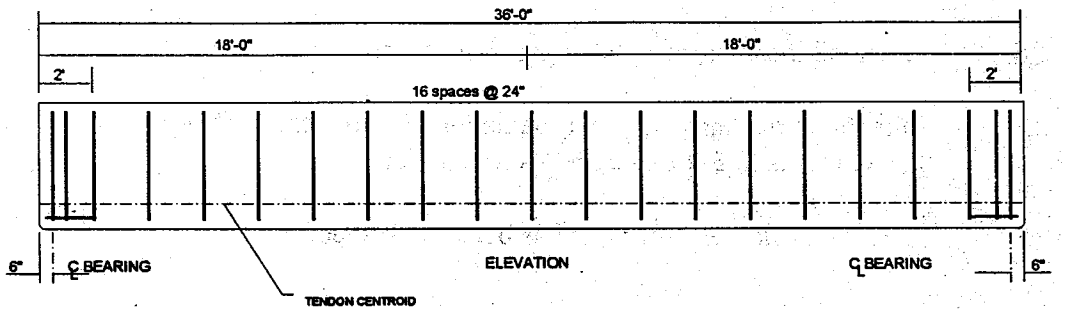

Figure 3-1. Elevation

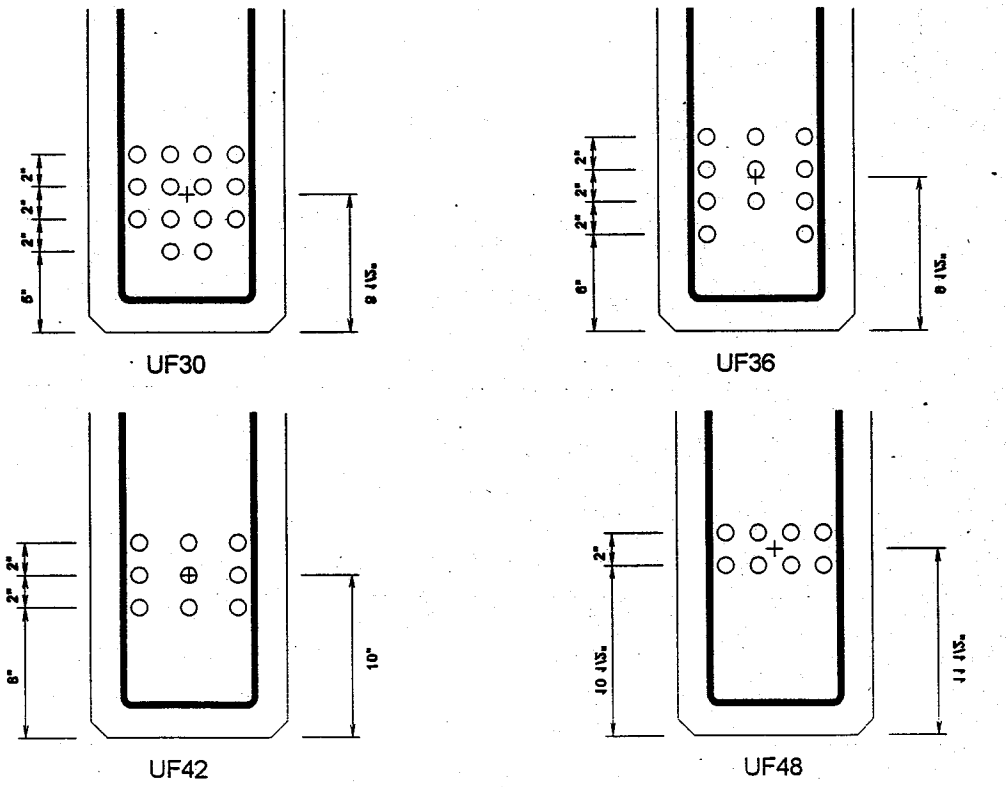

Figure 3-2. Tendon Layout

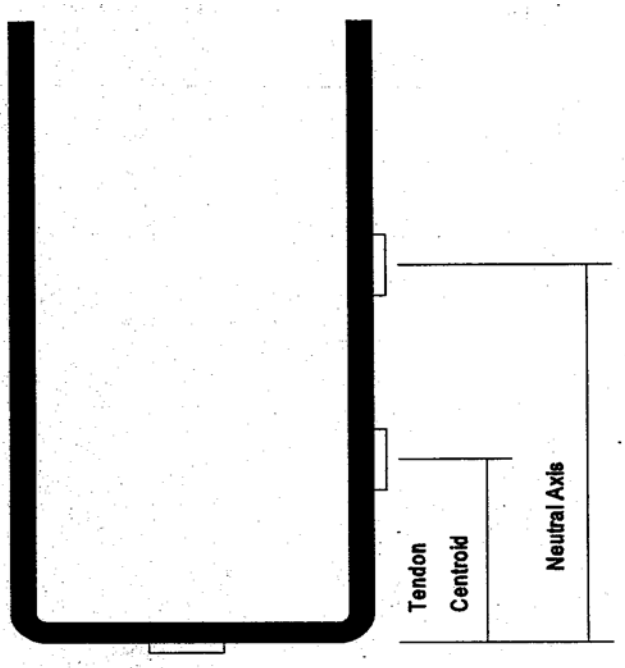

Figure 3-3. Typical Strain Gauge Location for Stirrups

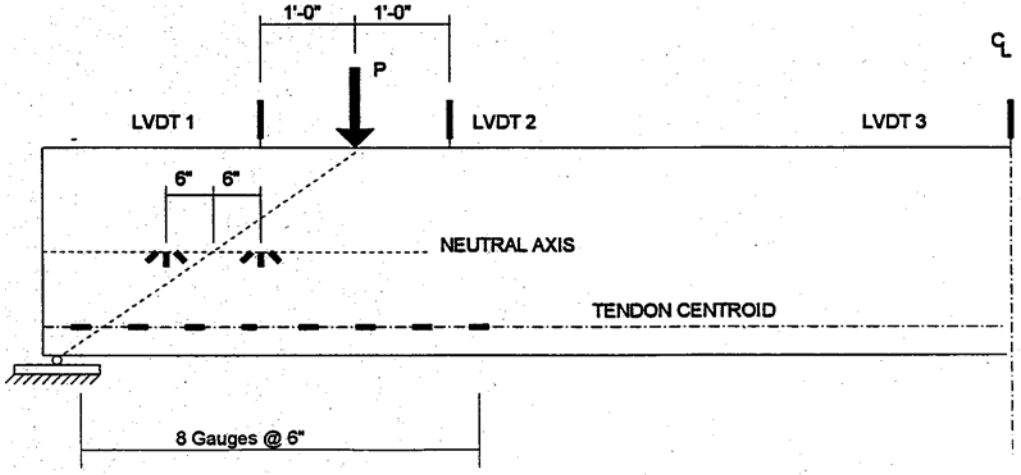

Figure 3-4. Typical Strain Gauge and LVDT Instrumentation

CHAPTER 4
TEST RESULTS

4.1 General

The measured data are presented in this chapter in order to generate a generalized representation of the relevant results of the investigation.

4.2 Description of Test Data

The data was reduced and displayed for each test in a suitable graphical format in order to permit a clear evaluation. The following is a list and description of the plots that are presented for each specimen:

1. Plot of load versus deflection (P-Delta). The deflection at the loading point and at midspan were continuously monitored and plotted during the loading and unloading of the specimen.
2. Plot of load versus strand slip. Tendon slip was monitored as load was applied in order to determine the load at which initial slip occurs and to what degree it affects behavior.
3. Plot of load versus stirrup strain. The internal strains in the stirrups at the bottom, tendon centroid and neutral axis are plotted at each load increment.

4. Plot of load versus principal tensile strain. The principal tensile strains from the rectangular rosette data are calculated from a Mohes Circle transformation and plotted versus the shear acting on the member.
5. Plot of longitudinal strain along the centroid of the prestressing steel. The strains at detensioning are plotted versus position along the beam in order to determine the transfer length.

4.3 Failure Modes

4.3.1 Beams Tested at 2D

A brief description of the testing-procedure for each beam loaded at twice its effective depth and its failure mechanism is given below. Failure is the load at which diagonal cracks develop and excessive crack widths are present or excessive deflections without further load carrying capacity. ACI recommends a maximum crack width of 0.012 inches for prestressed members located in areas subjected to high humidity. The loads at which the tests were terminated were called the collapse loads. The graphs referenced are found in Figures 4-1 through 4-24.

4.3.1.1 Specimen UF1-30-2D. This specimen was tested at a full span length of 35 feet. The P-Delta curve remained in the linear elastic range until a load of 100 kips was reached as shown in Figure 4-1. The first flexural cracks were observed at 100 kips and occurred at several locations as shown in Figure A-1. These cracks occurred at positions 5, 6, 8, and 10 feet from the support. These flexural cracks extended until a load of 135 kips. At 135 kips another sudden flexural crack formed at the stirrup located 12 feet from the support. Up until this load there were no noticeable slips in the tendons nor strains in

the stirrups. Existing cracks continued to extend until a-load of 165 kips. This load resulted in a sudden web-shear crack between the stirrups located 2 and 4 feet from the support. The slip associated with this load is shown in, Figure 4-2. At 170 kips a large flexure-shear crack was observed between the load and support. This was accompanied by additional slip. Crack width of 0.020 inches were-observed at this load. A web-shear crack appeared at a load of 200 kips. The test was terminated at a collapse load of 200 kips. The beam failed due to formation of excessive web and flexural shear cracks.

4.3.1.2 Specimen UF2-30-2D. This specimen was tested on a reduced span length of 25 feet and 6 inches in order, to remove the damaged portion of the beam. Figure A-3 shows the cracking pattern for this specimen. The P-Delta curve shown in Figure 4-4 remained in the linearly elastic range up to 115 kips and was accompanied by a flexural crack directly below the load. Cracks extended until 125 kips and another flexural crack formed at the 6-foot stirrup. All tendons exhibited continuous slippage with increasing load. All the flexural cracks continued to extend until a load of 170 kips with no sudden changes in the tests data. At 170 kips, two sudden vertical cracks developed directly under the load which did not extend to the bottom of the beam. Crack widths were unacceptable at this load. At 180 and 185, kips, sudden web-shear cracks developed with the latter terminating the test. The beam experienced a web shear failure.

4:3:1:3 Specimen UF1-36-2D. This specimen was tested with a full span length of 35 feet. The cracking pattern is shown. In Figure A-5. The P-Delta curve, shown in Figure 4-7, remained linear up to 120 kips. At this load a flexure crack formed near the stirrup located 6 feet from the support. At this crack, there were no noticeable slips in the tendons. At 120 and 141 kips, two flexural cracks formed. Figure 4-8 shows

in the tendons associated with this load. Between these two loads there were no change in strains of the stirrups. However, at 154 kips there was a sudden crack at the stirrup located 4 feet from the support. This was associated with high tensile strains at the tendon centroid. At this load crack widths became unacceptable. Between 154 and 171 kips the cracks extended and widened. There were no other significant events. At 171 kips crushing was observed under the load. The test was terminated at a collapse load 171 kips. The test was terminated due to excessive crushing under the load resulting in almost no compression zone.

Specimen UF2-36-2D. This specimen was. tested with a reduced span length of 28 feet. This was the first test in which the load position was tied to the effective depth. The racking pattern is shown in Figure A-7. The P-Delta curve, shown in Figure 4-10, remained in the linear elastic range up to a load of 140 kips at which several large cracks appeared directly under the load. The tendon slips are negligible as shown in Figure 4-11. After the first flexural crack formed, three other flexural cracks formed in the shear span. These cracks appeared at 154, 168 and 180-kips. Between each of these loads there were no slips in the tendons. The test was terminated at a collapse load 180 kips. The specimen failed in, flexure mixed with flexural shear cracks.

4.3.1.5 Specimen UF1-42-2D. This beam was loaded with a span of 26 feet and 6 inches and developed its first flexural crack at 113 kips. A slight reduction of stiffness in the P-Delta curve as shown in Figure 4-13 also took place at this load increment. The cracking pattern is shown in Figure A-9. A flexure crack at a load of 113 kips formed directly under the load. The stirrup located 6 feet from the support which is in contact with this crack exhibited a sudden increase in tensile strain. Flexural cracks extended until

a load of 135 kips. At this load, there were sudden slips in the tendons. At 149 kips a sudden flexure crack formed at a position 11 feet from the support. There appeared to be no slips associated with this crack. At 169 kips a sudden flexure shear crack developed at the stirrup located 4 feet from the support. This crack extended to mid-height of the specimen. Figure 4-14 shows that a significant amount of tendon slip occurred at this loading point. A horizontal crack also developed at the tendon centroid at 170 kips. The stirrups experienced a sudden increase in tensile strain occurring simultaneously with the shear crack as shown in Figure 4-15. At a collapse load, 188 kips the test was terminated. This beam experienced a flexural failure combined with flexure shear failure.

4.3.1:6 Specimen UF2-42-2D. This specimen was loaded with a full span of 35 feet. The cracking pattern is shown in Figure A-11. The P-Delta Curve is shown in Figure 4-16. The P-Delta curve for this beam remained linearly elastic until 100 kips. The first flexure crack appeased at a load of 100 kips. The stirrup located at 6 feet from the support was indirect contact with this crack. A sudden increase in stirrup strain was associated with this cracks Between the load of 100 and 139 kips new flexural cracks appeared. There were no significant events associated with these cracks. At 139 kips a sudden flexural shear crack appeared. Stirrups located at 4 and 6 feet from the support showed sudden increases in tensile strain. This is shown in Figure 4-18 Up to this load crack widths are acceptable. Cracks extended until a load of 159 kips. At this load, a sudden flexural crack appeared associated with an increase in stirrup strain as shown in Figure 4-18. The test was terminated at a collapse load 177 kips. The specimen failed in flexure along with flexural shear.

4.3.1.7 Specimen UF1-48-2D. This specimen was tested with a full span length of 35 feet. The cracking pattern is shown in Figure A-13. The P-Delta curve shown in Figure 4-19 remained linearly elastic until a load of 113 kips. At 113 kips a flexure crack appeared under the load. At this event, all tendons showed a sudden slip. These are shown in Figure 4-20. Crack widths at this load are already unacceptable. At 136 kips a flexure crack appeared at the stirrup located 10 feet from the support. This was accompanied by sudden tendon slips shown in the Figure 4-20. At 158 kips a large flexure crack appeared at the stirrup located 4 feet from the support. This, crack extended up to near the load. Tendons continued to slip and the test was soon terminated at a collapse load 165 kips. The specimen failed primarily in flexure due to opening up of large flexural cracks as shown in Figure A-13.

4.3.1.8 Specimen UF2-48-2D. This specimen was tested with a reduced span length of 25 feet and 6 inches. The cracking pattern is shown in Figure A-15. The P-Delta curve, shown in Figure 4-22, remained linearly elastic up to a load of 115 kips. The first flexural crack appeared at this load. There were no slips associated with this crack nor it was associated with any increase in tensile strain in the stirrups. However, crack widths were already unacceptable. Nothing of significance occurred until, a load of 151 kips was applied on the beam. At the loads of 151 and 154 kips, two cracks appeared. The crack which appeared at the load of 154 kips caused a large slip in the tendons. This slip is shown in figure 4-23. These cracks continued to extend until the test was terminated at a collapse load 174 kips. The specimen failed in flexure due to large flexural cracks with excessive width.

4.3.2 Beams Tested at LD

A brief description of the testing procedure for each beam loaded at development length and its failure mechanism is given below. Failure is the load at which diagonal cracks develop and excessive crack widths are present or excessive deflections without further load carrying capacity. AC I recommends a maximum crack width of 0.012 inches for prestressed members located in areas subjected to high humidity. The loads at which the tests were used to be terminated are called as collapse loads. The graphs referenced to are found in Figures 4-25 through 4-48.

4.3.2.1 Specimen UF1-30-LD. This specimen was loaded on a reduced span length of 28 feet and 6 inches. The cracking pattern is shown in. Figure A-2. The P-Delta Curve shown in Figure 4-25 remained linearly elastic up to a load of 80 kips. The first flexural crack appeared at 80 kips directly under the load and through the stirrup located 8 feet from-the support. At 100 kips, two more flexural cracks appeared at locations 9 and 11 feet from the support associated with a tensile strain in the stirrup 8 feet from the support. Strain gages in stirrups located 4 feet and 6 feet from the support were not functioning. The tendon at RX1 exhibited a considerable slip at 125 kips corresponding to two sudden flexure cracks as shown in Figure A-2. Two large web-shear cracks between the load and support were observed at 145 kips and 150 kips. A load of 160 kips resulted in a catastrophic failure. The test was terminated at this collapse load. The failure mechanism of this beam was a total collapse due to the formation of web shear cracks.

4.3.2.2 Specimen UF2-30-LD. This specimen was tested with a full span of 35 feet. The cracking pattern of this beam can be observed in Figure A-4. The P-Delta Curve shown in Figure 4-28 remained linearly elastic until 60 kips. A flexural crack .

appeared at 70 kips directly under the load. This flexural crack did not result, in any increases in tendon slips or strains. There was no sudden change in behavior until a load of 110 kips. At 110 kips the stirrup located at 6 feet from the support indicated a sudden increase in strain at the tendon and section centroid. At 130 kips there was crushing observed under the load. Two flexure shear cracks appeared at this load. These cracks formed inside the shear span. The testing was terminated due: to excessive crushing and a reduction of the compression zone under the load at a collapse load 135 kips. This specimen failed as a result of excessive web shear cracking and crushing of the concrete under the load.

4.3.2.3 Specimen UFI-36-LD. This specimen was loaded with a reduced span of 28 feet. The cracking pattern is shown in Figure A-6. The first flexural crack appeared at 88 kips under the load and no slips were observed in the tendons. The reduction in stiffness of the P-Delta curve in Figure 4-31 did not occur until 115 kips. At l00 kips a flexural crack appeared at a location 6 feet from the support. This was accompanied by a large tensile strain in the stirrup. The crack intersected this stirrup at a load of 105 kips as shown in Figure A-6. At 118 kips there was an abrupt slip in the tendon R1C1. This corresponded to a flexural crack near the stirrup located 10 feet from the support. A sudden flexure crack appeared at 155 kips correlates to a sudden tendon slip as shown in Figure4-32. The specimen showed no other significant behavior patterns until the test was terminated due to formation of excessive flexural cracking and crushing under the load at a collapse load 165 kips. This beam experienced a flexural failure with the presence of flexural shear and crushing under the load.

4.3.2.4 Specimen UF2-36-LD. This specimen was tested with a full span of 35 feet. The cracking pattern is shown in Figure A-8. The P-Delta curve remained linear elastic until a load of 100 kips as shown in Figure 4-34. The stirrup 6 feet from the support abruptly developed high strains at 120 kips, just prior to the appearance of first flexural crack. As shown in Figure 4-35 tendon slips developed suddenly at 120 kips. The first flexure crack appeared at a load of 133 kips. The test was terminated at a collapse load 150 kips. This beam experienced a flexural failure with the presence of flexural shear.

4.3.2.5 Specimen UF1-42-LD. This specimen was loaded with a full span of 35 feet. The cracking pattern is shown in Figure A-10. The P-Delta curve, shown in Figure 4-37, remained linearly elastic until-80 kips. The first flexure crack also appeared at 90 kips at locations 6 and 8 feet from the support coinciding with stirrups. At 115 kips a new flexural crack appeared at a location 15 feet from the support. This appears to have an influence on the strain in the stirrup located 8 feet from the support. Sudden tendon slips took place as shown in Figure 4-38 at 134 kips which were load increments where large flexural cracks developed. There were also large horizontal cracks which developed at the tendon centroid at this point. Flexure cracks continued to grow with some crushing under the load point occurring at 150 kips. The test was terminated at a collapse load of 165 kips. This beam failed almost entirely in compression accompanied with excessive crushing under the load.

4.3.2.6 Specimen UF2-42-LD. This beam was loaded with a span of 26 feet and 8 inches with the first flexural crack appearing at 90 kips at which point the P-Delta curve in Figure 4-40 begins to loose stiffness. Sudden tendon slips in Figure 4-41

kips and 150 kips which correspond to initial cracking and the formation of flexural and flexural shear cracks. The cracking pattern can be seen in Figure A-12. At 105 kips the strain in the stirrup 6 feet from the support, as shown in Figure 4-42, exhibited a rapid increase which continued until failure of the specimen. This was the result of a crack at the stirrup located 6 feet from the support. At 145 kips a sudden large flexure crack developed accompanied by a sudden slip as shown in Figure 4-41. Also shown in Figure A-12 is a horizontal crack at 145 kips resulting in bond slip at this load. Only one flexure crack bent over at 10 feet from the support and it was formed at a load of 135 kips. At 157 kips two sudden flexure cracks occurred between the stirrups located 8 and 10 feet from the support with one not extending to the bottom of the beam. The test was terminated at a collapse load 157 kips. This beam failed due to the formation of large flexural cracks which led to the development of excessive flexural shear cracks.

4.3.2.7 Specimen UF1-48-LD. This beam was loaded with a span of 26 feet and 6 inches and formed its first flexural crack at 110 kips which corresponds to initial reduction in stiffness of the 'P-Delta curve in Figure 4-43. The first, flexure crack was associated with no sudden slips in the tendons. Flexure cracks continued to grow and-at a load of 140 kips one bent over slightly as shown in Figure A-14. At 134 kips one tendon slipped considerably as shown in Figure 4-44. This was a reflection of the horizontal crack at the tendon centroid and flexure crack. At 174 kips the flexure crack 10 feet from the support became very wide. The test was terminated at a collapse load 174 kips. The specimen failed in flexure with flexure shear cracks and loss of bond.

4.3.2.8 Specimen UF2-48-LD. This beam was loaded with a full span of 35 feet and formed its initial flexural crack at 92 kips which corresponds to a slight kink in the

P-Delta curve shown in Figure 4-46. The cracking pattern can be seen in Figure A-16. Two tendons exhibited slips at this load. The largest of these occurring to the tendons located at the bottom row. At 140 kips a large flexure shear crack appeared between the load and support extending up to near the load. The compression zone was small at this load. There were also several horizontal cracks those developed along the tendon centroid at this load. The test was terminated at a collapse load 140 kips. This beam developed some shear forces but appeared to fail by the formation of a hinge under the load and the beam rotating about this point.

4.4 Transfer Length Results

The plot of the longitudinal strain on the concrete surface along the tendon centroid at transfer for the 30 inch beams are shown in Figures 4-49 and 4-50 and the 36-inch beams are shown in Figures 4-51 and 4-52. The strains due to the dead weight of the beam have been subtracted from the field data. Thus, the following graphs represent the strains due to the initial prestress, P_i, only. The data for the 42- and 48-inch beams are unavailable due to problems with the data acquisition equipment during the transfer operation.

An determining the transfer length, measured strains were plotted versus distance from the end of the beam. A regression analysis was then performed to determine an equation that best represented the data. This equation was then used to plot a curve through the data points.

The transfer length is assumed to be the distance from the end of the beam to the point onward which the tendons had constant strain. Generally, the strain values increased

linearly from zero at the end of the beam up to a point where they became, approximately constant. It is assumed that at this point the full prestress force is transferred to the concrete. It can be seen from Figures 4-49 through 4-52 that the lines of "constant strain" exhibit some random fluctuations between data points. This is partially, due to experimental error that is inherent in this type of field test.

A summary of all of the transfer length test results and a comparison of transfer length results according to ACI equations, the equation proposed by Zia and Mostafa (Ref. 4) and the equations proposed by Shahawy (Ref 5) are presented in Table 4-1. These equations are presented in Chapter 2.1.3.

Table 4-1. Transfer Length Results

BEAM	ACI l_t	Zia & Mostafa l_t	Shahawy l_t	TEST l_t
UF1-30	18.05	11.3	22.6	24
UF2-30	18.05	17.0	22.6	30
UF1-36	18.85	18.0	23.6	24
UF2-36	18.85	16.8	23.6	24

The transfer lengths determined from Figures 4-49 through 4-52 are higher than the predicted value according to ACI. Based on these observations it appears that Shahawy's suggestion of using f_{si} instead of f_{se}. in the ACI/AASHTO equation is a reasonable approach for estimating the transfer length in prestressed concrete beams.

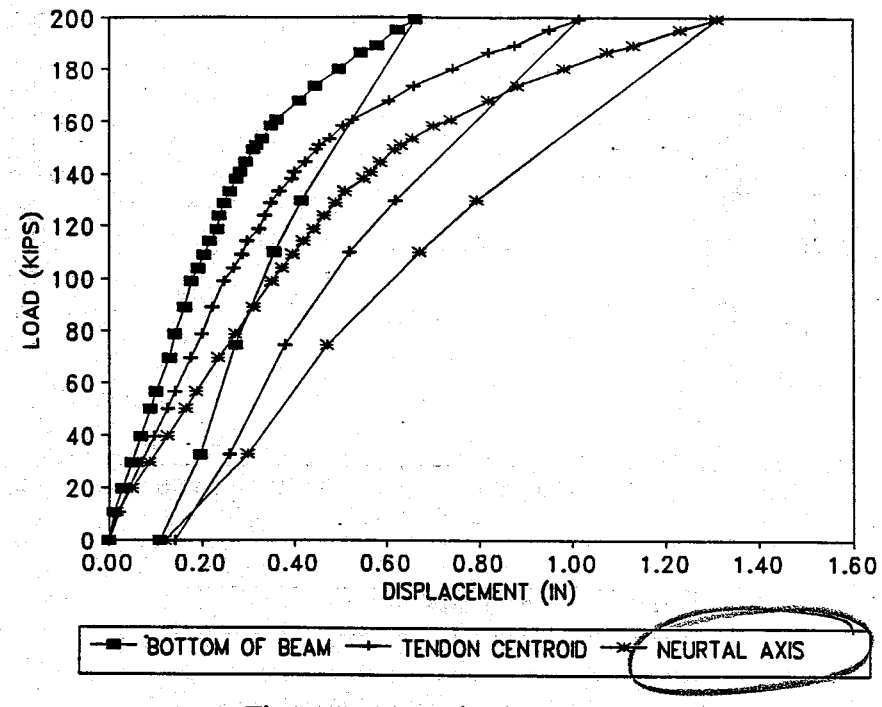

Figure 4-1 P-Delta (UF1-30-2D)

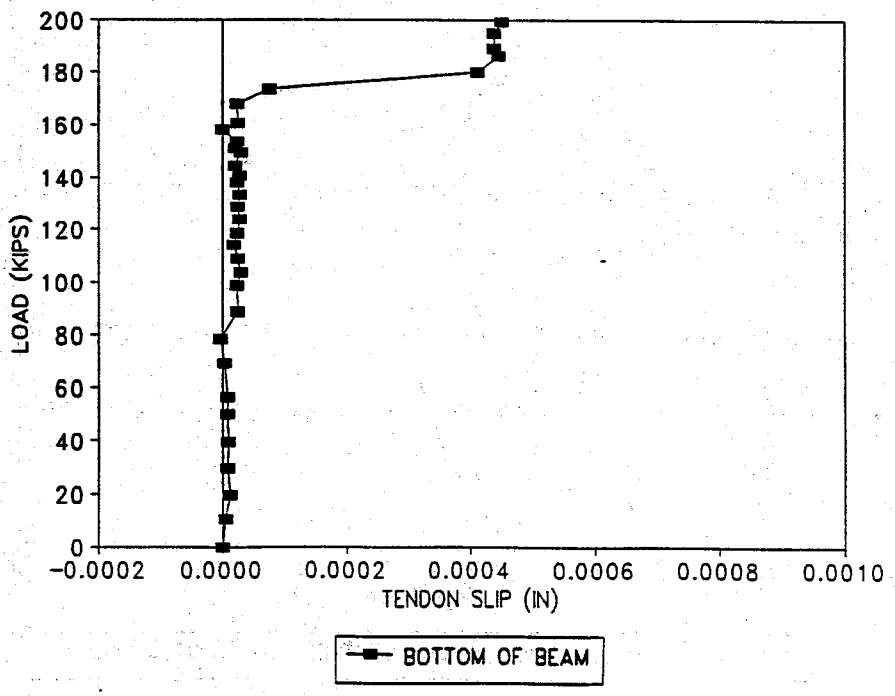

Figure 4-2 Tendon Slip (UF1-30-2D)

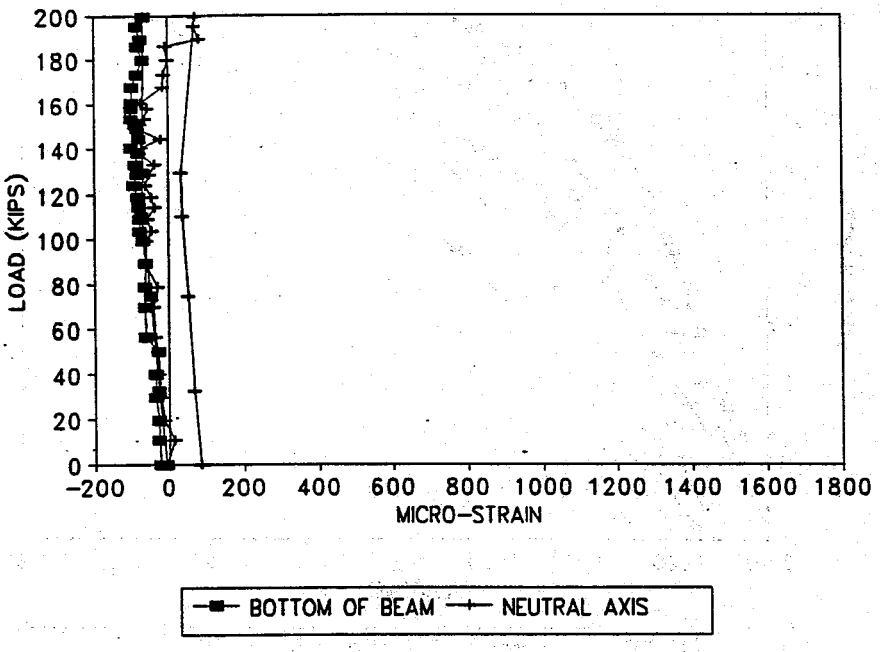

Figure 4-3 Stirrup Strain (UF1-30-2D)

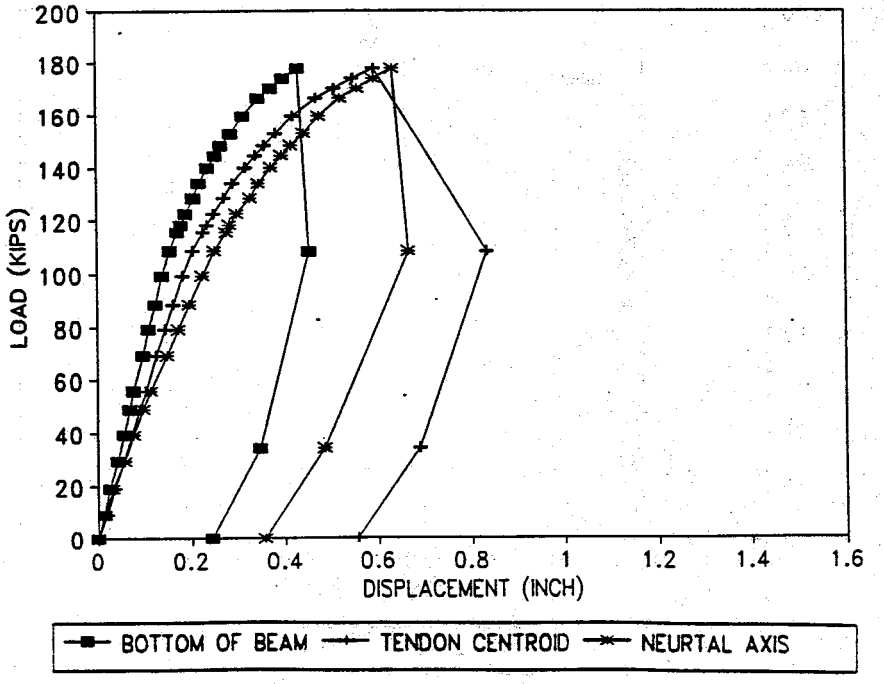

Figure 4-4 P-Delta (UF2-30-2D)

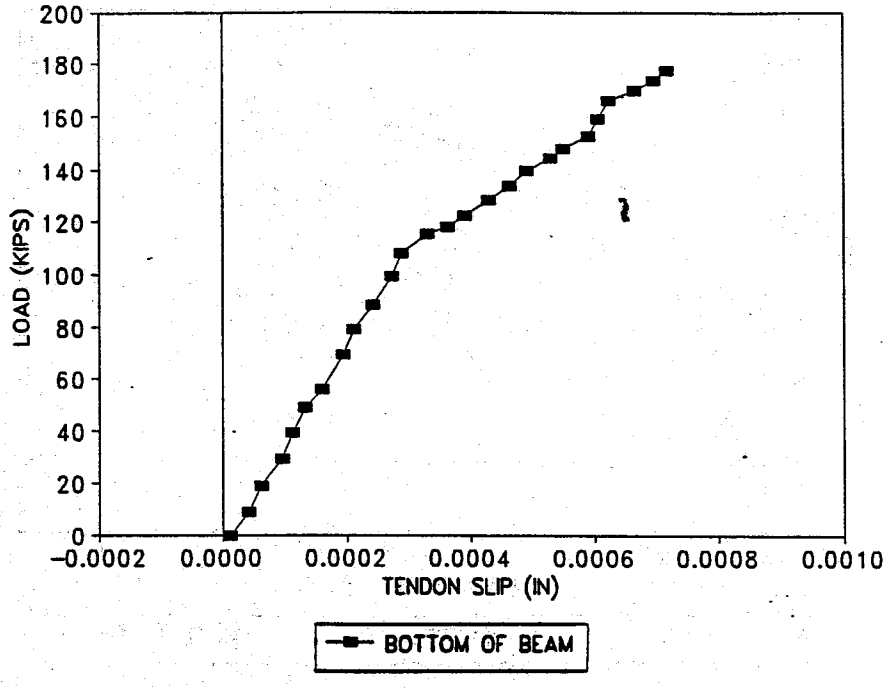

Figure 4-5 Tendon Slip (UF2-30-2D)

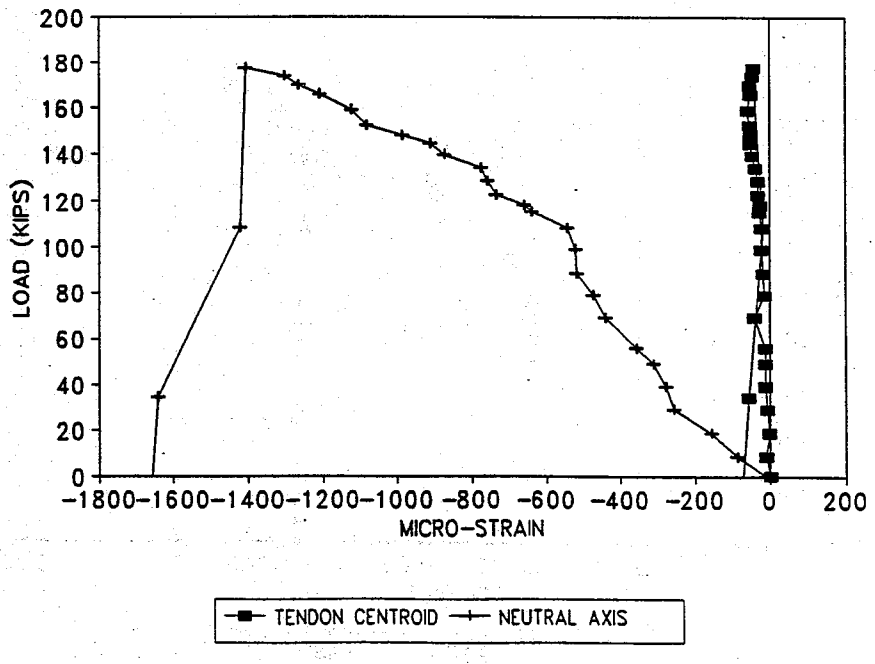

Figure 4-6 Stirrup Strain (UF2-30-2D)

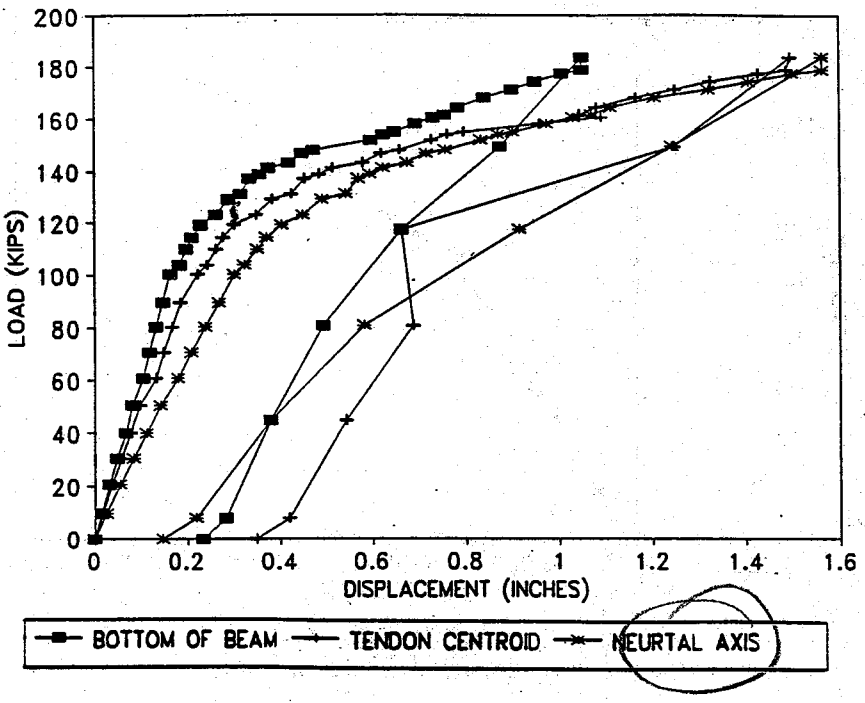

Figure 4-7 P-Delta (UF1-36-2D)

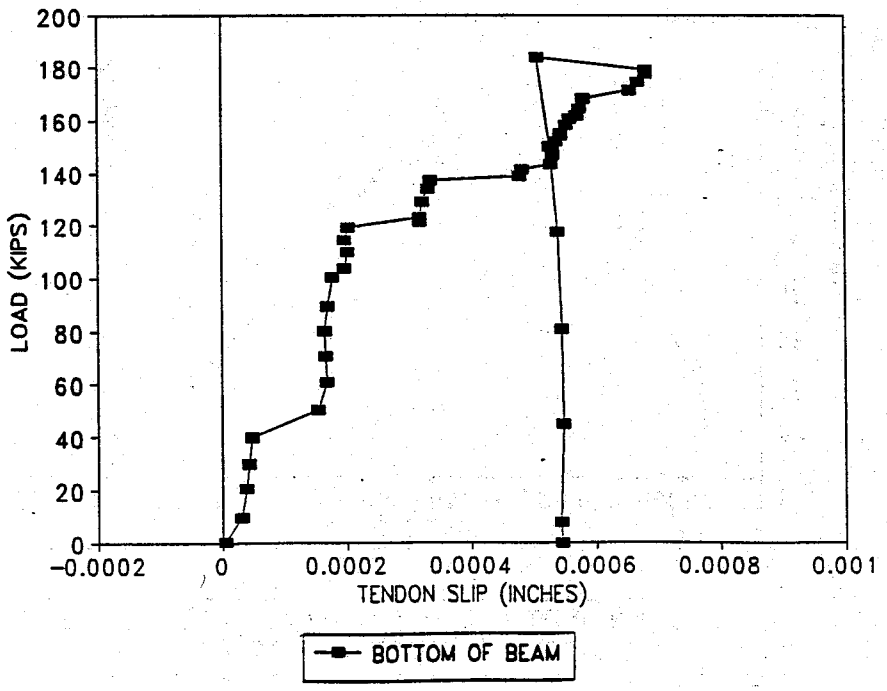

Figure 4-8 Tendon Slip (UF1-36-2D)

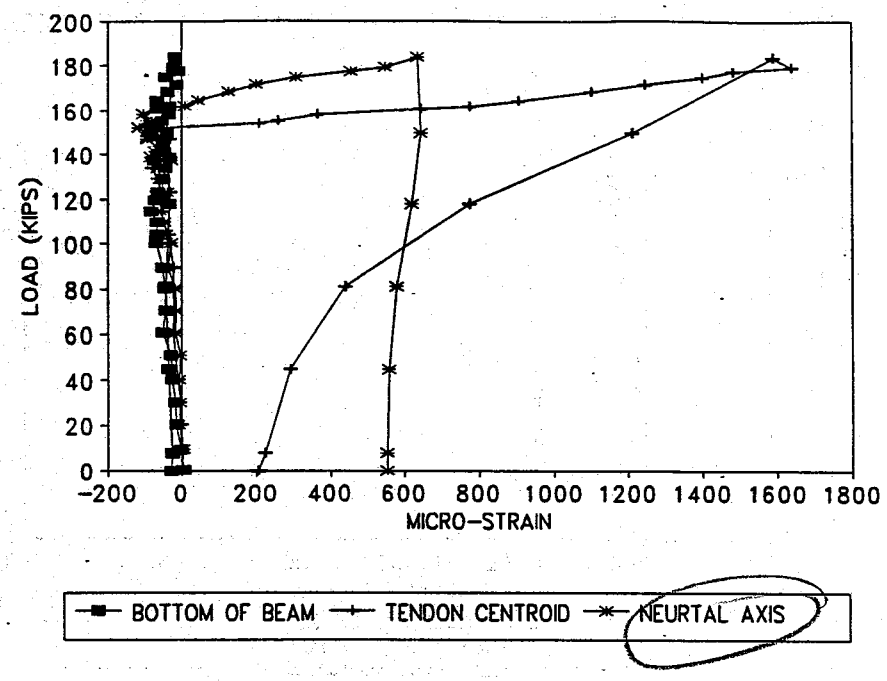

Figure 4-9 Stirrup Strain (UF1-36-2D)

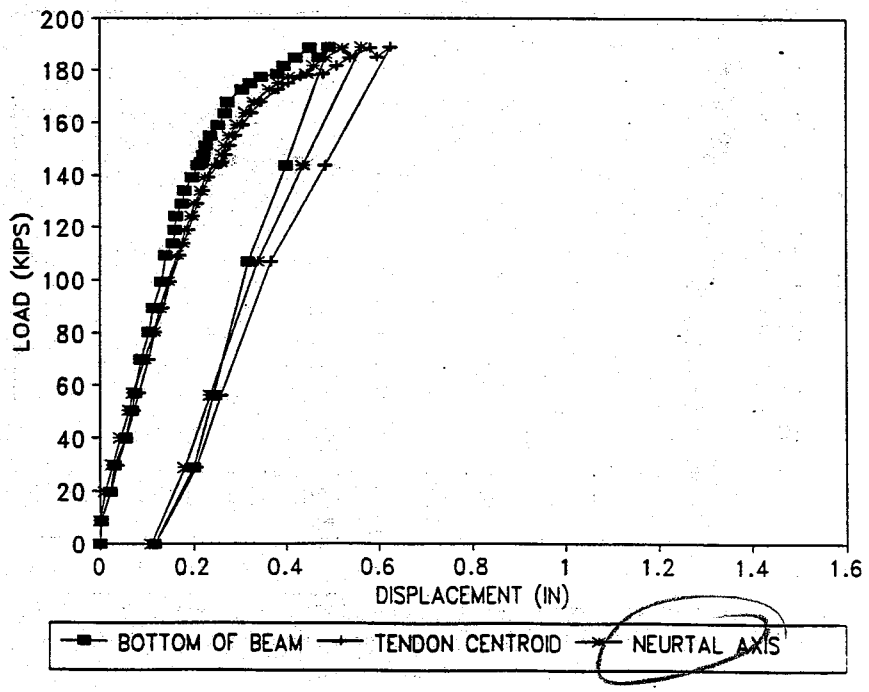

Figure 4-10 P-Delta (UF2-36-2D)

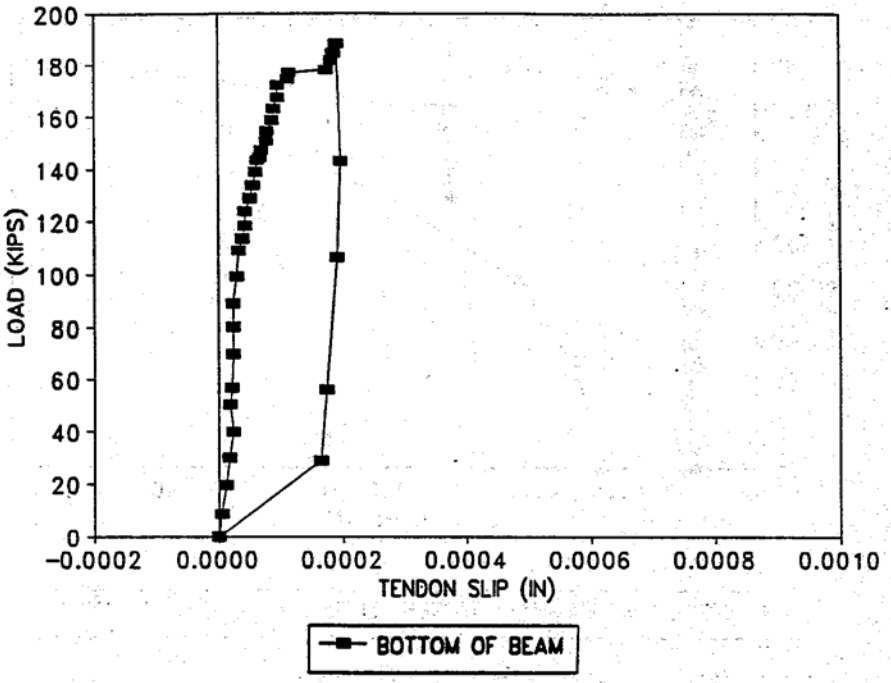

Figure 4-11 Tendon Slip (UF2-36-2D)

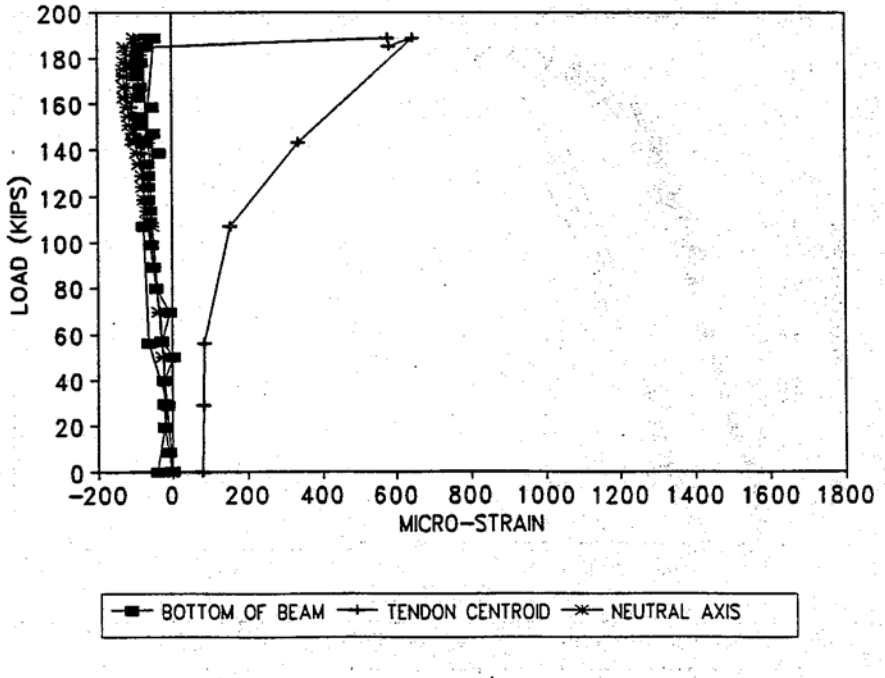

Figure 4-12 Stirrup Strain (UF2-36-2D)

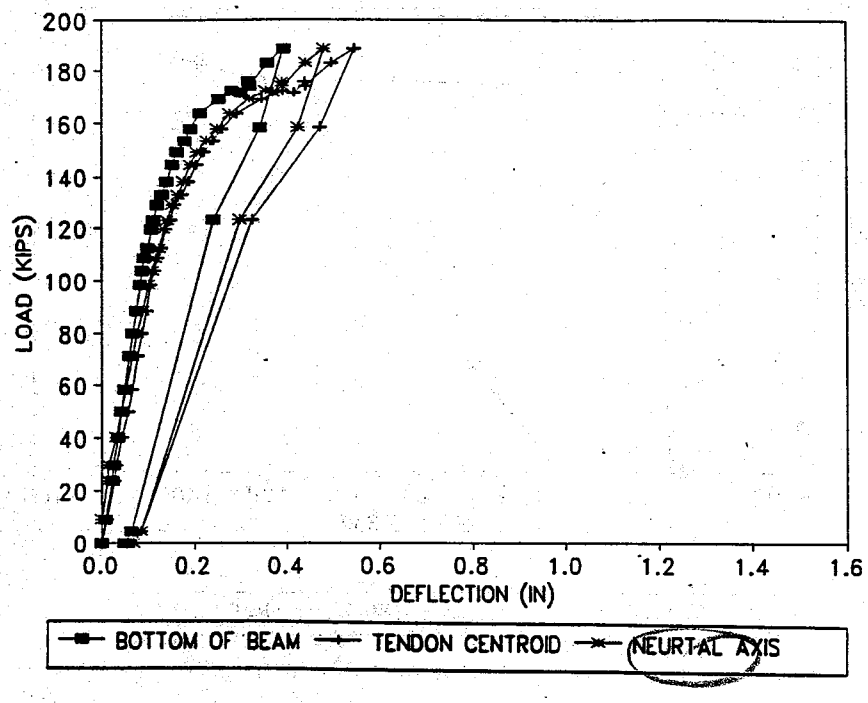

Figure 4-13 P-Delta (UF1-42-2D)

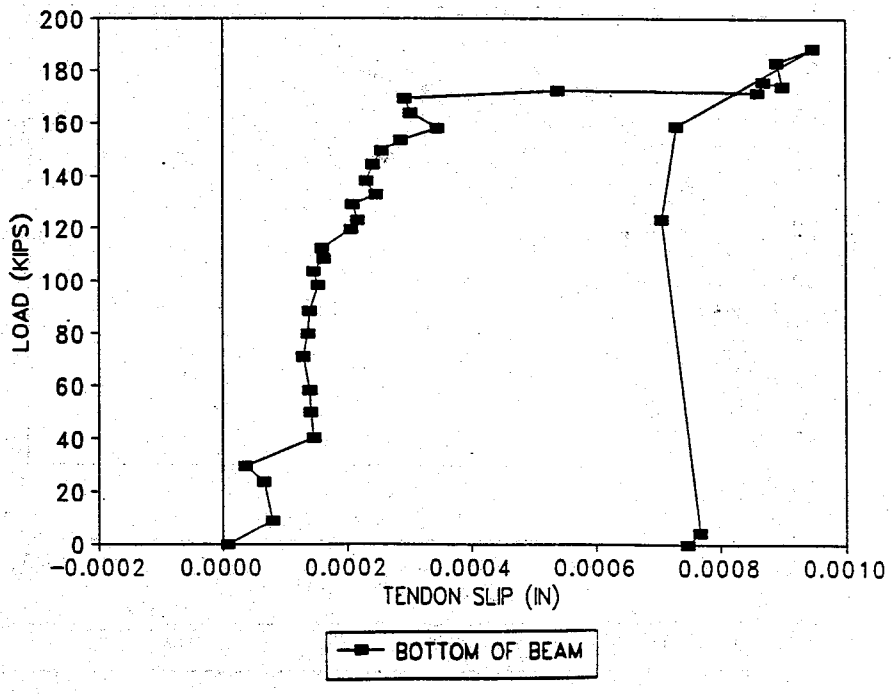

Figure 4-14 Tendon Slip (UF1-42-2D)

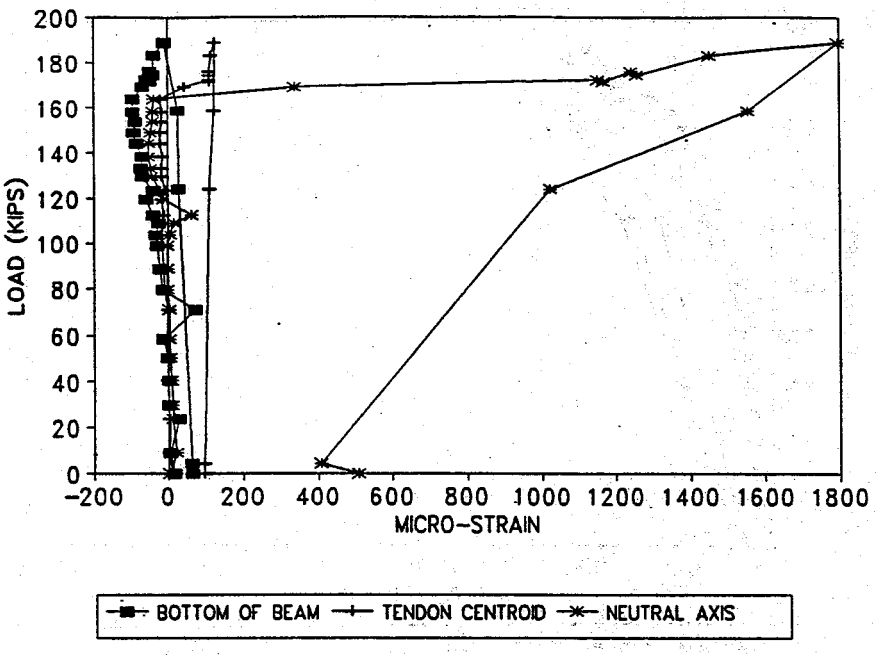

Figure 4-15 Stirrup Strain (UF1-42-2D)

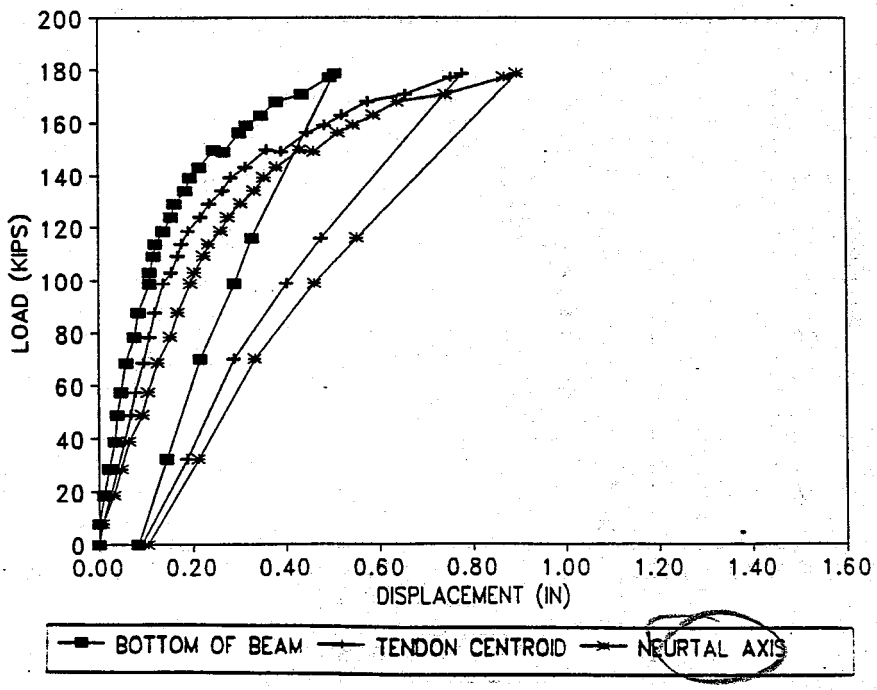

Figure 4-16 P-Delta (UF2-42-2D)

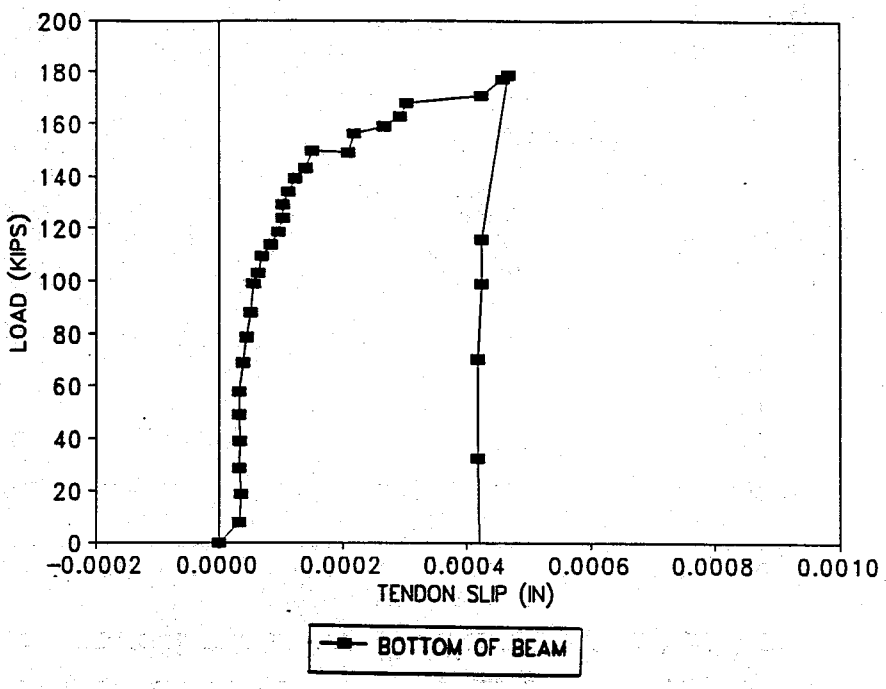

Figure 4-17 Tendon Slip (UF2-42-2D)

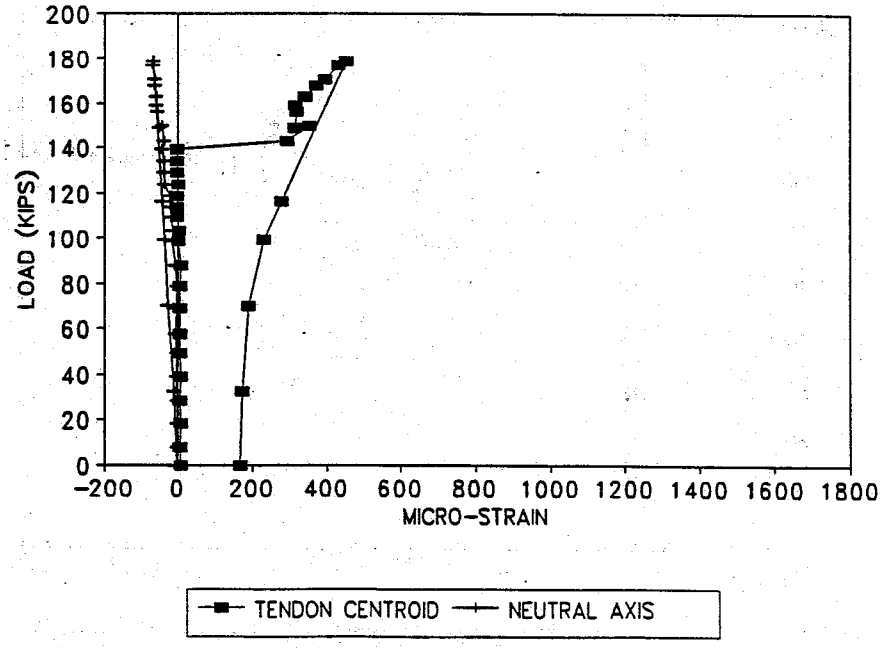

Figure 4-18 Stirrup Strain (UF2-42-2D)

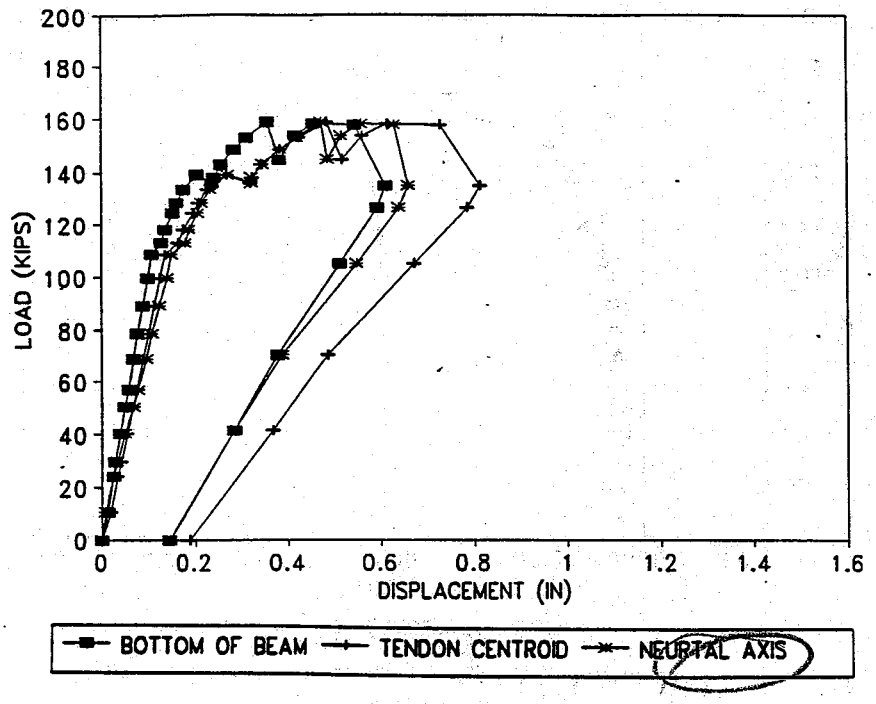

Figure 4-19 P-Delta (UF1-48-2D)

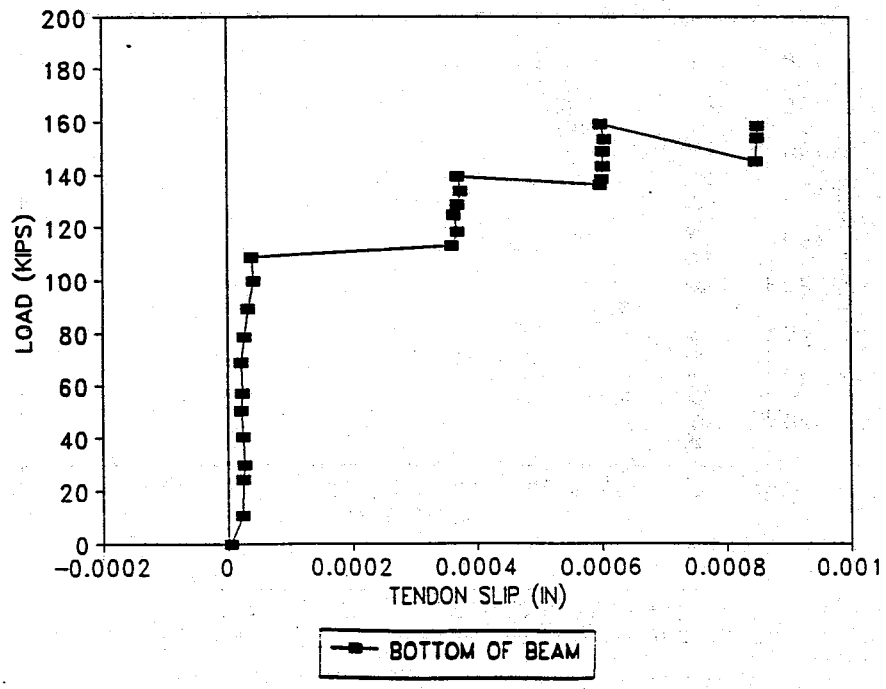

Figure 4-20 Tendon Slip (UF1-48-2D)

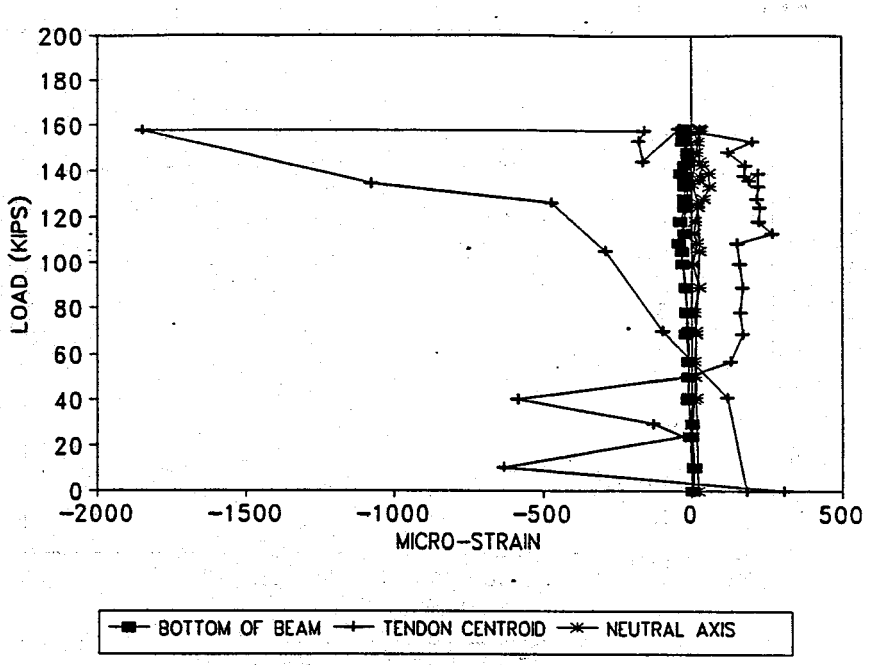

Figure 4-21 Stirrup Strain (UF1-48-2D)

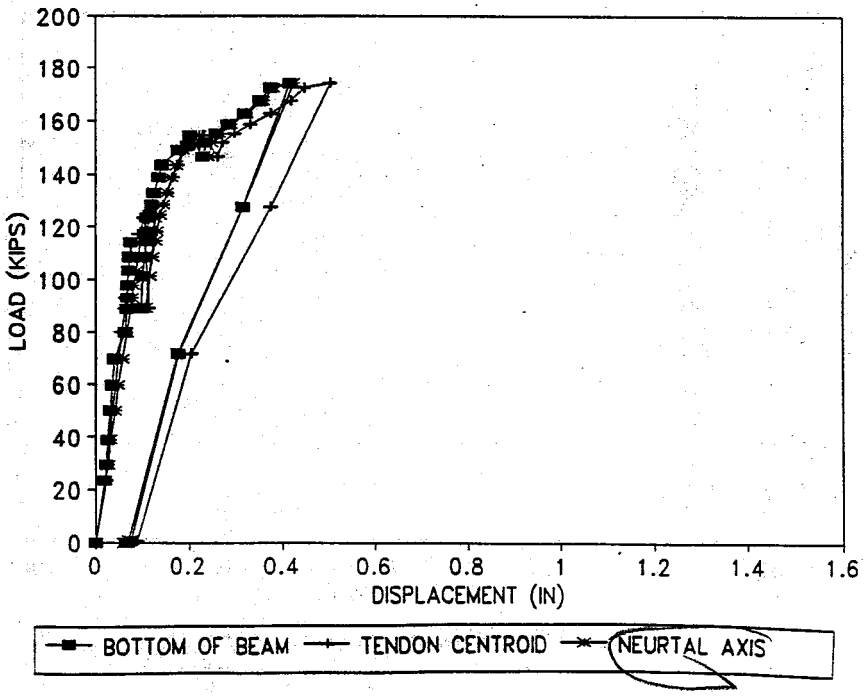

Figure 4-22 P-Delta (UF2-48-2D)

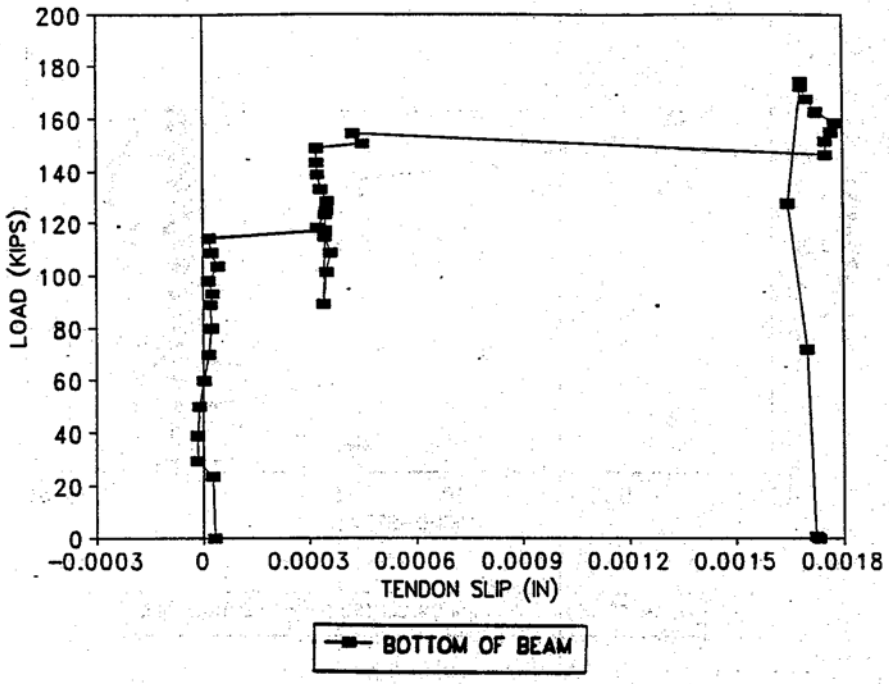

Figure 4-23 Tendon Slip (UF2-48-2D)

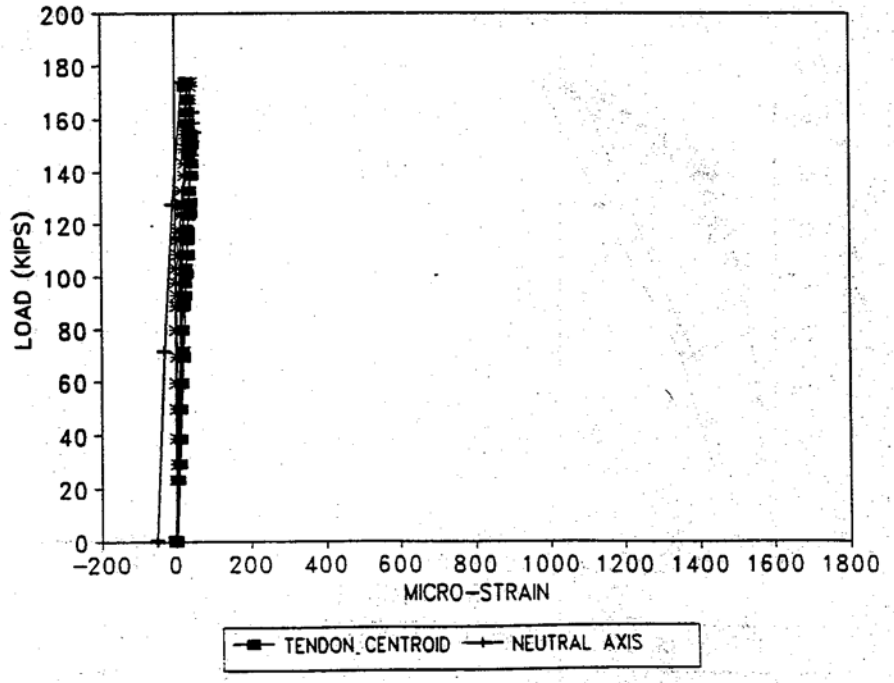

Figure 4-24 Stirrup Strain (UF2-48-2D)

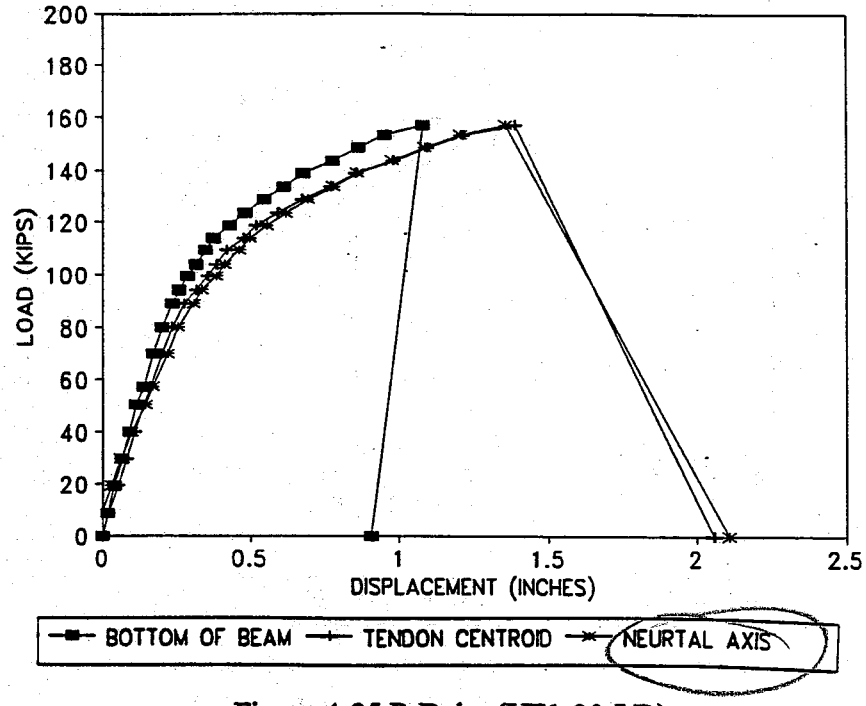

Figure 4-25 P-Delta (UF1-30-LD)

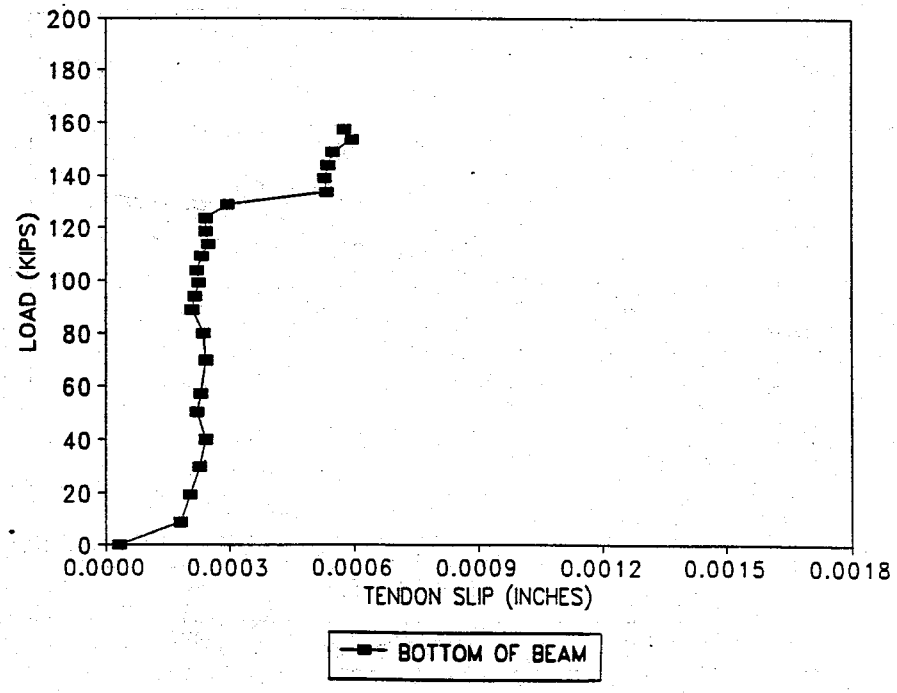

Figure 4-26 Tendon Slip (UF1-30-LD)

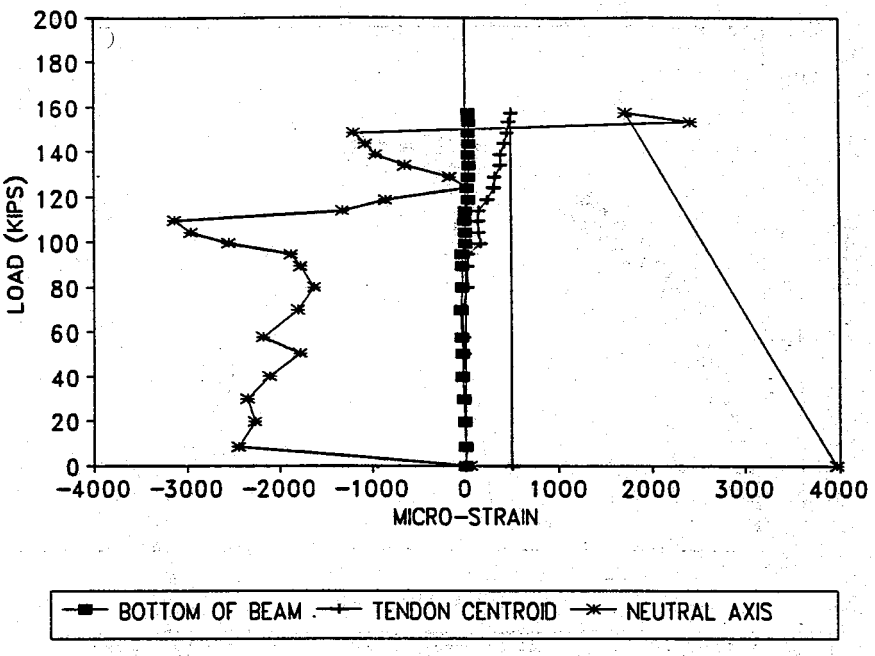

Figure 4-27 Stirrup Strain (UF1-30-LD)

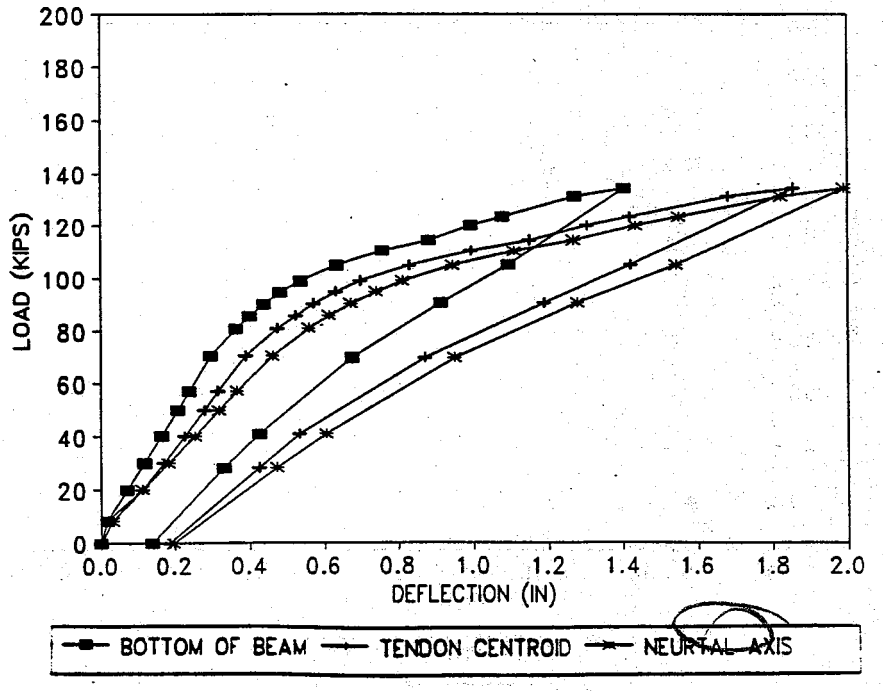

Figure 4-28 P-Delta (UF2-30-LD)

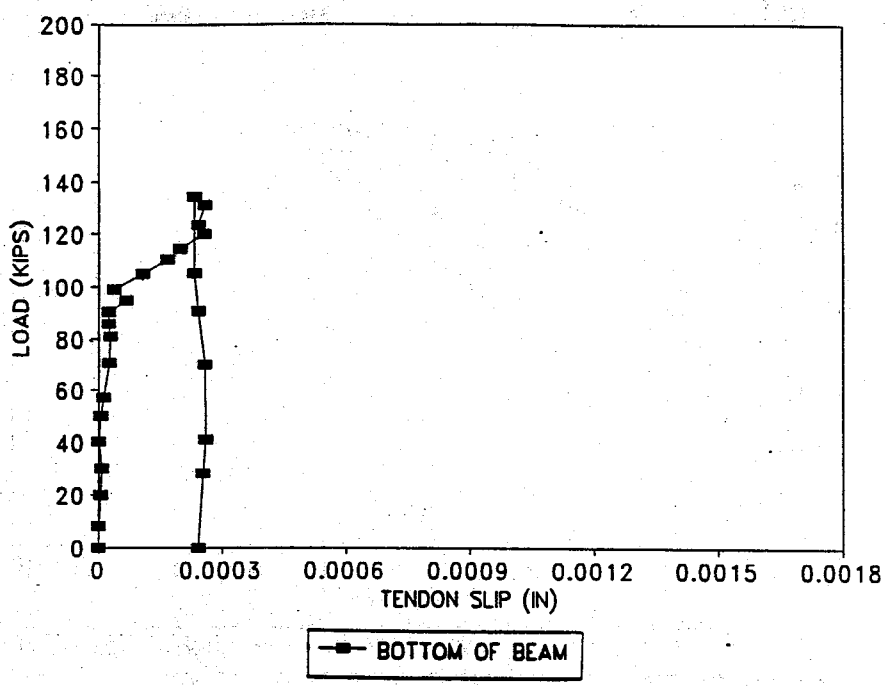

Figure 4-29 Tendon Slip (UF2-30-LD)

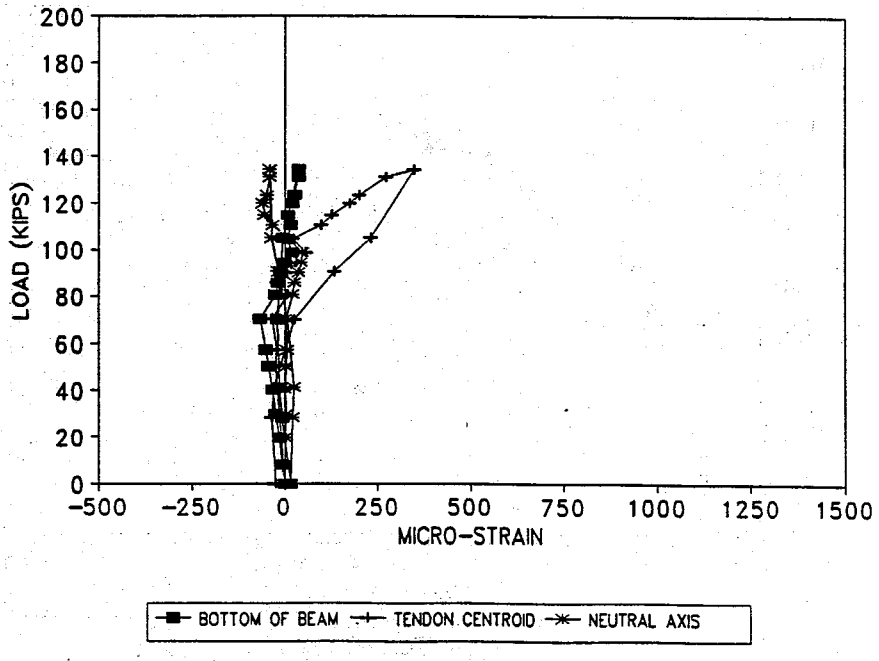

Figure 4-30 Stirrup Strain (UF2-30-LD)

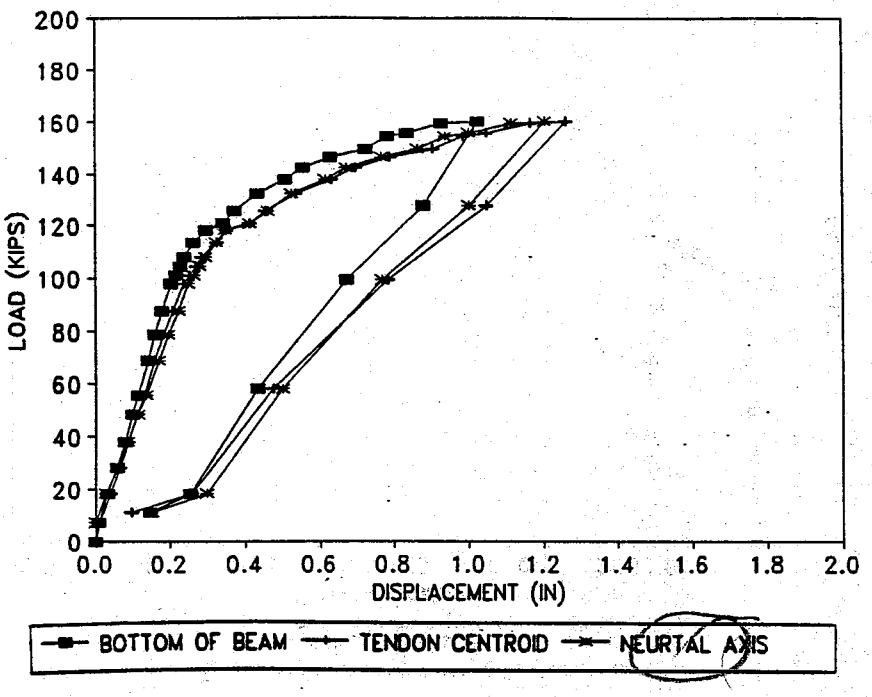

Figure 4-31 P-Delta (UF1-36-LD)

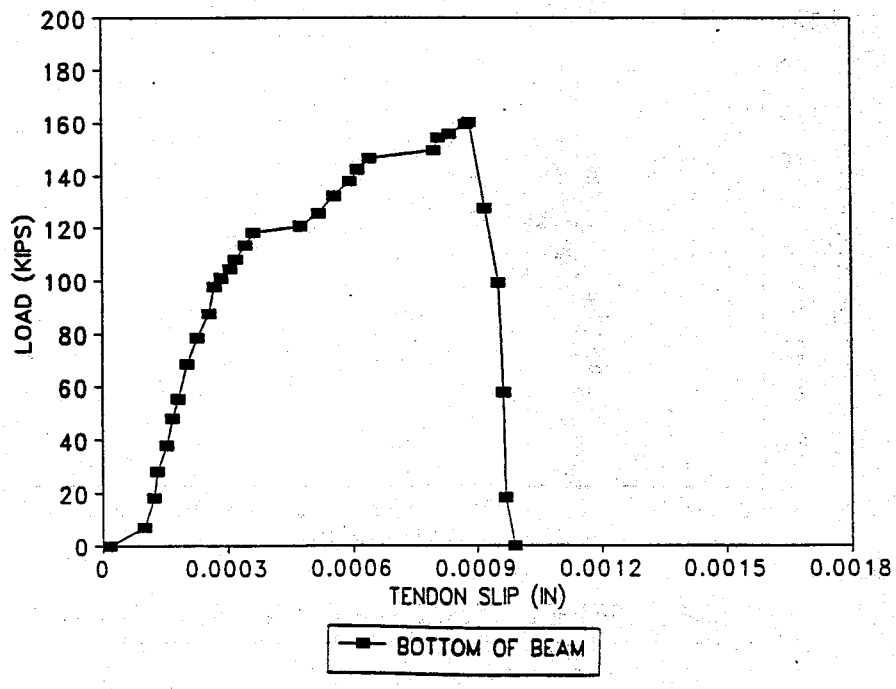

Figure 4-32 Tendon Slip (UF1-36-LD)

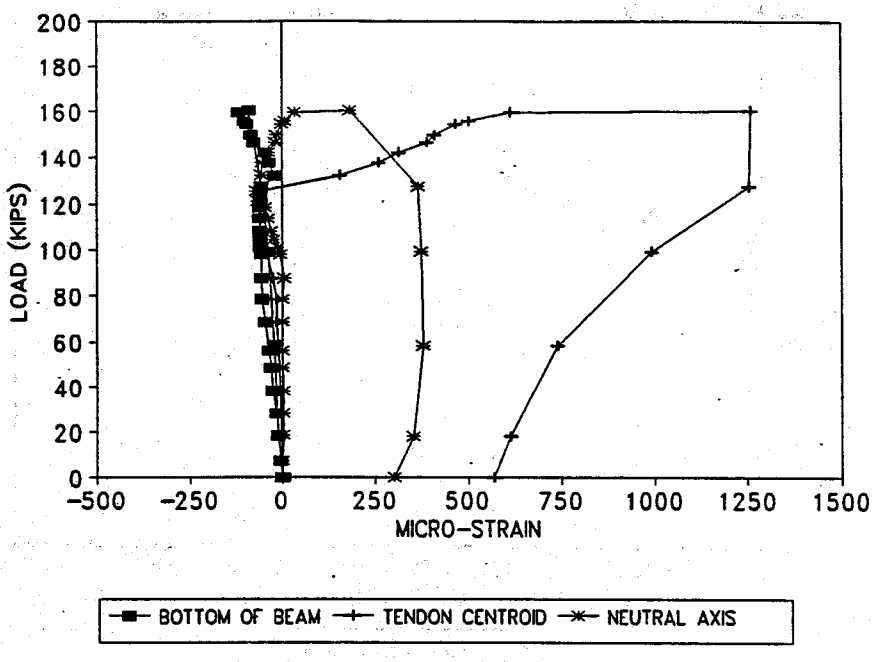

Figure 4-33 Stirrup Strain (UF1-36-LD)

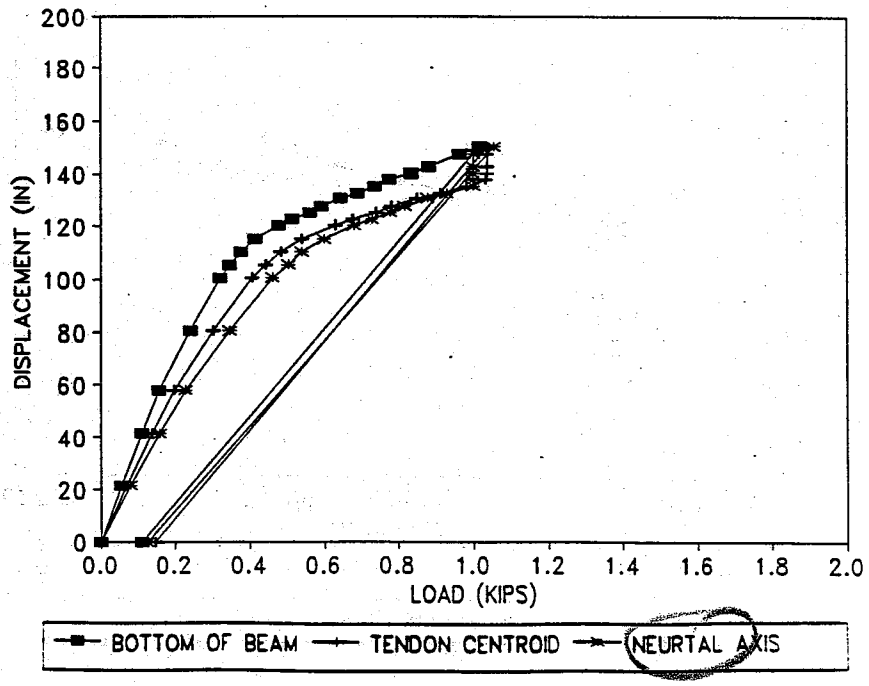

Figure 4-34 P-Delta (UF2-36-LD)

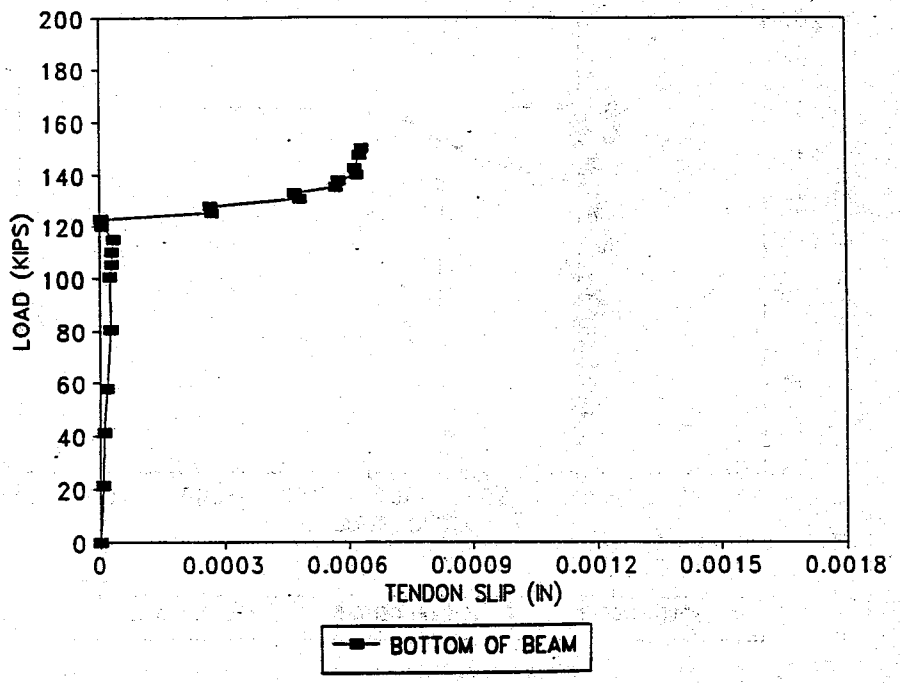

Figure 4-35 Tendon Slip (UF2-36-LD)

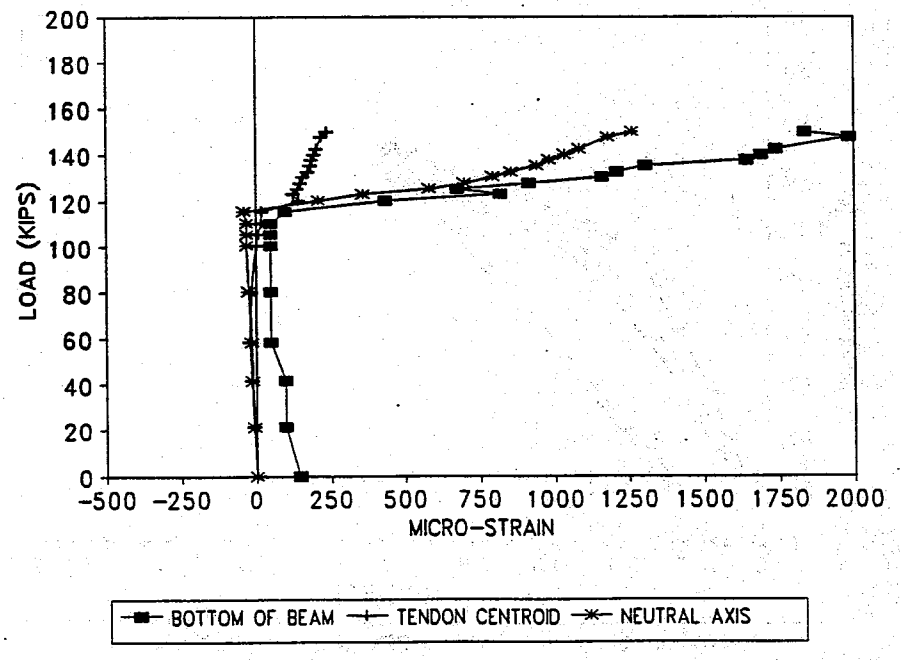

Figure 4-36 Stirrup Strain (UF2-36-LD)

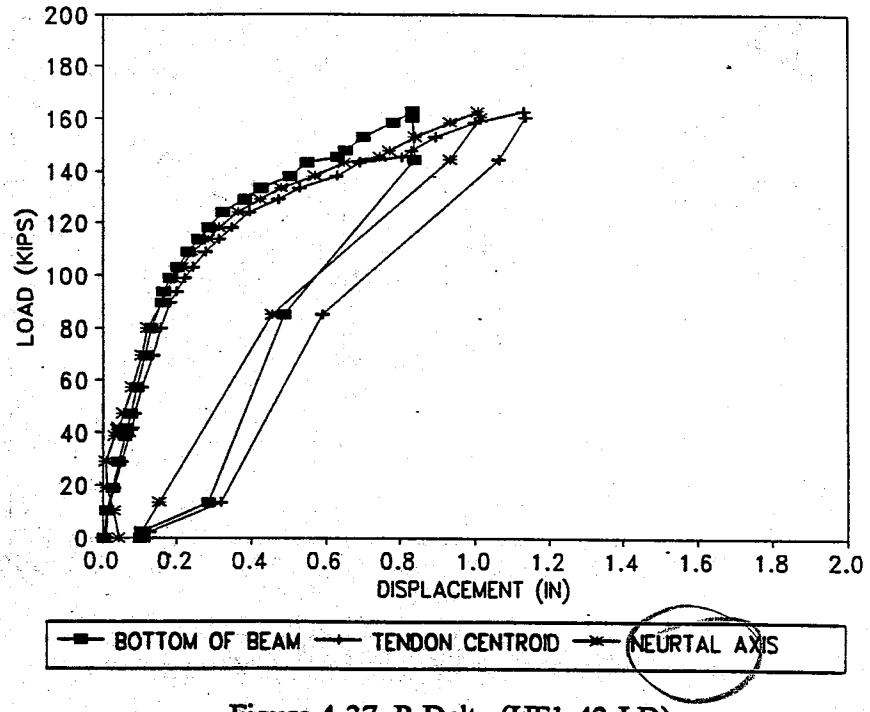

Figure 4-37 P-Delta (UF1-42-LD)

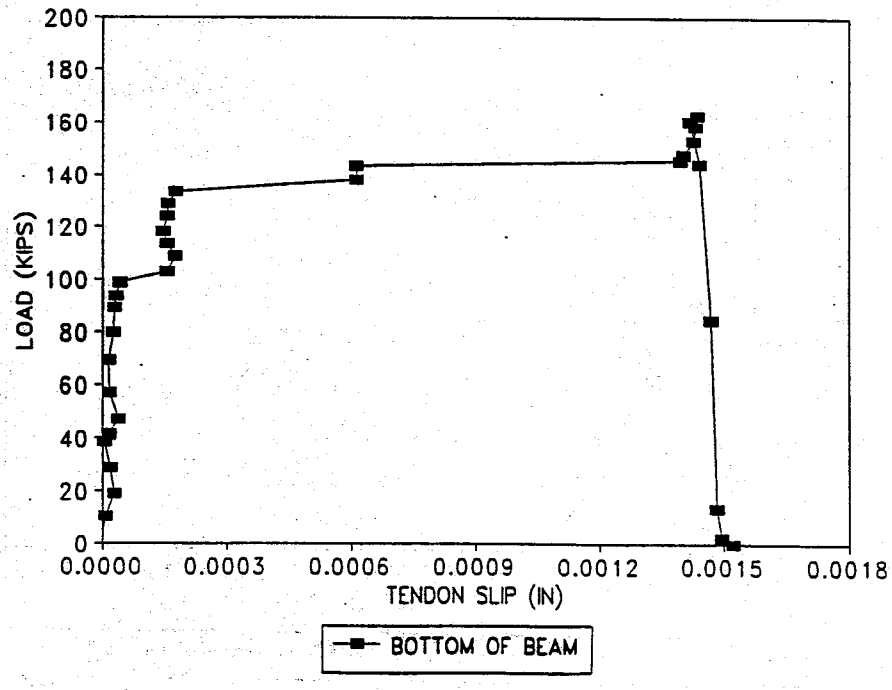

Figure 4-38 Tendon Slip (UF1-42-LD)

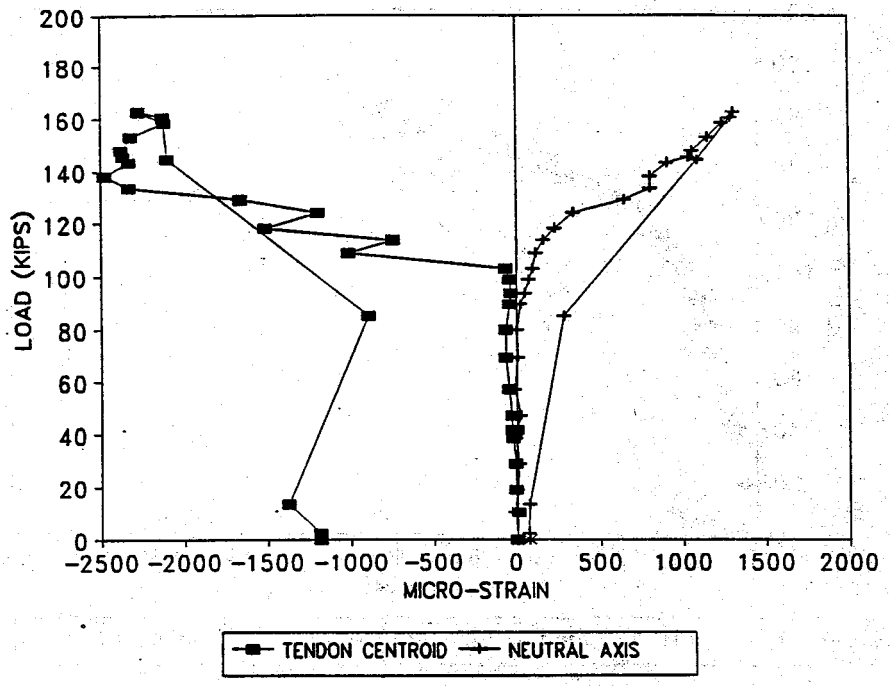

Figure 4-39 Stirrup Strain (UF1-42-LD)

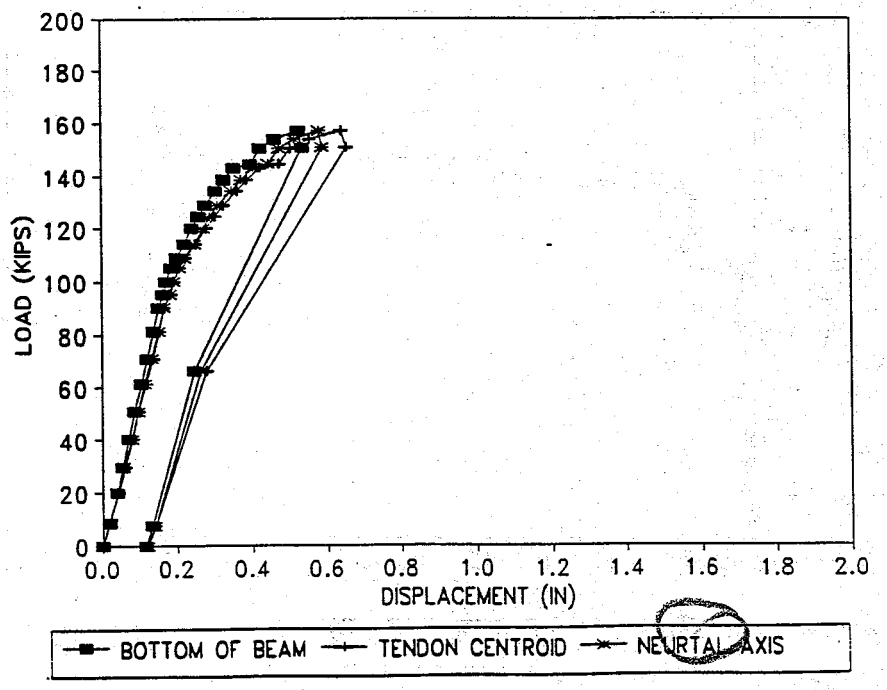

Figure 4-40 P-Delta (UF2-42-LD)

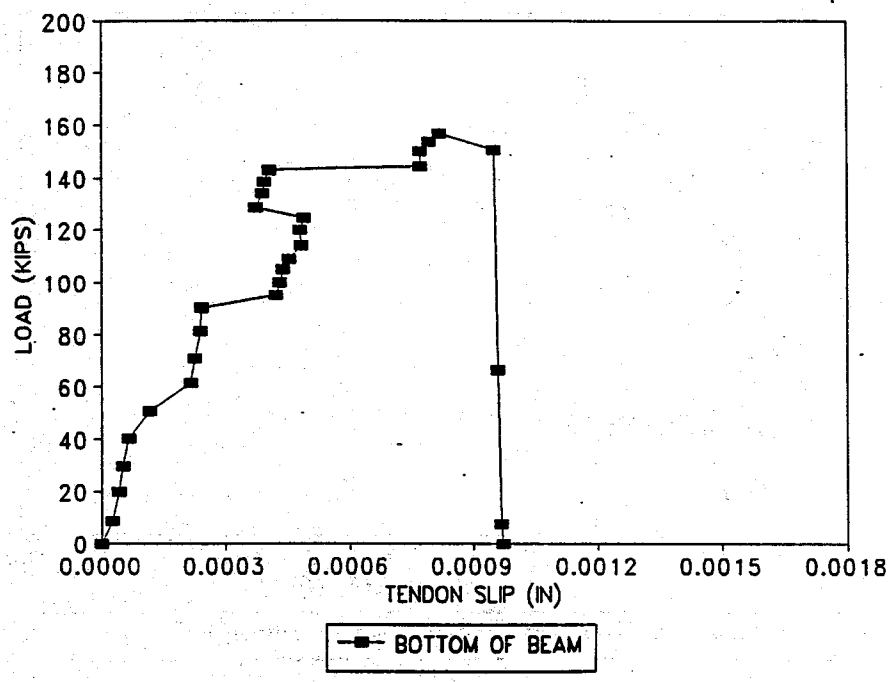

Figure 4-41 Tendon Slip (UF2-42-LD)

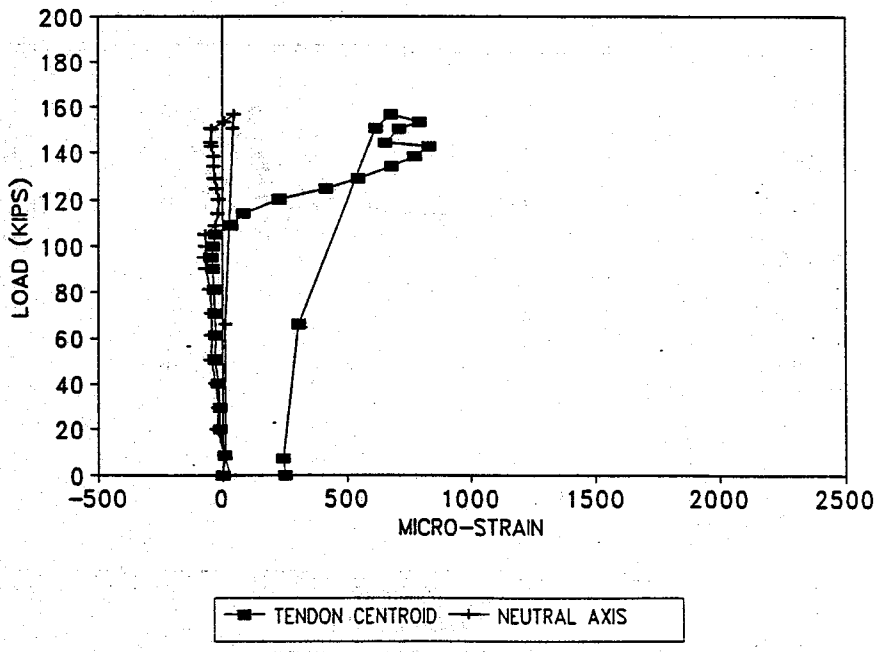

Figure 4-42 Stirrup Strain (UF2-42-LD)

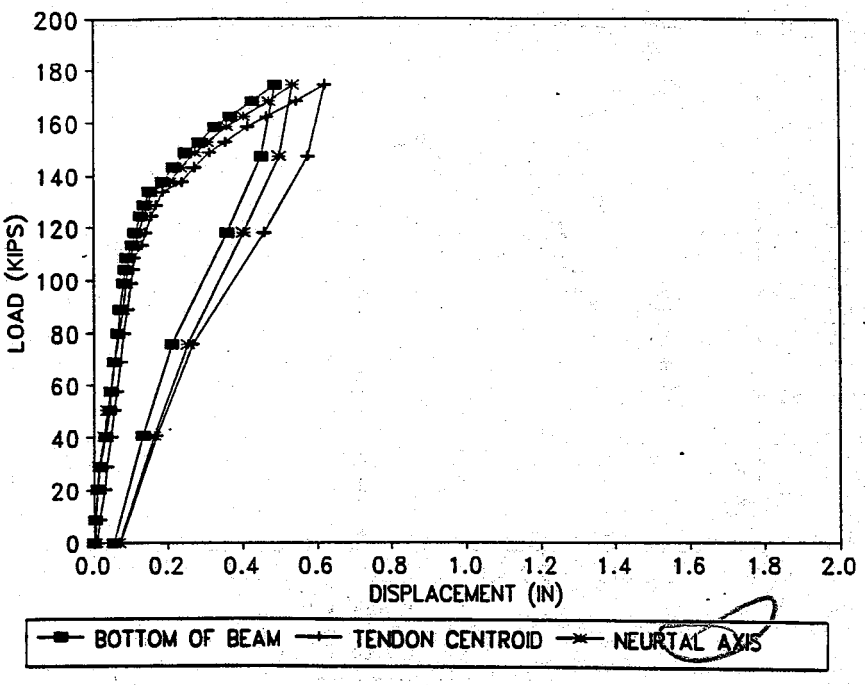

Figure 4-43 P-Delta (UF1-48-LD)

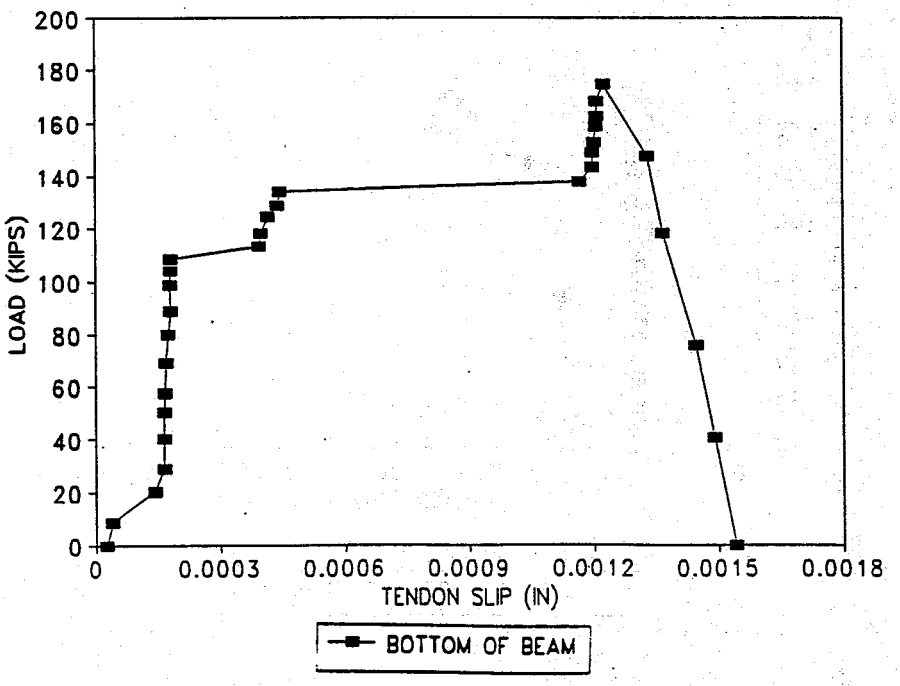

Figure 4-44 Tendon Slip (UF1-48-LD)

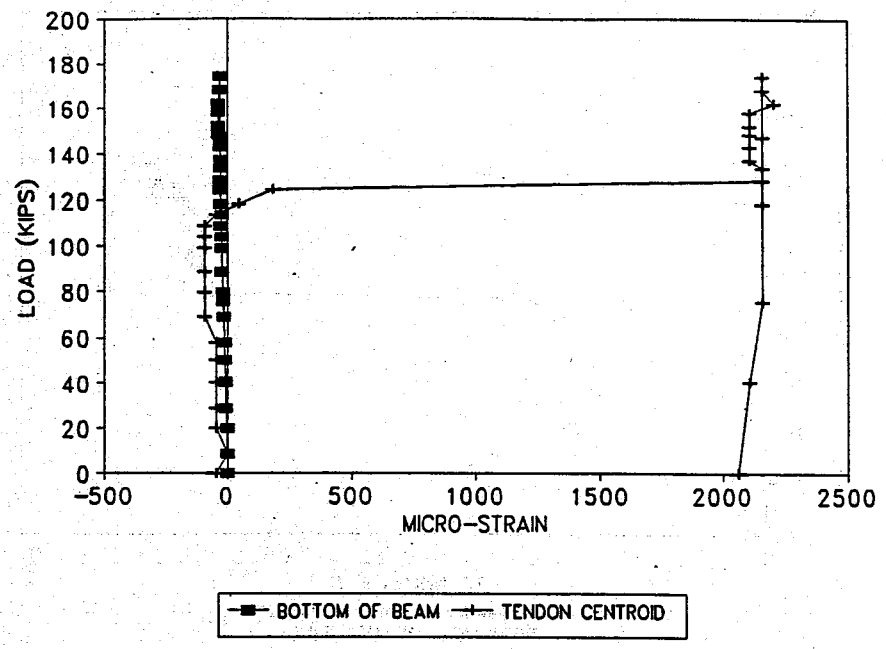

Figure 4-45 Stirrup Strain (UF1-48-LD)

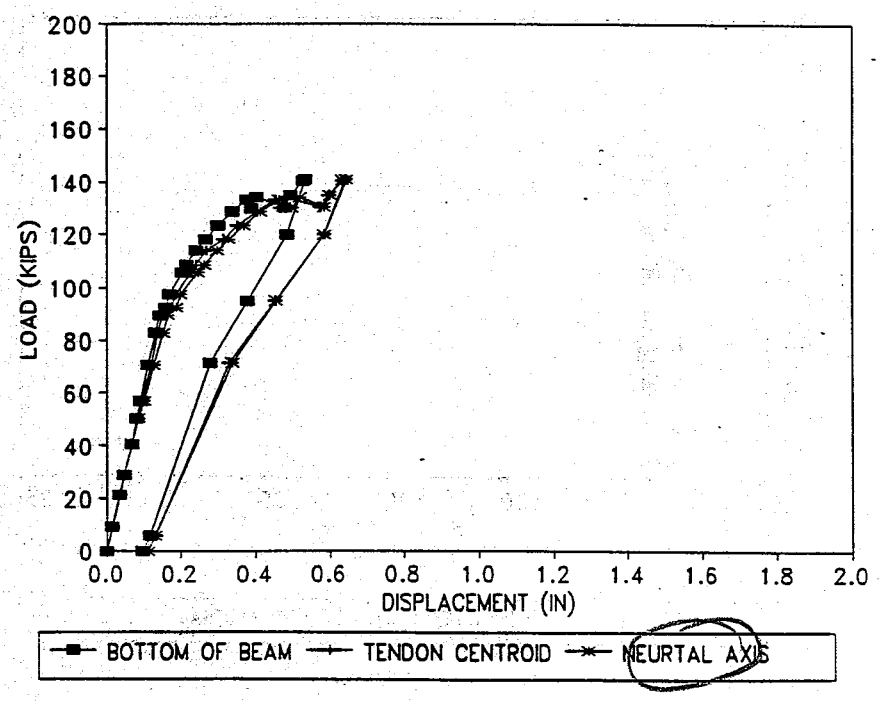

Figure 4-46 P-Delta (UF2-48-LD)

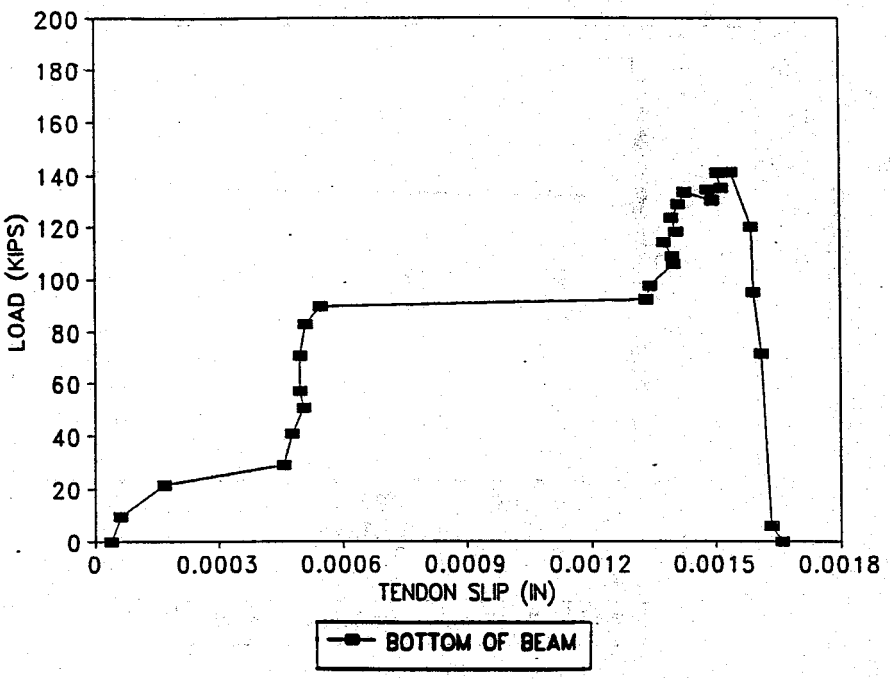

Figure 4-47 Tendon Slip (UF2-48-LD)

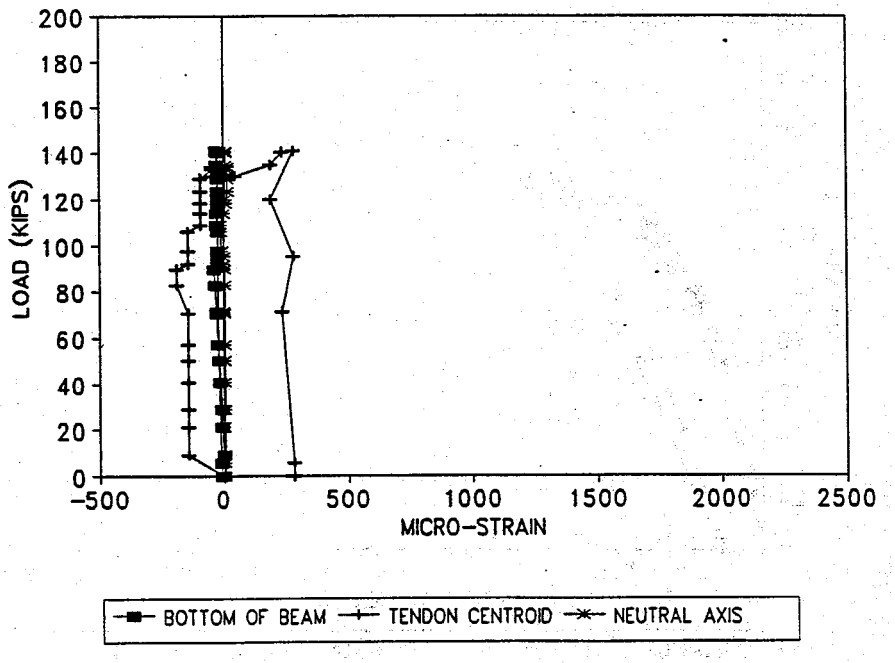

Figure 4-48 Stirrup Strain (UF2-48-LD)

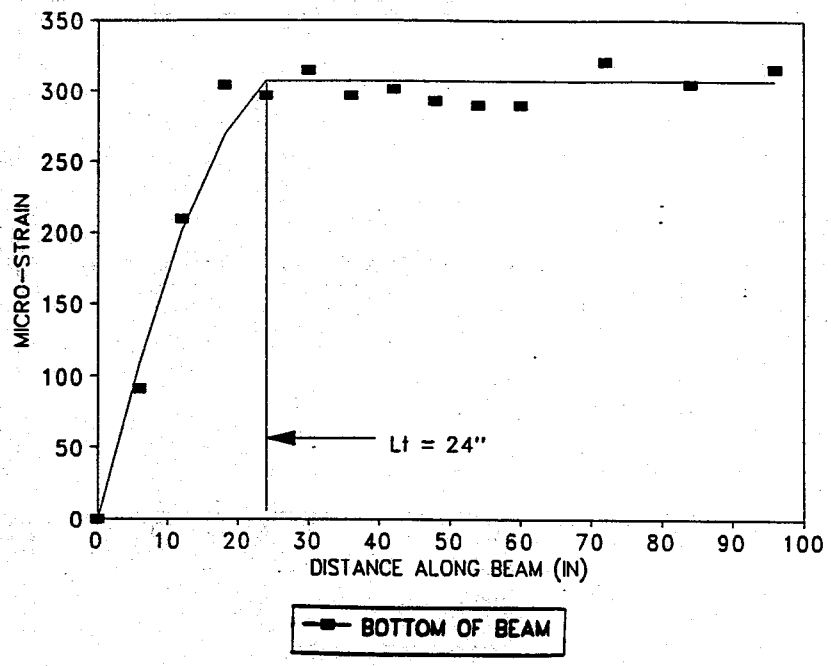

Figure 4-49 Transfer Length for UF1-30

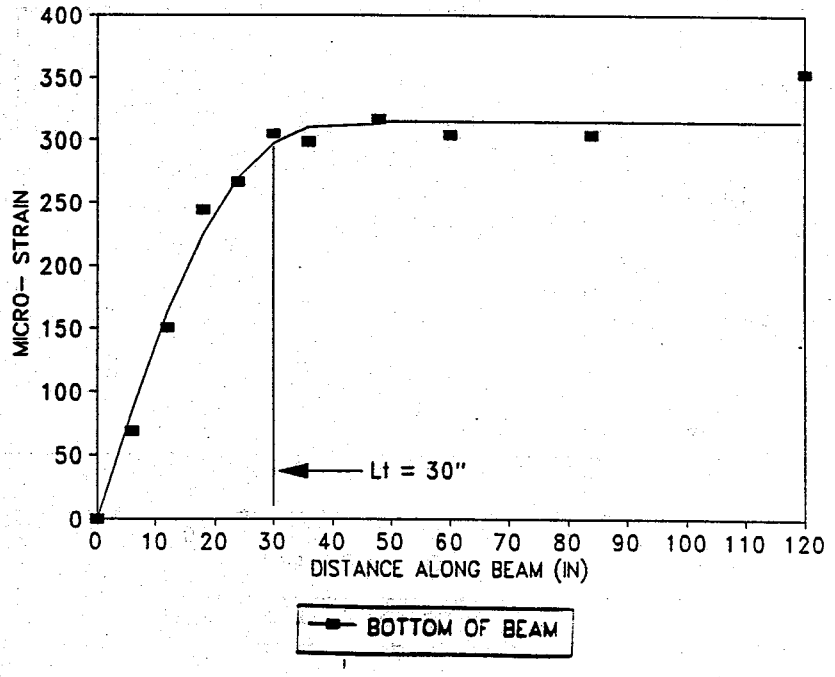

Figure 4-50 Transfer Length for UF1-30

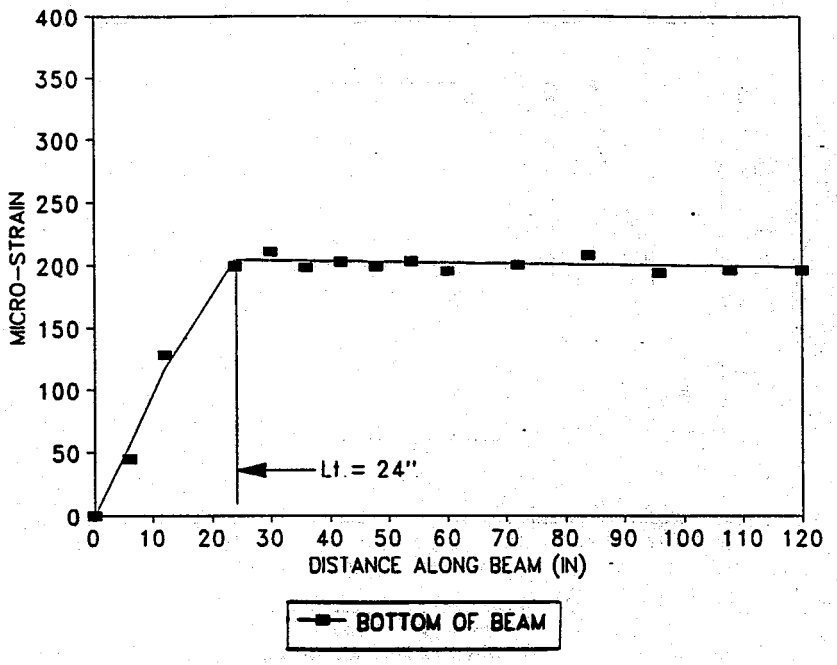

Figure 4-51 Transfer Length for UF1-36

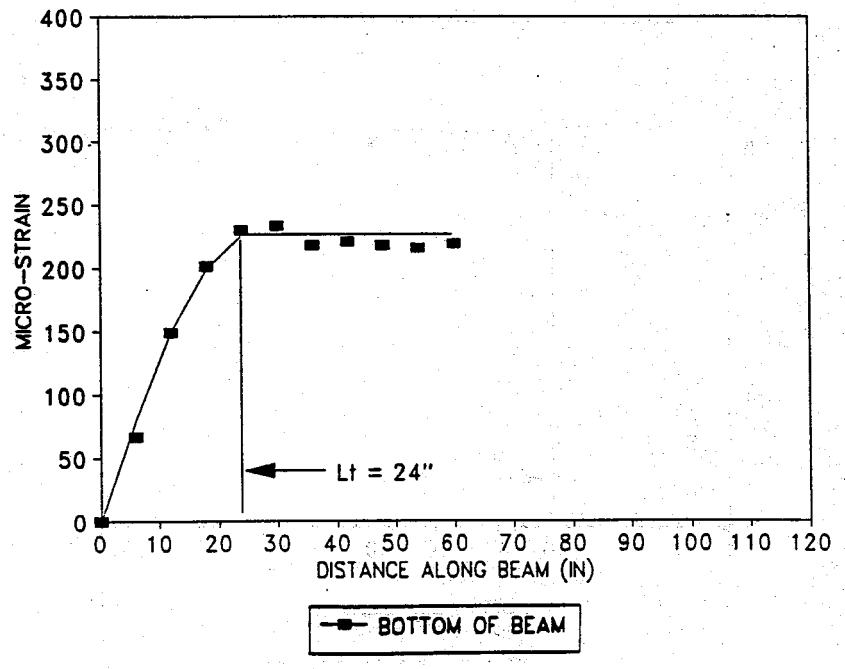

Figure 4-52 Transfer Length for UF2-36

CHAPTER 5
BEHAVIORAL MODELS

5.1General Information.

The prestressed concrete members were observed very carefully during testing in order to determine the load and corresponding shear force at which it developed the first diagonal crack. Throughout this study this particular load is referred as the failure load. The load at which the tests were terminated is called the collapse load.

The prestressed concrete members have clear spans ranging from 35 feet to 25 feet and 6 inches and effective depths ranging from 21.5 to 36.5 inches. In each case there is a clear span to depth ratio, l_n/d, greater than 5.0 and according to ACI 11.8.1 (Ref. 1) these beams may be treated as slender members. However, the loading point of 2D with a single concentrated load causes the short shear span to act as a deep beam. Since the shear spans and the effective depths varied in our testing the same behavioral model may not be valid for every test situation. The test variables for each beam are listed in Table 5-1.

Where, a/d = shear span to depth ratio

l_n = clear span

d = effective depth of the member

V_u = shear acting at the loading point at the appearance of first diagonal crack

b = member width

f'_c = compressive strength of the concrete.

Table 5-1. Test Variables

BEAM	a/d	l_n (ft)	l_n/d	V_u/bdf_c'	$V_u/bd\sqrt{f_c'}$
UF1-30-2D	2.00	35.0	19.53	.089	6.68
UF1-30-LD	3.58	28.5	15.91	.053	4.38
UF2-30-2D	2.00	25.5	14.23	.083	5.33
UF2-30-LD	3.58	35.0	19.53	.053	4.09
UF1-36-2D	2.00	35.0	15.85	.055	3.75
UF1-36-LD	2.91	28.0	12.68	.047	3.68
UF2-36-2D	2.00	28.0	12.68	.069	4.06
UF2-36-LD	2.91	35.0	15.85	.054	3.75
UF1-42-2D	2.00	26.5	9.94	.044	4.04
UF1-42-LD	2.41	35.0	13.13	.040	3.60
UF2-42-2D	2.00	35.0	13.13	.042	3.76
UF2-42-LD	2.41	28.7	10.00	.038	3.40
UF1-48-2D	2.00	35.0	11.51	.029	3.29
UF1-48-LD	2.11	25.7	8.44	.028	2.83
UF2-48-2D	2.00	25.5	8.38	.038	3.20
UF2-48-LD	2.11	35.0	11.51	.037	3.04

5.2 Plastic Truss Model/Strut and Tie

Based on the presentation in Chapter 2 the plastic truss model consists of compression struts inclined at an angle 6 to the horizontal, tension chords, stirrups and longitudinal chords. The longitudinal reinforcement provides the tension chord while the compression strut is provided by the concrete compression zone.

The concentrated loads and reactions in slender beams are transmitted to several stirrups by compression struts radiating from the load point which are referred to as compression fans. Between the compression fan there is a compression field of uniformly sloped compression struts.

Generally, a deep beam is any beam in which a significant amount of the load is carried to the supports by a compression thrust joining the load and the supports. This condition occurs at the loading point of 2D which provides a shear span to depth ratio (a/d) of 2.0, thus causing deep beam behavior. This type of behavior causes the compression an regions to overlap so that no compression field can exist. The net result is the formation of a major compression diagonal.

The load carrying mechanism for the beams tested at 2D is best modeled by strut and tie action. The 42-inch beam that was loaded at the assumed development length of 77 inches has a shear span to depth ratio of 2.4. Therefore, its behavior is also governed by the strut and tie model.

5.2.1 Implementation of the Strut and Tie Model

The primary task in developing the strut and tie model is the determination of the size of the compression strut. The size of this strut is strongly influenced by details such as the size of the bearing plate under the loading and the bearing plate at the support as well as the anchorage conditions.

Mitchell and Collins (Ref. 7) suggest the following method of determining the shear capacity of a prestressed concrete beam using the strut and tie model. The first step -is the determination of the smallest angle existing between the tension tie and the compression strut, 6. The following equation is used to calculate this angle with the variables illustrated in Figure 5-2:

$$\tan\theta = \frac{h - 0.5h_a - 0.5d_a}{a} \qquad \text{Eq. 5-1}$$

where, h = the overall height of the beam

$0.5h_a$ = the distance from the bottom the bottom face of the beam, to the centroid of the tension reinforcement

d_a = depth of the top horizontal compression strut

a = shear span.

All of the variables in this equation are known but the depth of the horizontal compression strut, d_a. Therefore, an initial guess of this value must be made.

From the equilibrium conditions in the strut and tie model in Figure 5-1 it can be seen that the tension, T, in the horizontal tie must equal the compression, C, in the compression strut and that these two forces are related to the applied load, V. Thus

$$C = T = V \cot \theta \qquad \text{Eq. 5-2}$$

The capacity of the top horizontal strut can be found by

$$C = \phi A_c f_{2\max} \qquad \text{Eq. 5-3}$$

where, $\Phi = 0.70$, strength reduction factor for axial compression

A_r = effective cross sectional area of the top strut

f_{2max} = effective compressive strength of the strut.

For the top horizontal strut f_{2max} is assumed to be $0.85f'_c$, since this strut is not crossed by a tension tie.

The load necessary to reach the capacity of the top horizontal strut can be found by Equation 5-3. The compressive force in the diagonal is found by

$$D = \frac{V}{\sin\theta} \qquad \text{Eq. 5-4}$$

The top end of the diagonal also is not crossed by a tension tie so f_{2max} can be assumed as 0.85 f_c'. The capacity is still calculated from Equation 5-3 except in this case the effective cross sectional area, A_c, is dependent on the anchorage conditions. The top end of the diagonal consists of a strut anchored by a bearing plate and another strut as. seen in Figure 5-2, View B. Therefore,

$$A_c = [l_b \sin\theta + d_a \cos\theta] width \qquad \text{Eq. 5-5}$$

The bottom end of the diagonal is crossed by a tension tie and hence it is necessary to determine f_{2max} from the following equation:

$$f_{2\max} = \frac{f_c'}{0.8 + 170 \in_1} \qquad \text{Eq. 5-6}$$

where, $\in_1 = \in_s + (\in_s + 0.002) \cot^2 \theta$ (strain in concrete)

$\in_s$ = tensile strain in tension-tie reinforcement

The bottom end of the diagonal consists of a strut anchored by a bearing plate and a tension-tie. The capacity is still calculated from Equation 5-3 and A_c, is governed by the anchorage conditions shown in Figure 5-2, View A. Therefore,

$$A_c = [l_b \sin\theta + H_a \cos\theta] width \qquad \text{Eq. 5-7}$$

The capacity of the compression diagonal is assumed to be the smaller of the top or bottom capacity and then compared to the force existing in the diagonal. If thus value is close to the initial guess a new estimate of d_a has to be made and the procedure repeated until the values converge.

5.2.2 Comparison of Predicted and Experimental Results

The process mentioned above was used to determine the shear capacity of the diagonal compression strut at shear span to depth ratios ranging from 1 to 7. The shear force at the loading point towards the support at failure was then normalized by dividing by bdf'_c, and was plotted against the different shear span to depth ratios.

The strut and tie model yields very consistent results when compared with the test results as seen in Figures 5-3 through 5-5 This model illustrates how the shear strength of a simply supported prestressed concrete beam loaded with a concentrated load changes as the shear span changes. In every case the beams can resist very high shear forces if the shear is a result of a load near the support but the shear strength is greatly reduced as the shear span to depth ratio (a/d) increases.

All four of the normalized shear forces for the 48-inch beams are plotted against their aspect ratios in Figure 5-6. The beams tested at 2D and ID have shear span to depth ratios of 2.0 and 2.14 respectively. If these beams exhibited normal deep beam behavior then it would be expected that the strut and tie model would yield accurate predictions. From Figure 5-6 it can be seen that all four of the beams failed at loads lower than predicted. All of the beams formed an initial crack under the load which acted as a hinge.

Both ends of the beam then acted as rigid bodies rotating about the hinge. This type of failure mechanism is typical behavior for an under reinforced section.

Because of this behavior the beams never had a chance to develop a compression strut or a compression field. Therefore, neither the strut and tie model nor the modified compression field theory correctly models this situation.

5.3 Modified Compression Field Theory Analysis

5.3.1 Implementation of MCFT

The modified compression field theory analysis is based on the information presented in Chapter 2. Since analysis using the modified compression field is a highly iterative procedure, it was not practical for normal calculations. The computer program RESPONSE, written by Mitchell and Collins (Ref. 7), was used to complete the analysis.

RESPONSE is an interactive menu-driven program used to determine the load deformation response of a prestressed concrete cross-section subjected to combined moment, axial load and shear. In order to perform any analysis using this program the material properties as well as the section properties must be supplied as data.

5.3.1.1 Concrete material properties. The following is a sample representation of the concrete properties for UF1-36 that were required for this analysis:

Compressive strength of concrete, f_c' = 6.800 ksi

Strain at max compressive stress, $\in '_c$ = -2.36 millistrain

Tensile strength of concrete, f_{cr} = 300 psi

Tension Stiffening Factor, α

α_1 = 1.00 deformed bars under short term monotonic loading

α_1 = 0.70 plain bars, wires and bonded strands for short-term monotonic loading

α_1= 0.00 for unbonded reinforcement

α_2 = 0.49 for plain bars, wires and bonded strand for sustained or repeated loading

This tension stiffening factor, accounts for the complex situation that develops in concrete after the formation of cracks. There are no tensile stresses in concrete at crack locations whereas tensile stresses do exist between these cracks due to the concrete bonded to the reinforcement. These tensile stresses between the cracks tend to increase the stiffness of the member. In order to account for this "tension stiffening" the following estimate of the average tensile stress in the concrete is used:

$$f_c = \frac{\alpha_1 + \alpha_2 + f_{cr}}{1 + \sqrt{500 \in_{cf}}} \qquad \text{Eq. 5-8}$$

These tensile stresses will be concentrated in a zone of concrete around the reinforcement called the "effective embedment zone" which is suggested as 7.5 d_b above and 7.5 d_b below the longitudinal reinforcement.

5.3.1.2 Steel material properties. The steel material properties that were used for the regular reinforcement and the prestressing steel are listed below:

REINFORCING STEEL

Elastic modulus of reinforcing steel,	E_s	=	28200 ksi
Yield stress of reinforcing steel,	f_y	=	60 ksi
Strain when strain hardening begins,	$\in_{sh}$	=	40 millistrain
Strain when reinforcing steel reaches ultimate strength,	$\in_{rupt}$	=	40 millistrain
Ultimate reinforcing stress,	f_u	=	60 ksi

PRESTRESSING STEEL

Elastic modulus of prestressing steel,	E_p	=	28200 ksi
Ultimate tensile stress,	f_{pu}	=	270 ksi
Strain when prestressing steel reaches ultimate strength,	$\in_{rupt}$	=	40 millistrain

5.3.1.3 Section properties. The program requires that all of the section dimensions be input. The program prompts the user for the standard dimensions such as width, effective depth and stirrup spacing. The crack control characteristics of the longitudinal and transverse reinforcement, characterized by s_{mx} and s_{mv} respectively, must be calculated. Both of these expressions are found in Section 2.2.7. The only other requirements are that the section be divided into a series of no more than 20 finite concrete layers and longitudinal steel elements and that the location and initial prestress of the tendons be defined.

5.3.2 Comparison of Predicted and Experimental Results

The smaller beams that were loaded at the development length, Ld, had shear spans of 2.5 or greater. The background theory presented in Chapter 2 suggests that deep beam behavior becomes less likely to dominate the failure modes. The beams begin to form a diagonal compression field when loaded at these higher aspect ratios, thus the modified compression field theory appears to be an acceptable method of analysis.

A summary of these results and a comparison between the ACI nominal shear strength ($V_n = V_c + V_s$) is presented in Table 5-2.

It can be seen from the data in Table 5-2 that the theoretical results from the modified compression field theory agree very well with the results for the beams tested at LD but is inconsistent for the beams tested at 2D. The calculated shear capacities of the beams tested at LD were within 7% of the experimental results.

The prestressed concrete members UF1-36-LD, UF1-36-2D and UF1-42-LD were instrumented along the compression strut with strain gauges in the form of a rectangular rosette. Principal tensile strains were calculated from these strain readings at every

Table 5-2. Comparison of MCFT, ACI and Test Results

BEAM	V_c	V_s	V_n	Test V	MCFT V	%ACI	%MCFT
UF1-30-2D	100.0	11.8	111.8	148	94.8	1.32	1.56
UF1-30-LD	61.3	11.8	73.1	97	94.8	1.33	1.02
UF2-30-2D	107.0	11.8	118.9	133	94.8	1.12	1.40
UF2-30-LD	63.0	11.8	74.8	102	94.8	1.36	1.07
UF1-36-2D	103.0	14.6	117.6	109	115	0.93	0.95
UF1-36-LD	71.4	14.6	86.0	107	115	1.24	0.93
UF2-36-2D	101.2	14.6	115.8	118	115	1.02	1.02
UF2-36-LD	71.6	14.6	96.2	109	115	1.13	0.95
UF1-42-2D	95.2	17.6	112.8	128	118.3	1.13	1.08
UF1-42-LD	96.5	17.6	104.2	114	118.3	1.09	0.96
UF2-42-2D	96.6	17.6	104.2	126	118.3	1.21	1.07
UF2-42-LD	93.74	17.6	101.3	114	118.3	1.13	0.96

loading increment. These principal tensile strains, $\in_1$ are-plotted versus the shear force Figures 5-7 through 5-9.

Results for beam UF1-36-LD as shown in Figure 5-7 with a shear span to depth ratio of 3.58, demonstrate the formation of a diagonal compression field. The stirrups in this beam registered tensile strains as shown in Figure 4-36 which is an indication that a compression field develops. It can be seen from Figure 5-7 that the measured shears and principal tensile strains correlate very well with the results predicted by the modified compression field theory. Only the experimental data up to the failure load is shown in Figure 5-7 which corresponds very well with the failure load that is predicted. This analytical procedure appears to provide a rational analysis for prestressed concrete beams subjected to these loading conditions.

The prestressed concrete member UFI-36 2D as shown in Figure 5-8 has a shear span to depth ratio of 2.0. As can be seen in Figure 5-8 the principal tensile strains and shear values do not agree very well to the response predicted by the modified compression field theory. The random fluctuations in the principal tensile strain readings and high shear value are a result of the loading point being in a disturbed region. From Figure 5-8 it is apparent that a compression field never existed for this test and that the modified compression field theory is not an acceptable method of analysis for this situation.

The 42-inch, beams that were loaded at LD have a shear span to depth ratio of 2.4 which is right on the border line between deep and slender beam behavior. From Figure 5-9 it appears that UF1-42-LD is following the response predicted by the modified compression field theory but the collapse load was little bit less than predicted. This implies that the beam is still behaving as a deep beam and that the strut and tie model is a more accurate method of analysis.

The primary reason the modified compression field theory can not properly estimate the shear capacity of disturbed regions is that it is a sectional model that assumes that plane sections remain plane. Therefore, it is not capable of predicting the local effects caused by the support and loading conditions. At loading conditions with aspect ratios of 2.5 and lower a significant portion of the load is carried by strut action. Thus, the beneficial transverse compressive stresses induced by the support are ignored and the shear capacity is not justly estimated.

5.4 Moment Curvature Analysis

5.4.1 Compatibility and Equilibrium Conditions

The hypothesis that plane sections remain plane is the fundamental assumption that forms the basis of modern beam theory. Because of this assumption, it is possible to develop the compatibility conditions for prestressed concrete members. The concrete strain distribution is defined by two variables; the strain at the op face and the strain at the bottom face of the member. This is a linear strain distribution defined by the strain at the centroid, $\in_{cen}$, and the curvature, Φ. The curvature is equal to the change in slope per unit length along the member. Thus, the strain in the concrete at any level y is given by

$$\in_c = \in_{cen} - \Phi y \qquad \text{Eq. 5-9}$$

In prestressed members, the strain in the tendons at any level y is equal to the strain in the surrounding concrete plus the initial strain due to prestressing.

$$\in_p = \in_{cen} - \Phi y + \Delta \in_p \qquad \text{Eq. 5-10}$$

The sign convention for the preceding equations assumes that tensile strains are, negative and compressive strains are positive.

The section stresses, when integrated over the section, must add up to the required sectional forces M and N in order to satisfy equilibrium.

5.4.2 Predicting the Response of Flexural Members

The response of flexural members can be predicted using the preceding compatibility and equilibrium conditions together with the material stress-strain relationships.

The stress-strain relationship used to describe the behavior of the concrete was the Hognestad parabola, shown in Figure 5-9 (Ref. 11). The rising portion of this curve is approximated by a parabola with its vertex at the maximum stress. The. parabola is followed by a sloping line terminating at a limiting strain of 0.0038. The concrete stress corresponding to a given strain, $\in_c$ is given by the following:

$$f_c = f_c^{'}\left[2\frac{\in_c}{\in_o} - \left(\frac{\in_c}{\in_o}\right)^2\right] \qquad \text{Eq. 5-11}$$

where, $\in o = 1.8\ f'_c / E_c$.

The stress-strain response for prestressing strand is obtained using the modified Ramberg-Osgood function recommended by Mattock (Ref. 12) given as:

$$f_p = E_p \in_{pf} \left\{A + \frac{1-A}{\left[1+\left(B\in_{pf}\right)^C\right]^{1/c}}\right\} \le f_{pu} \qquad \text{Eq. 5-12}$$

This function which consists of two straight lines joined by a smooth curve is defined by three constants A, B and C. The typical values for these constants, 0.025, 118.0 and 10.0 were used for the determination of f_p.

If the strain distribution across the section is known, then the stress-strain relationships can be used to determine the distribution of stresses across the section. Once the stresses are known; then the moment and axial load acting at that section can be determined using the equilibrium conditions.

In determining the moment curvature response of a typical section with zero axial load, an initial value of the top concrete strain is chosen and then the bottom strain that will result in zero axial load is found by trial and error. The moment and curvature associated

with the chosen strain distribution can then be found. Repeating this process for several different values of top strain allows the complete moment curvature response of the section to be developed.

5.4.3 Comparison of Predicted and Experimental Results

The procedure mentioned above was used to develop a moment curvature response for each beam. The cracking moment, M is taken as the force that will cause a tensile strain of 0.00015 at the bottom of the concrete. This point is labeled for each beam. A spreadsheet was used to assist in the calculations. The predicted responses for the 30-, 36-, 42- and 48-inch beams are found in Figures 5-11 through 5-14.

The moment that was developed in each test specimen at the formation of the first crack is shown in Table 5-3 and compared to the calculated cracking moment, M_{cr}.

From the moment curvature relationships it is possible to calculate the deflected shapes for each beam. This was done using the conjugate beam method for calculating deflections. In the conjugate beam method, the deflection at a given point equals the bending moment at that point for a beam loaded with the curvature diagram.

For each moment curvature relationship a regression analysis was performed to determine an equation that would best represent the data. In order to obtain a more accurate fit, the moment curvature graph was divided into three sections and three separate second order curves were fit through the data points. Once an equation for every section along the graph is known, the curvature can be calculated for any given moment. After the curvature at any given point has been calculated the deflection at that point can

Table 5-3. Comparison of Predicted and Experimental M_{cr}

BEAM	TEST M_{cr} (k-in)	CALCULATED M_{cr} (k-in)	% DIFFERENCE
UF1-30-2D	4945	5000	1.11
UF1-30-LD	6160	5000	18.83
UF2-30-2D	4730	5000	5.71
UF2-30-LD	5390	5000	7.24
UF1-36-2D	5300	5707	7.68
UF1-36-LD	6930	5707	17.65
UF2-36-2D	5830	5707	2.11
UF2-36-LD	8470	5707	32.62
UF1-42-2D	7360	5942	19.27
UF1-42-LD	6930	5942	14.26
UF2-42-2D	6400	5942	7.16
UF2-42-LD	6930	5942	14.26
UF1-48-2D	8760	6645	24.14
UF1-48-LD	8470	6645	21.55
UF2-48-2D	8541	6645	22.19
UF2-48-LD	7084	6645	6.19

be calculated. By discretising the beam into a series of finite segments and calculating the deflection at each point, the deflected shape for the entire member can be calculated.

The equations that were determined for each moment curvature response are expressed in units of kips and inches. The equations are presented in the following pages.

UF-30:

$$M = 2013.84 + 1.595 \times 10^{8}\,\Phi - 1.781 \times 10^{12}\Phi^{2}$$
$$\text{for } -1.2 \times 10^{-5} < \Phi < 2.8 \times 10^{-5}$$

$$M = 4401.99 + 2.693 \times 10^{7}\,\Phi - 3.6 \times 10^{10}\,\Phi^{2}$$
$$\text{for } 2.8 \times 10^{-5} < \Phi\ 29.0 \times 10^{-5}$$

$$M = 7203.84 + 9.73 \times 10^{6}\,\Phi - 9.431 \times 10^{9}\,\Phi^{2}$$
$$\text{for } 29.0 \times 10^{-5} < \Phi < 57.9 \times 10^{-5}$$

UF36:

$$M = 2556.19 + 2.394 \times 10^{8}\phi - 5.851 \times 10^{12}\phi^{2}$$
$$\text{for } -.77 \times 10^{-5} < \phi < 2.32 \times 10^{-5}$$

$$M = 5421.03 + 3.612 \times 10^{7}\phi - 6.57 \times 10^{10}\phi^{2}$$
$$\text{for } 2.32 \times 10^{-5} < \phi < 24.6 \times 10^{-5}$$

$$M = 9252.8 + 5.987 \times 10^{6}\phi - 6.343 \times 10^{9}\phi^{2}$$
$$\text{for } 24.6 \times 10^{-5} < \phi < 49.4 \times 10^{-5}$$

UF42:

$$M = 2278.83 + 5.171 \times 10^{8}\phi - 1.196 \times 10^{13}\phi^{2}$$
$$\text{for } -.42 \times 10^{-5} < \phi < .793 \times 10^{-5}$$

$$M = 5465.73 + 4.256 \times 10^{7}\phi - 9.96 \times 10^{10}\phi^{2}$$
$$\text{for } .793 \times 10^{-5} < \phi < 16.6 \times 10^{-5}$$

$$M = 9266.63 + 4.449 \times 10^{6}\phi - 3.795 \times 10^{9}\phi^{2}$$
$$\text{for } 16.6 \times 10^{-5} < \phi < 64.7 \times 10^{-5}$$

UF48:

$$M = 2515.17 + 8.639 \times 10^{8}\phi - 4.730 \times 10^{13}\phi^{2}$$
$$\text{for } -.26 \times 10^{-5} < \phi < .882 \times 10^{-5}$$

$$M = 6083.91 + 4.442 \times 10^{7}\phi - 1.112 \times 10^{11}\phi^{2}$$
$$\text{for } .882 \times 10^{-5} < \phi < 14.5 \times 10^{-5}$$

$$M = 9900.58 + 2.864 \times 10^{6}\phi - 1.685 \times 10^{9}\phi^{2}$$
$$\text{for } 14.5 \times 10^{-5} < \phi < 79.3 \times 10^{-5}$$

The deflected shape was determined for each specimen for the load at which initial cracking took place, the failure load and an intermediate point. A typical deflected shape for a beam loaded at 2D and at LD are illustrated in Figures 5-15 and 5-16.

The moment curvature relationship can also be used to determine the deflections at a single point for the entire loading sequence. Therefore, a predicted P-Delta relationship can be determined at any point along the span of the member. The deflections were calculated at one foot toward midspan of the load for each prestressed concrete member. Each specimen was instrumented with LVDT's one foot to either side of the load. Thus, a direct comparison of experimental and predicted values can be made. Typical results are illustrated in Figures 5-17 through 5-19. Figures 5-17 and 5-18 represent the typical P-Delta curves where the predicted and experimental curves correlate very well. The events that occurred during testing are associated quite closely to the predicted values. The moment curvature analysis is a flexural analysis that does not consider shearing strains nor the effects of inclined cracking. Since the predictions are so close to the experimental in most cases it is evident that flexure played a dominant role in the failure mechanisms.

Figure 5-19 illustrates a P-Delta curve that exhibited less correlation between the test and theoretical results than the others. The beam UF2-30-2D was supported with neoprene pads between the beam and the support. The deviation of the experimental data from the predicted data may be the result of a rigid body deformation due to the compression of the neoprene pad.

5.5 Effect of Shear Force on Bond Slip

To study the impact of shear force on longitudinal tendon slip in the prestressed concrete members the longitudinal slips of the tendons were monitored with the help of the LVDTs. The shear force at which tendons develop considerable slipping was monitor ed. The effects of different variables such as normalized ratio (V/bd$\sqrt{f_c^{'}}$), diagonal

cracks and aspect ratio on the interaction between shear force and the first longitudinal bond slip are discussed in subsequent sub-sections. The results of test beams loaded at the development length are represented graphically in the Figure 5-20. Test results are also presented in tabulated form in Table 5-4.

Table 5-4. Shear Force at First Longitudinal Tendon Slip

NAME	SPAN (ft)	a/d	V @ 1st. slip (kips)	M @ 1st. slip (kip-ft)
UF1-30-2D	35.00	2	148	531
UF2-30-2D	25.50	2	138	493
UF1-36-2D	35.00	2	114	502
UF2-36-2D	28.00	3	122	809
UF1-42-2D	26.50	2	135	720
UF2-42-2D	35.00	2	127	678
UF1-30-LD	28.50	3.58	112	721
UF2-30-LD	35.00	3.58	102	655
UF1-36-LD	28.00	2.91	112	717
UF2-36-LD	35.00	2.91	114	734
UF1-42-LD	35.00	2.44	109	702
UF2-42-LD	26.67	2.44	117	750

5.5.1 Effect of Diagonal Crack

Figure 5-20 shows the variation of the percentage shear with aspect ratio of the prestressed concrete girders. Percentage shear is defined as the ratio of the shear force when a longitudinal strand slipped considerably to the shear force when the first diagonal crack appeared. Referring to Figure 5-20 it seems that the value of the percentage shear is always greater than one. The formation of diagonal cracks always precedes longitudinal tendon slip. At the appearance of a diagonal crack the loading was stopped. Usually longitudinal slip was observed with the next increment of load. The formation of diagonal

crack always preceded the longitudinal bond slip of tendon for all the tests performed in the laboratory.

5.5.2 Effect of Normalized Ratio

To normalize the section properties, material properties and the ratio of the shear force at which the diagonal crack first appeared to the product of the width, effective depth and the square root of compressive strength of concrete are determined for each test beam. The values of this normalize and dimensionless ratio for each beam are tabulated in Table 5-1.

The ACI code suggests a simplified approach to: the prediction of the shear strength for members with an effective prestress force not less than 40 percent of the tensile strength of the flexural reinforcement. The shear strength expression is as follows:

$$V_c = \left[0.6\sqrt{f_c'} + 700\frac{V_u d}{M_u} \right] b_w d \qquad \text{Eq. 5-13}$$

where, V_c = assumed nominal shear strength at the appearance of the first diagonal crack.

f_c = concrete compressive strength

b_w = width of the web

d = effective depth

V_u = factored shear force acting at the section

M_u = factored moment acting at the section

In Equation 5-13 the quantity $V_u d/M_u$ is not to be taken greater than 1.0. The above expression for shear strength has got a lower bound and a upper bound as follows:

$$2\sqrt{f_c'}b_w d \le V_c \le 5\sqrt{f_c'}b_w d \qquad \text{Eq. 5-14}$$

Equation 5-13 reduces to the following form for beams loaded with a single concentrated load acting at a distance "a" from the support:

$$\frac{V_u d}{M_u} = \frac{V_u d}{V_u a} = \frac{d}{a} \qquad \text{Eq. 5-15}$$

Substituting Equation 545 into Equation 5-13 and dividing both sides of the equation by $\sqrt{f_c'}$ $b_w d$ we get:

$$\frac{V_c}{\sqrt{f_c'}b_w d} = 0.6 + \frac{700}{\sqrt{f_c'}}\frac{d}{a} \qquad \text{Eq. 5-16}$$

In order to include the term ρ, percentage reinforcement ratio in Equation 5-13; a new factor k is defined as follows:

$$700 = k\rho \qquad \text{Eq. 5-17}$$

Thus,

$$k = \frac{700}{\rho} \qquad \text{Eq. 5-18}$$

Equation 5-13 further reduces to the following:

$$\frac{V_c}{\sqrt{f_c'}b_w d} = 0.6 + k\frac{\rho}{\sqrt{f_c'}}\frac{d}{a} \qquad \text{Eq. 5-19}$$

If we define the variable "x" as follows:

$$x = \left(\frac{\rho}{\sqrt{f_c'}} \frac{d}{a} \right) \qquad \text{Eq. 5-20}$$

where, ρ = reinforcement ratio in percentage

f_c' = concrete compressive strength

d = effective depth

a = shear span

and the variable "y" as follows: .

$$y = \frac{V_c}{\sqrt{f_c'} b_w d} \qquad \text{Eq. 5-21}$$

the final form of the Equation 5-13 reduces to the following:

$$y = 0.6 + k\,x \qquad \text{Eq. 5-22}$$

A plot of normalized ratio versus the variable "x" for the test beams is presented in Figure 5-21. Figure 5-21 shows that as the variable "x" for the test beams increases the normalized ratio increases.

The Equation 5-22 is of the form of a straight line. A regression analysis is computed for the test results. A straight line is fitted through the test results on the basis of a least squares analysis. The variable "x" is assumed to be the independent variable and the normalized ratio "y" is assumed to be dependent variable. Figure 5-22 represents the

equation of the straight fine obtained by the regression analysis of the test results. The equation is as follows:

$$y = 1.85 + 82882x \qquad \text{Eq. 5-23}$$

Assuming the value of percentage reinforcement ratio to be the average value of the test beams the value of the factor k is determined as 140,000. Analyzing the test beams it has been found that a following equation containing the term ρ fits the test results, very well as shown in Figure 5-21.

$$y = \frac{V_c}{\sqrt{f_c^{'}}\, b_w d} = 0.6 + 140000 \frac{\rho}{\sqrt{f_c^{'}}} \frac{d}{a} \qquad \text{Eq. 5-24}$$

Equation 5-24 proves to be a very good approximation to predict the shear strength at the appearance of first crack of the prestressed concrete beams under consideration. Equation 5-23 shows that the test results follow a definite linearly increasing relation between the variable "x" and the variable "y" as described in earlier paragraphs. It appears that the ACI equation is conservative as expected. Particularly for the higher values of the variable "x" the ACI equation is overly conservative since an upper bound is imposed on the ACI equation.

The value-of the strength reduction factor for shear recommended in the ACI code is 0.85. Equation 5-24 reduces to Equation 5-25 with the strength. reduction factor for shear as follows:

$$y = \frac{\phi V_c}{\sqrt{f_c'} b_w d} = 0.85\left[0.6 + 140000\frac{\rho}{\sqrt{f_c'}}\frac{d}{a}\right] \qquad \text{E q. 5-25}$$

Both the Equations 5-24 and 5-25 are represented graphically in Figure 5-20. The upper bound for the normalized ratio according to Equation 5-24 is assumed as 5 and the lower bound as 2 as recommended by ACI code. The upper bound and lower bound for the normalized ratio according to Equation 5-25 are 1.7 and 4.25 respectively. It will be of interest to determine the effect of transverse reinforcement, spacing of stirrups and include these terms in the simplified expression predicting the shear strength of a prestressed concrete beam at the appearance of first diagonal crack.

5.5.3 Effect of Aspect Ratio

Aspect ratio plays an important role in the utilization of the full shear capacity of a prestressed concrete member. The prestressed concrete members which were tested in the laboratory had aspect ratios ranging from 2 to 3.58. As the aspect ratio of the beams in the moment arm also increases. Thus for the same shear force the beam having higher aspect ratio develops a higher bending moment. Higher bending moment induces higher amount of longitudinal stress in the tendons of the members. The tendons tend to slip more as a result of the development of this longitudinal stress due to flexure. The development of this: longitudinal flexural stress seems to lower the shear force causing the first longitudinal bond slip. Table 5-4 shows that at first longitudinal bond slip the bending moments are higher and shear forces are lower for the test beams loaded at LD than the test beams loaded at 2D.

5.6 Summary

Comparison of shear strength predicted by different behavioral models, such as, strut and tie model, modified compression field theory and shear strength of the tests beams as determined from the performed tests were presented in Tables 5-2. The comparison shows that the strut and tie model proved to be an acceptable method of analysis for prestressed concrete members subjected to loading conditions with a shear span to depth ratios less than 2.5. On the contrary the modified compression field theory provides a rational and comprehensive analytical procedure for analyzing prestressed concrete members with shear span to depth ratios greater than 2.5.

The moment curvature relationship for each test specimen was developed and presented in Figures 5-11 through 5-14. The moment curvature analysis used does not account for shearing strains nor the effects of inclined cracking. It can be seen from Table 5-3 that the predictions of the cracking moments were very close to the experimental results in most cases.

The test results regarding the effect of shear force on first longitudinal bond slip presented in Table 5-4. The results show the shear force at first longitudinal tendon slip decreases as the aspect ratio of the test beams increases. The results also, point, out that shear force at first appearance of diagonal cracks are always lower than shear force at first longitudinal bond slip. The formation of diagonal crack always preceded the longitudinal bond slip of tendon for all the tests performed in the laboratory.

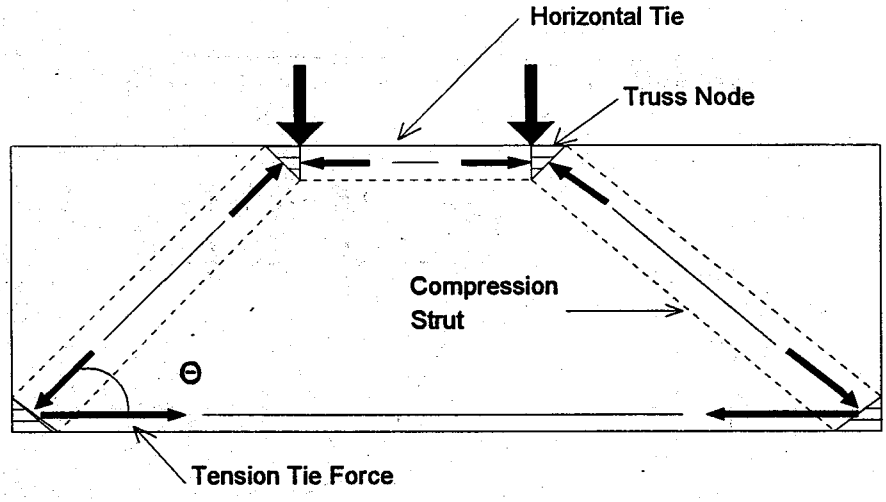

Figure 5-1. Strut and Tie Model for Deep Beams

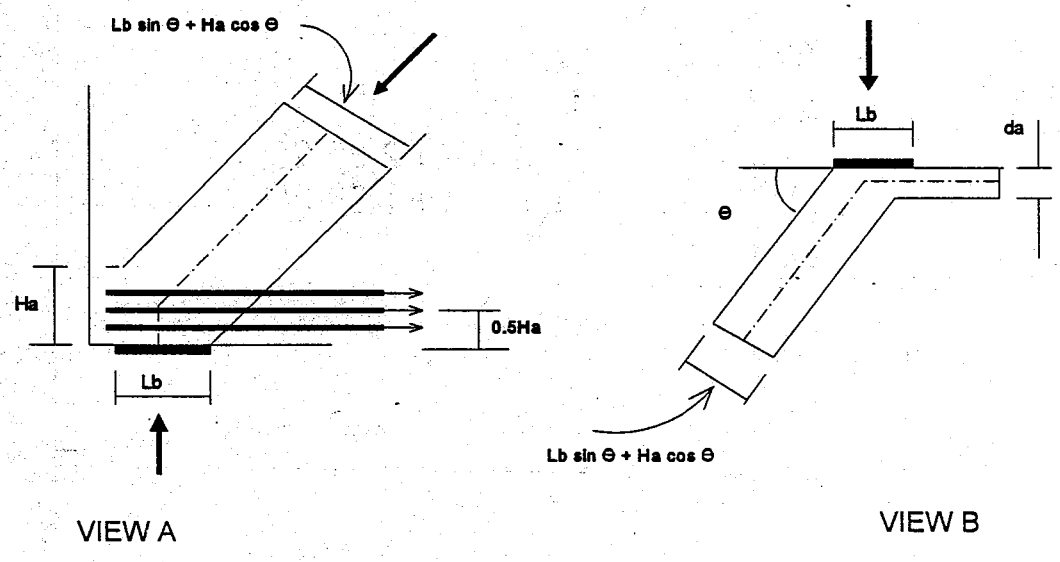

Figure 5-2. Influence of Anchorage Conditions on A_c

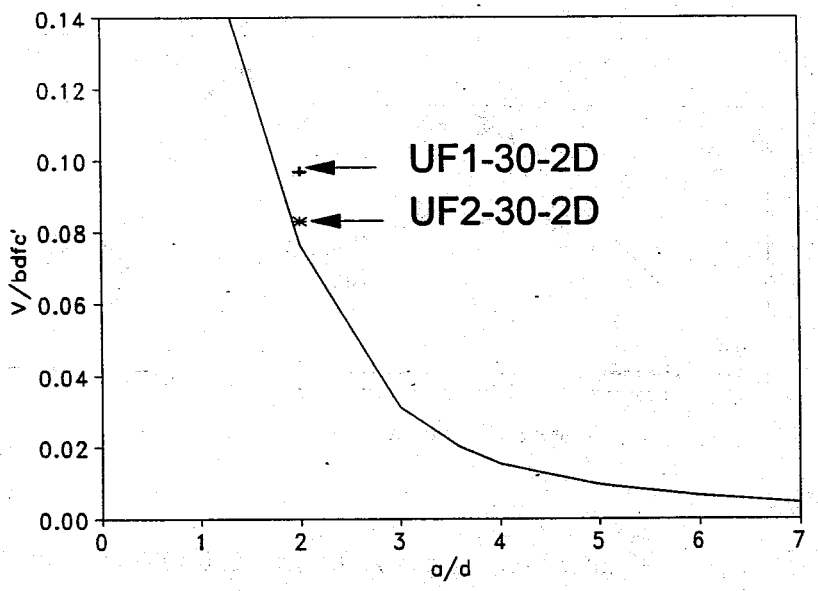

Figure 5-3. Strut and Tie Model Strength Predictions (UF1-30-2D and UF2-30-2D)

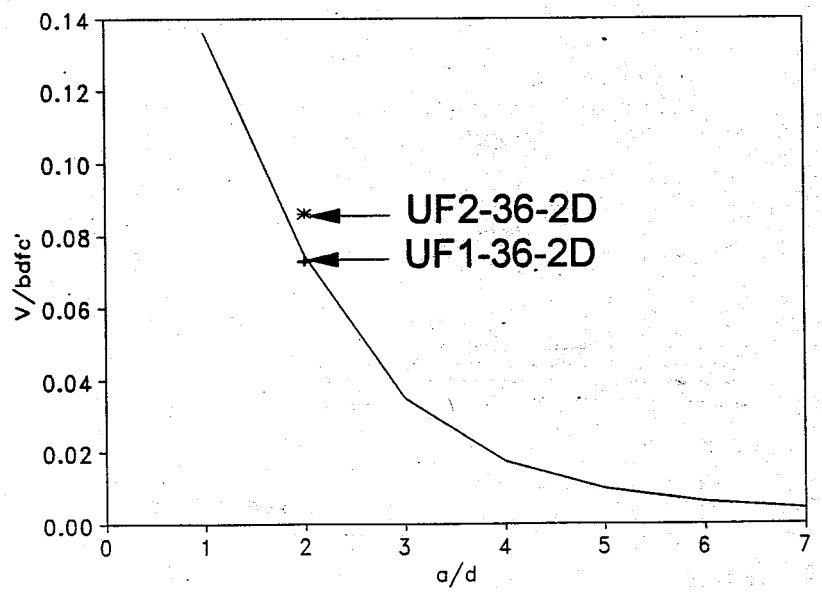

Figure 5-4. Strut and Tie Model Strength Predictions (UF1-36-2D and UF2-36-2D)

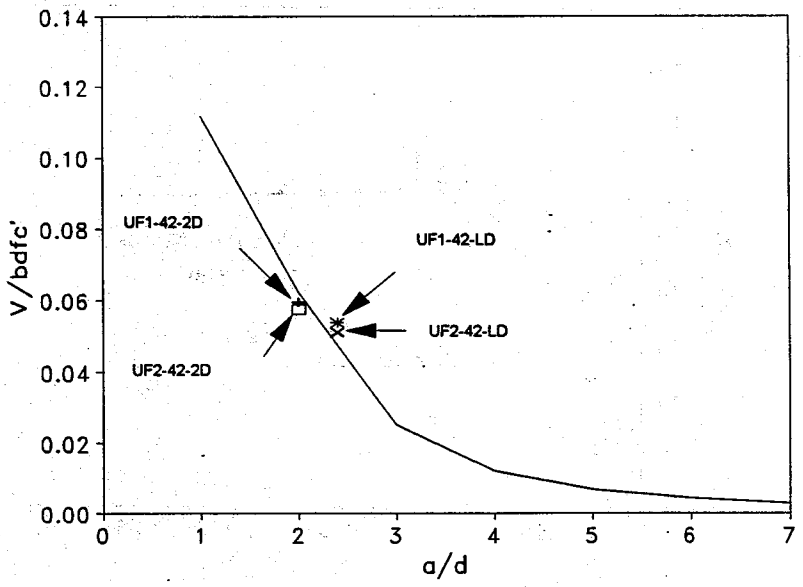

Figure 5-5. Strut and Tie Model Strength Predictions (UF1-42-2D & LD, UF2-42-2D & LD)

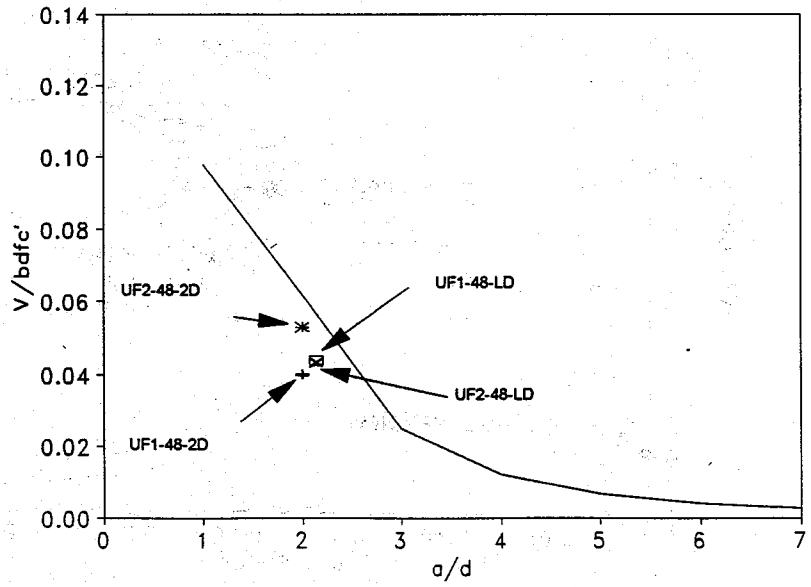

Figure 5-6. Strut and Tie Model Strength Predictions (UF1-48-2D & LD, UF2-48-2D & LD)

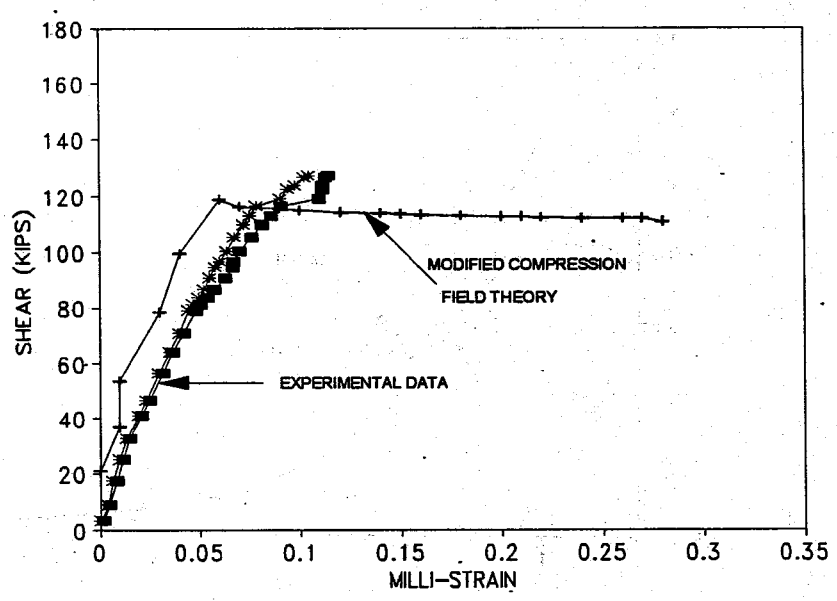

Figure 5-7. Shear versus Principal Tensile Strain (UF1-36-LD)

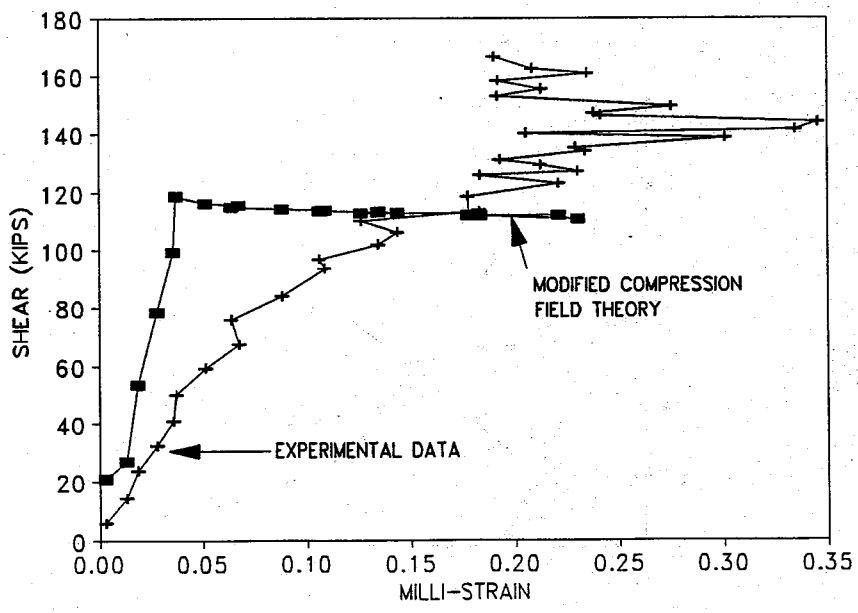

Figure 5-8. Shear versus Principal Tensile Strain (UF1-36-2D)

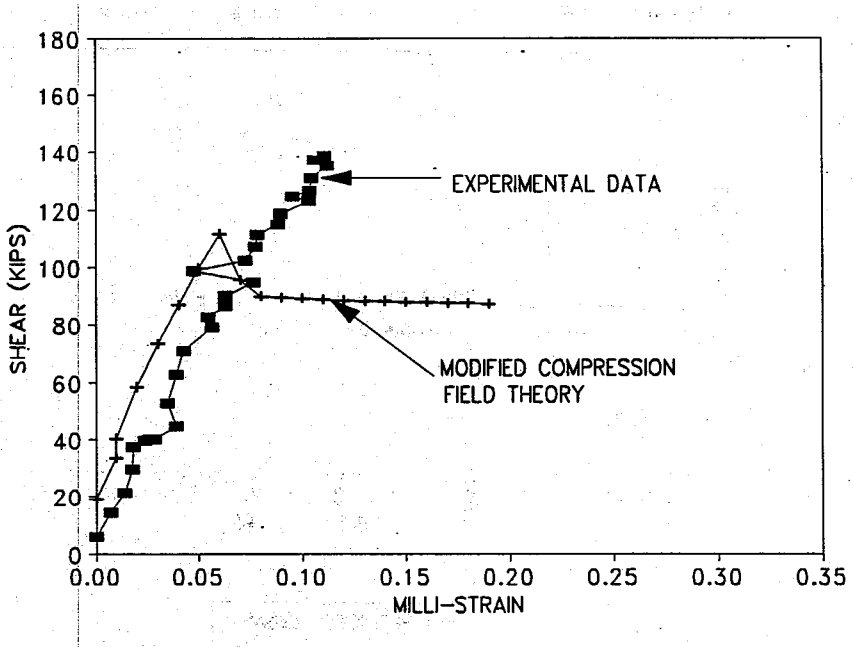

Figure 5-9. Shear versus Principal Tensile Strain (UF1-42-LD)

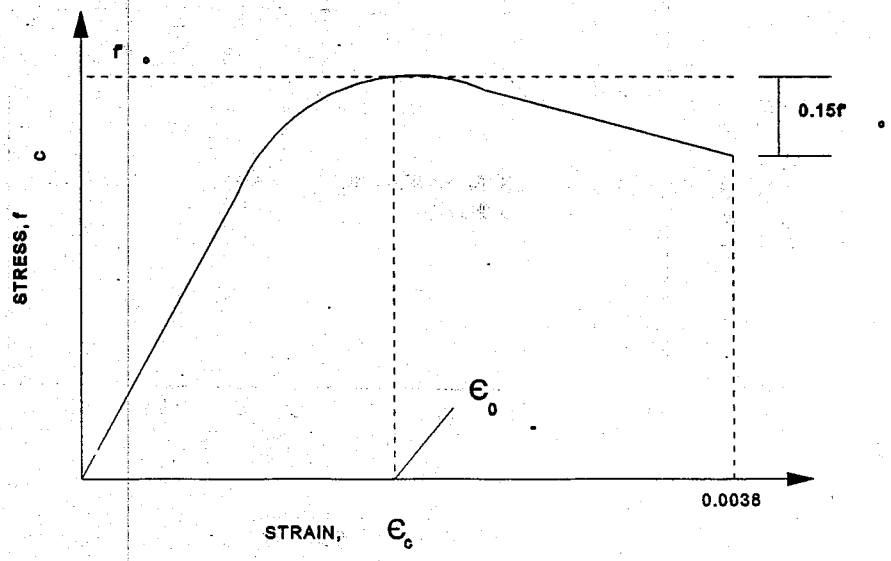

Figure 5-10. Hognestad Stress-Strain Curve

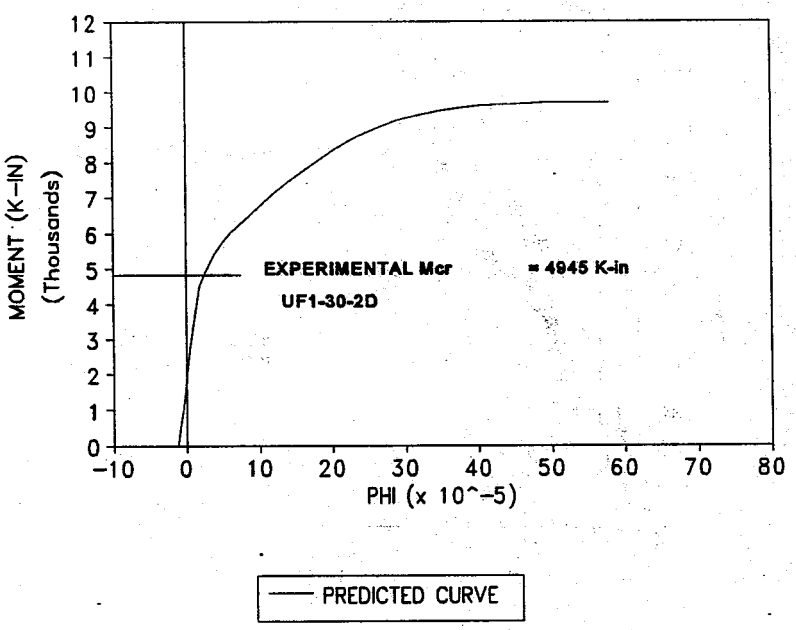

Figure 5-11 Moment Curvature Response (UF-30)

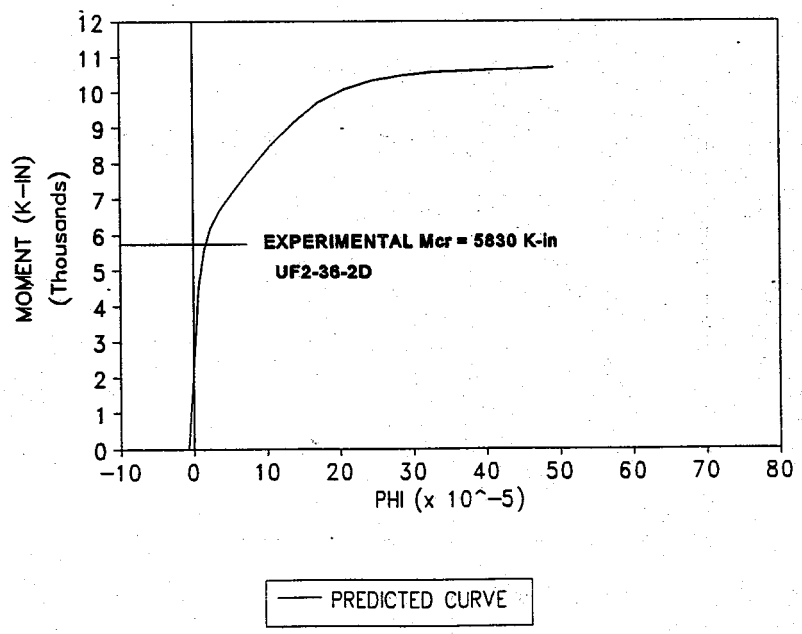

Figure 5-12. Moment Curvature Response (UF-36)

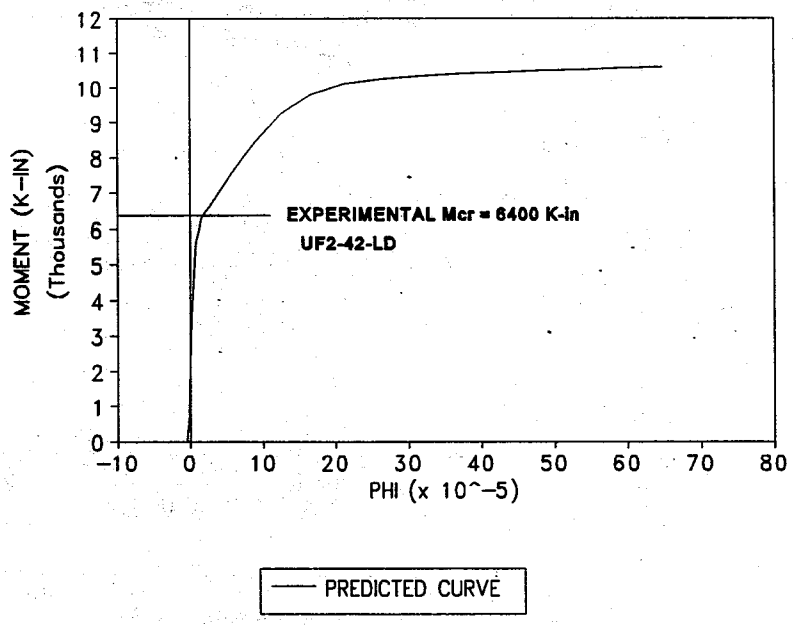

Figure 5-13. Moment Curvature Response (UF-42)

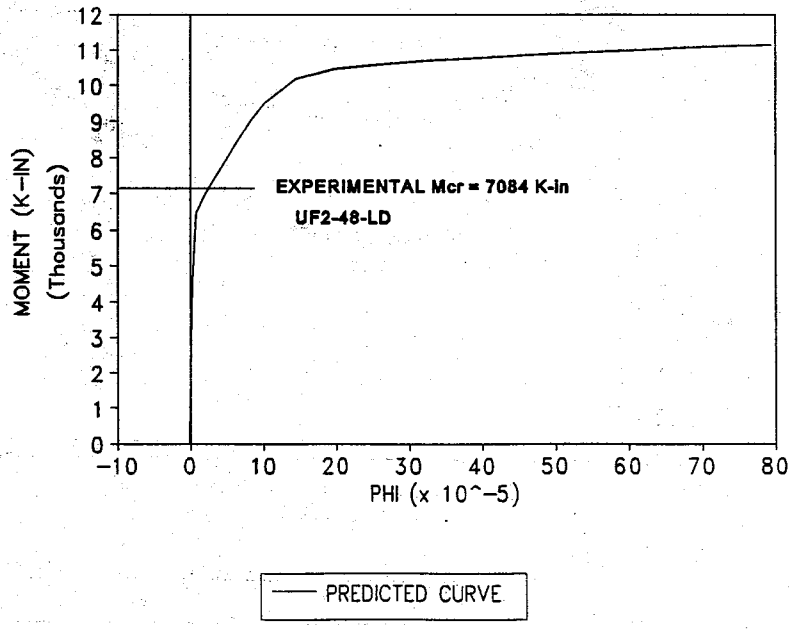

Figure 5-14. Moment Curvature Response (UF-48)

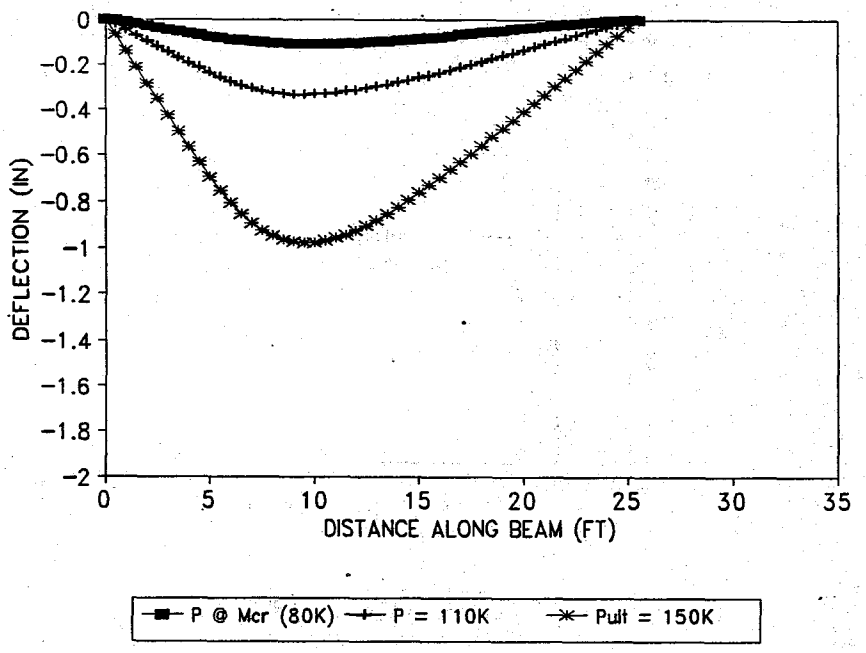

Figure 5-15. Deflected Shape (UF2-30-2D)

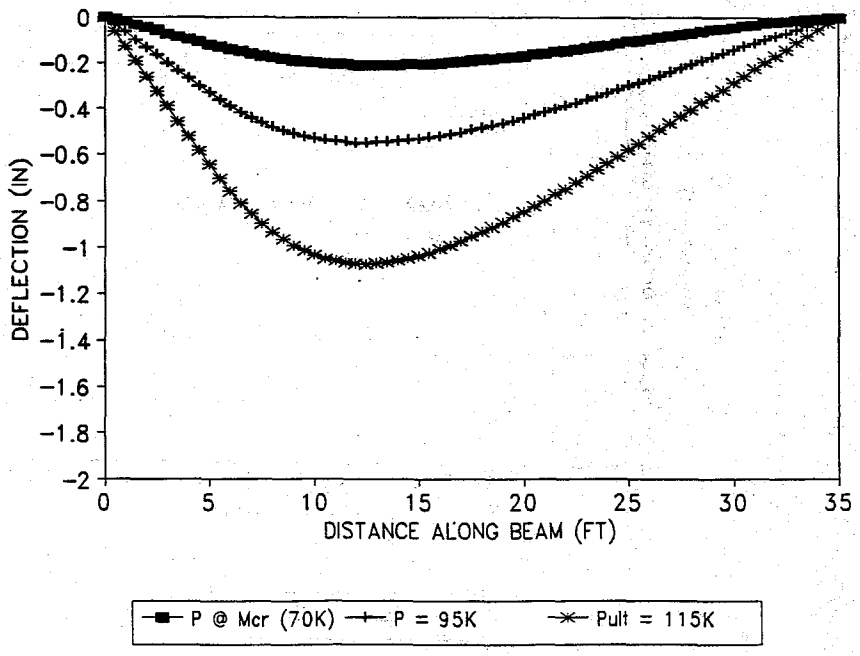

Figure 5-16. Deflected Shape (UF2-30-LD)

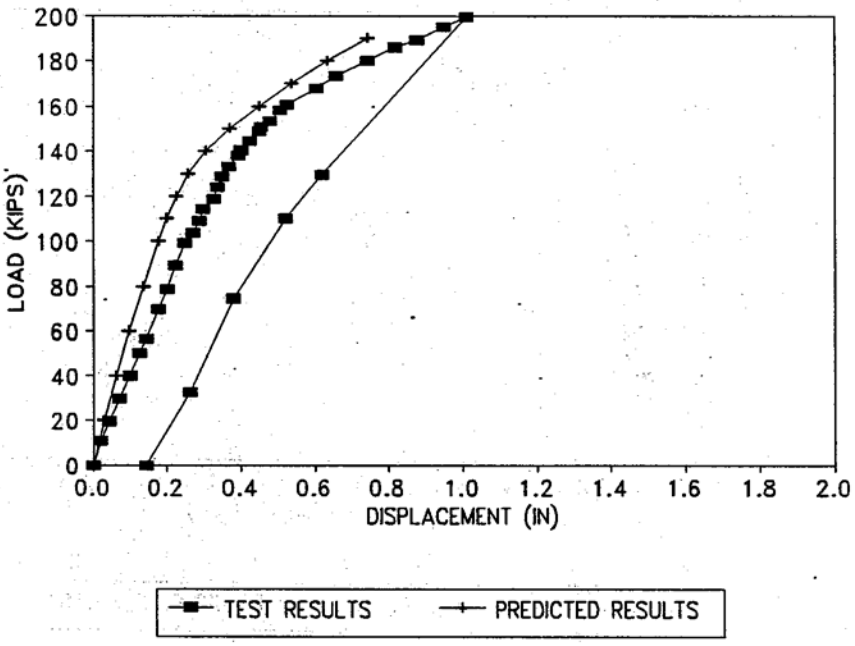

Figure 5-17. P-Delta Comparison (UF1-30-2D)

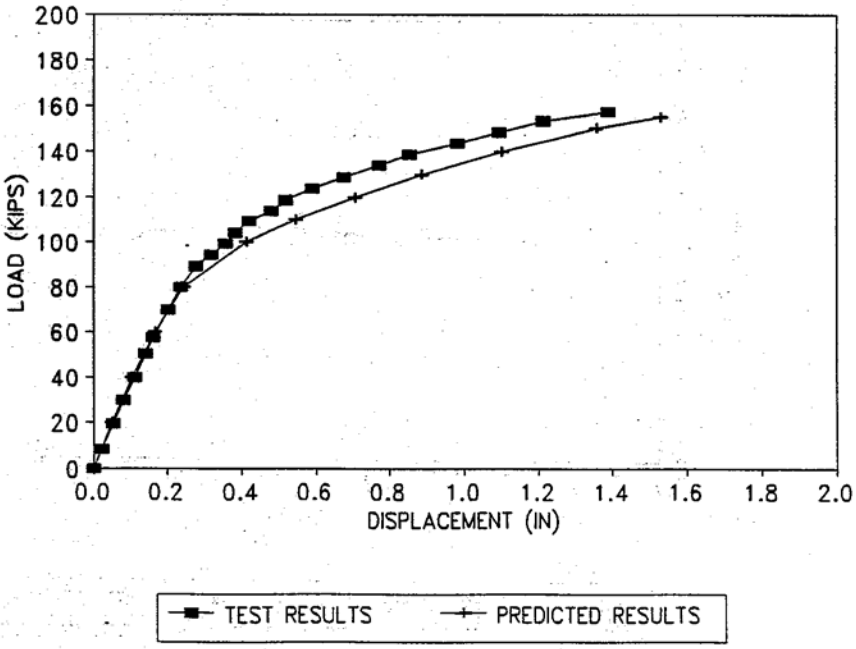

Figure 5-18. P-Delta Comparison (UF1-30-LD)

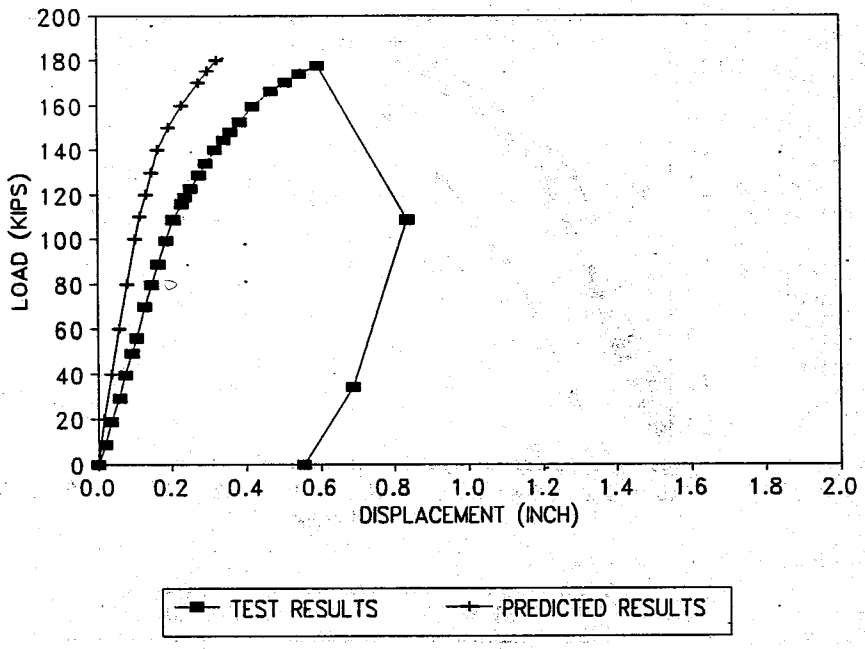

Figure 5-19. P-Delta Comparison (UF2-30-2D)

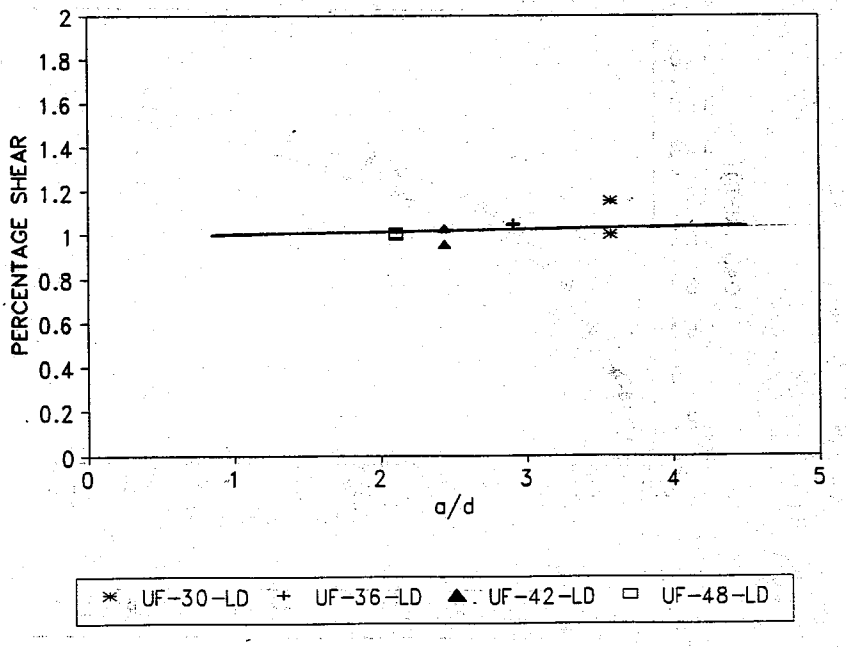

Figure 5-20. Percentage Shear vs. Aspect Ratio

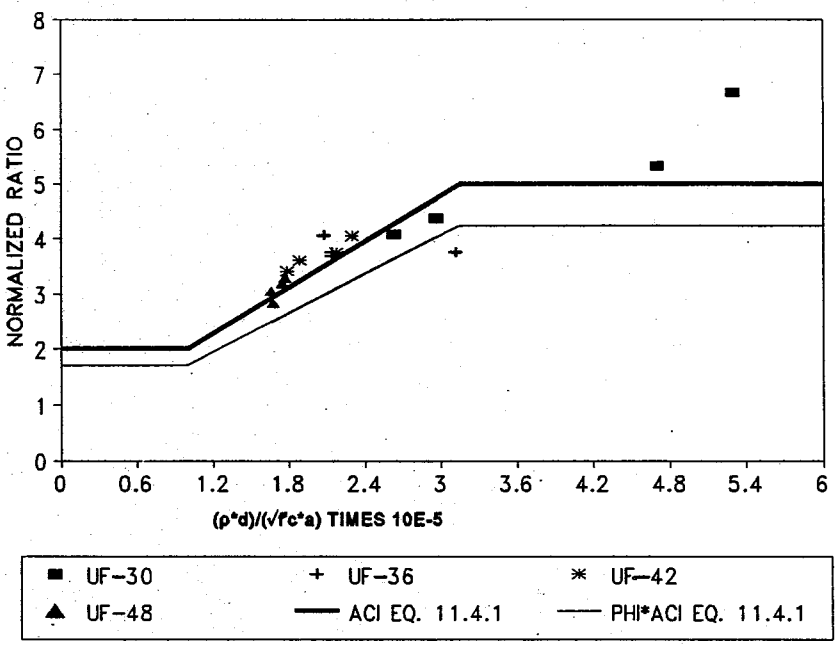

Figure 5-21. ACI Equation vs. Experimental Results

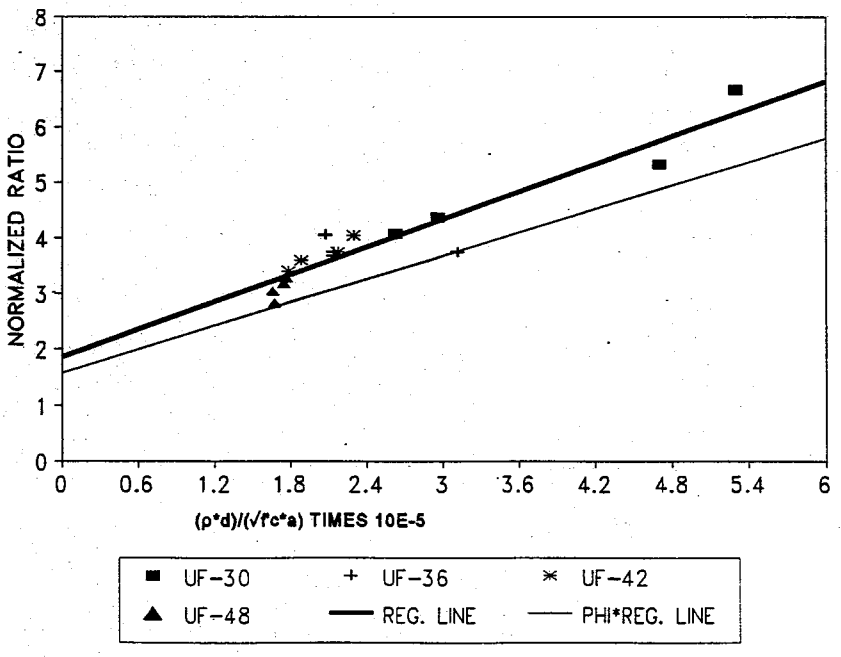

Figure 5-22. Regression Analysis of Experimental Results

CHAPTER 6
SUMMARY, CONCLUSIONS

6.1 Summary

6.1.1 General Information

The objectives of this project outlined in Chapter 1.3.2 were accomplished by testing a series of 8 beams at each end for a total of 16 individual tests. This was done by holding the testing point of 77 inches (LD) a constant at one end of the beam and testing the other end at twice its effective depth (2D). Both ends of each beam were instrumented with internal and external strain gauges to collect data to study the effects of shear forces. Only one end of each beam was instrumented with strain gauges along the tendon centroid in order to measure the transfer and development lengths.

6.1.2 Testing Performed at 2D

The beams, tested at 2D, had low shear span to depth ratios ($a/d < 2.5$) resulting in shear stresses becoming dominant. As seen from the analysis in Chapter 5 the behavior of these beams is governed by strut and tie action due to the presence of the disturbed regions. The majority of the load is carried by a major compression diagonal, thus the web reinforcement was never fully mobilized. Therefore, the capacity of the sections is governed by the strength of the concrete and the load required to develop diagonal cracks.

The presence of the shear cracks in these beams appeared to deteriorate the bond stress between the tendons and the surrounding concrete. As the shear cracks formed there were sudden increases in tendon slip in every case. In the cases when excessive tendon slip occurred there was also the simultaneous formation of a flat shear crack which split along the tendon centroid or a separate horizontal crack formed at the tendon centroid. The location and orientation of these cracks is an indication of a bond failure taking place. The failure mechanism of these beams tended to be more brittle than the beams tested at LD.

6.1.3 Testing Performed at LD

The 30 and 36 inch beams tested at LD had a shear span to depth ratio greater than 2.5 allowing the shear flow to be uninterrupted by a disturbed region. Therefore, they had a chance to develop a compression field which was evident from the generation of tensile strain in the stirrups in every case.

The formation and propagation of shear cracks in these beams resulted in loss of bond between the strand and the concrete which led to significant tendon slip. Increasing the load resulted in failure of the beam from excessive crack. widths and flexural and shear cracks leading to excessive crushing of the concrete near the loading point and significant reduction of the compression zone. The failure of these beams tended to be more ductile than the beams tested at 2D.

6.1.4 Transfer Length

The experimental transfer lengths were compared with analytical predictions presented by the ACI/AASHTO code, Zia and Mostafa and by Shahawy. The comparison between the measured results, and the analytical predictions is presented in Table 4-1. It can be seen from Table 4-1 that the present ACI/AASHTO code equation far transfer length, $(f/3)d_b$, appears to be unconservative. The calculated values based on the ACI equations underestimate the measured transfer length by an average, of 38%.

In the report presented by Shahawy, he suggested that the value of f_{si} be used instead of f_{se} in the ACI/AASHTO equation for transfer length. This equation provides a much closer approximation of the actual transfer length with results an average of 10% less than the experimental.

The equation presented by Zia and Mostafa has been accepted to be applicable for concrete strengths ranging from 2,000 to 8,000 psi. This is evident by the relatively close comparison in l_t for UF2-36 as shown in Table 4-1. This equation gives comparable results to the ACI/AASHTO code for low concrete strengths at transfer but as the concrete strengths increase the results become increasingly more unconservative.

6.1.5 Effect of Shear Force on Longitudinal Bond Slip

The comparison of shear force at first longitudinal tendon slip and shear force at first appearance of diagonal cracks was presented in Chapter 5. The ratio of the shear force when a longitudinal strand slipped considerably to the shear force when the first diagonal crack appeared, always seems to be greater than one. The formation of diagonal cracks always precedes longitudinal tendon slip. At the appearance of a diagonal crack

the loading was stopped. Usually longitudinal slip was observed with the next increment of load.

6.2 Conclusions

Based on the results of this tests, the following conclusions have been drawn:

1) The modified compression field theory provides a rational and comprehensive analytical procedure for analyzing prestressed concrete members with shear span to depth ratios greater than 2.5. The strut and tie mode proved to be an acceptable method of analysis for prestressed concrete members subjected to loading conditions with a shear span to depth ratio less than 2.5.

   Attention should be given to ensuring the development of: a compression field and avoiding the formation of a strut and tie which tends to produce a brittle failure. The development of a uniform compression field can be accomplished by providing sufficient amount. of hear reinforcement within the development length region of a beam. Additional detailing requirements should be such that adequate shear reinforcement is provided in order to develop the full capacity of the beam and a compression field.

2) The ACI/AASHTO equations.-for transfer length should be reevaluated. The suggestion of using $f_{si}/3$ instead of $f_{se}/3$ appears to provide a closer comparison with test results.

3) Tendon slip and shear forces appear to be related. There appears to be a direct correlation between the formation of shear cracks and the initiation of a bond slip. This is evident from the sudden increases in tendon slip that occurred immediately

after the formation of diagonal shear cracks as well as the horizontal cracking along the tendon centroid in the test beams. Deep beams with a/d less than 1 tend to develop inclined cracks that join the load and the support which, in effect, destroy the horizontal shear flow from the longitudinal steel to the compression zone. Thus, the behavior changes from beam to arch action. In this type of beam the most common mode of failure is an anchorage failure at the ends of the reinforcement. The lowest aspect ratio (a/d) of the test beams was 2 and none of the test beams collapsed due to loss of bond in the anchorage region.

APPENDIX A

CRACKING PATTERN OF SPECIMENS

The following pages are the sketches of the cracks as they appear in the photographs taken.

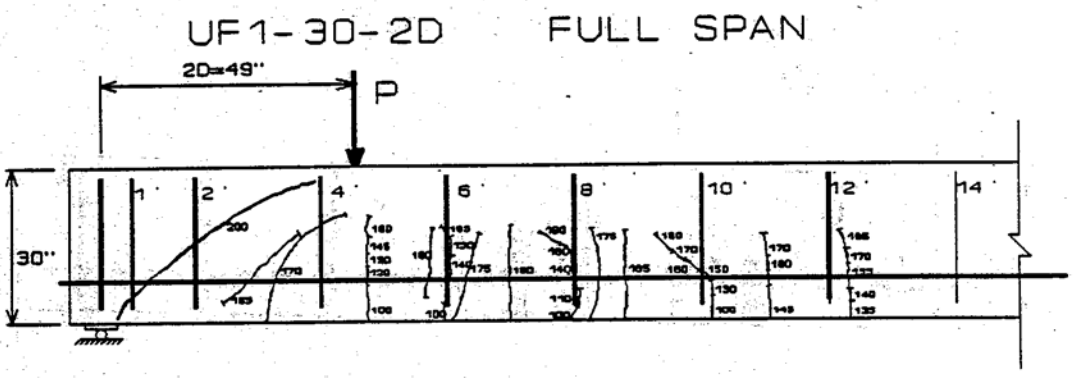

A-1. Cracking Pattern, UF1-30-2D

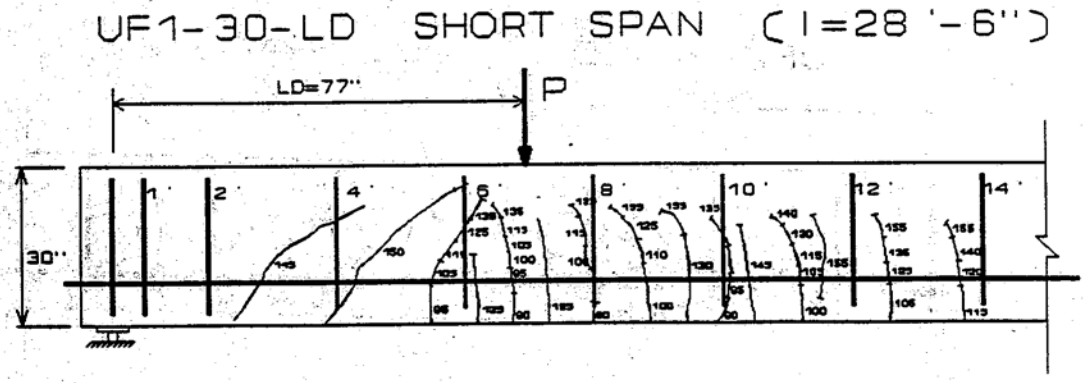

A-2. Cracking Pattern, UF1-30-LD

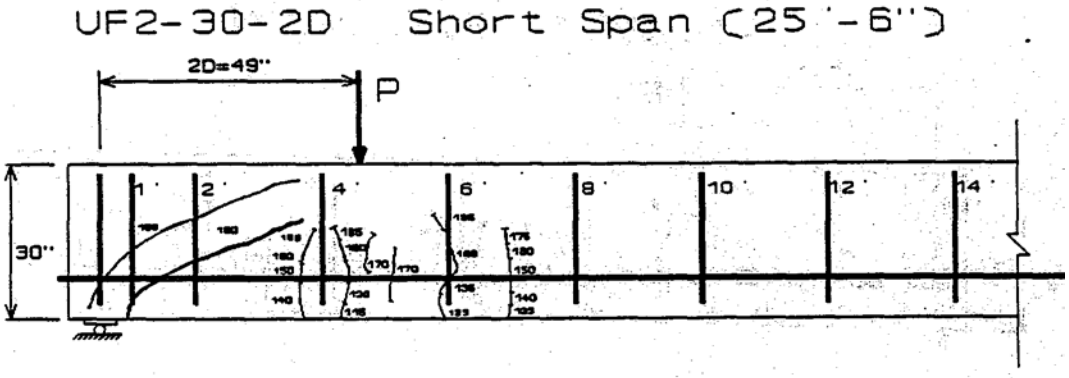

A-3. Cracking Pattern, UF2-30-2D

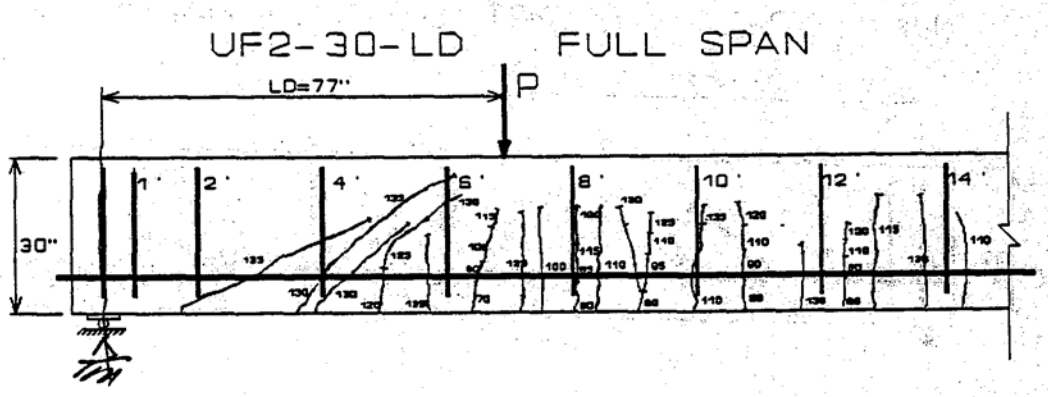

A-4. Cracking Pattern, UF2-30-LD

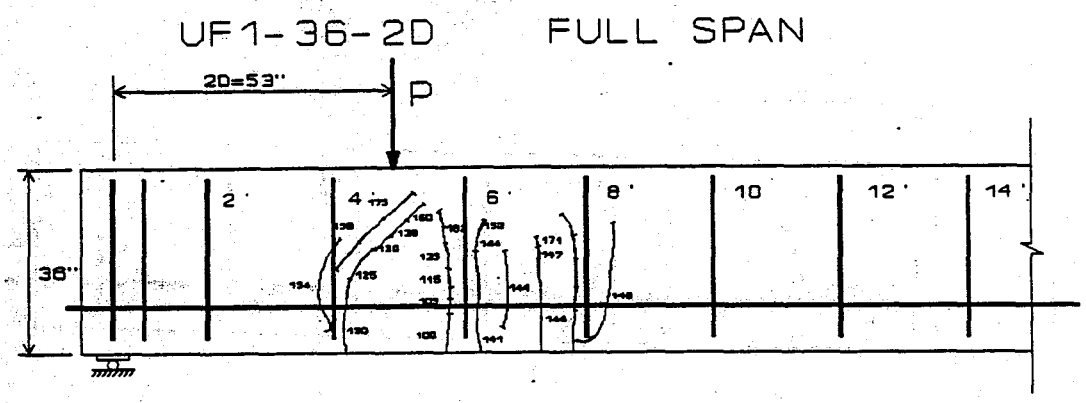

A-5. Cracking Pattern, UF1-36-2D

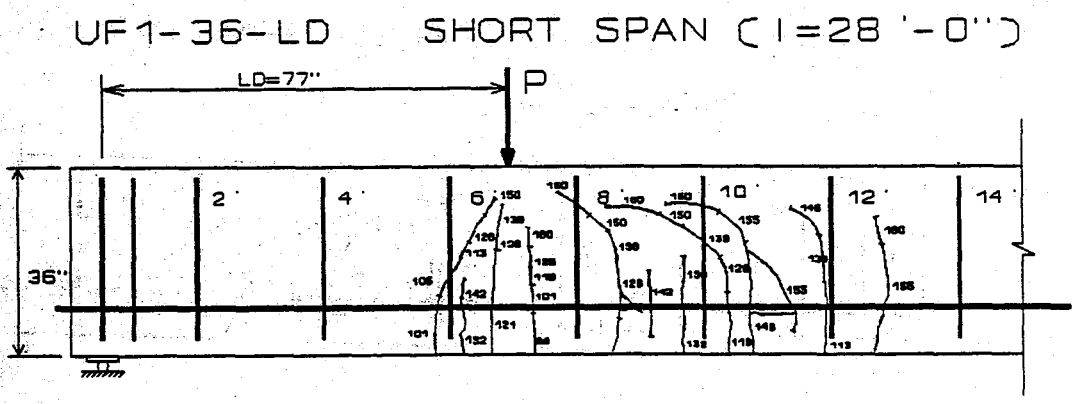

A-6. Cracking Pattern, UF1-36-LD

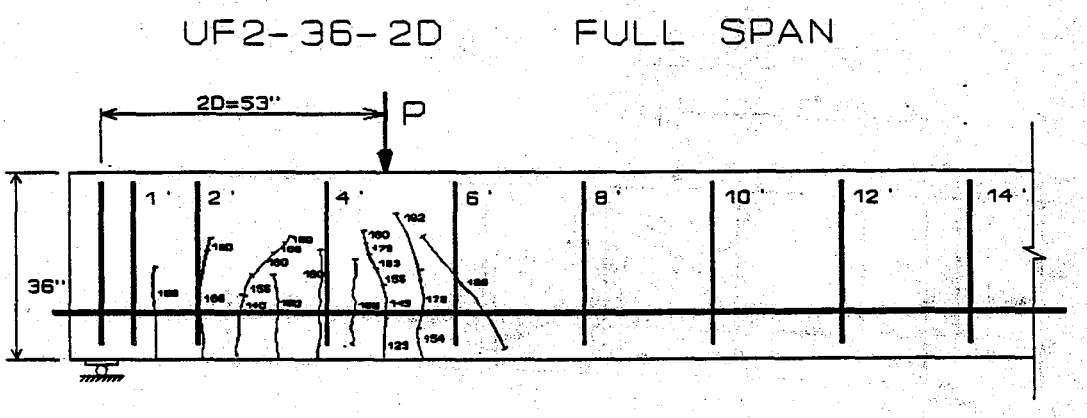

A-7. Cracking Pattern, UF2-36-2D

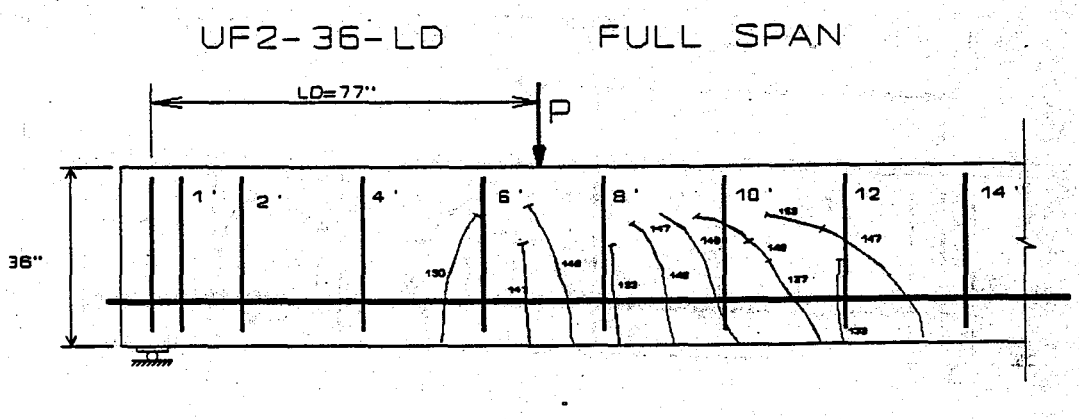

A-8. Cracking Pattern, UF2-36-LD

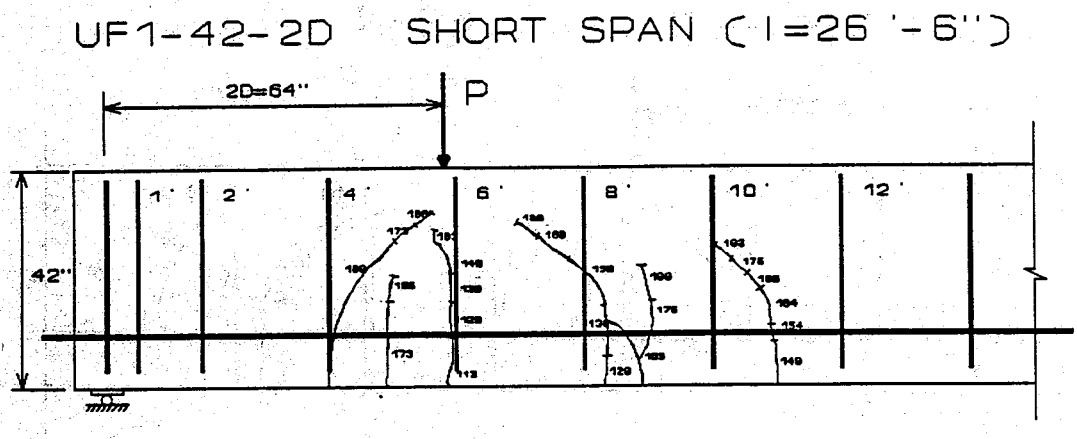

A-9. Cracking Pattern, UF1-42-2D

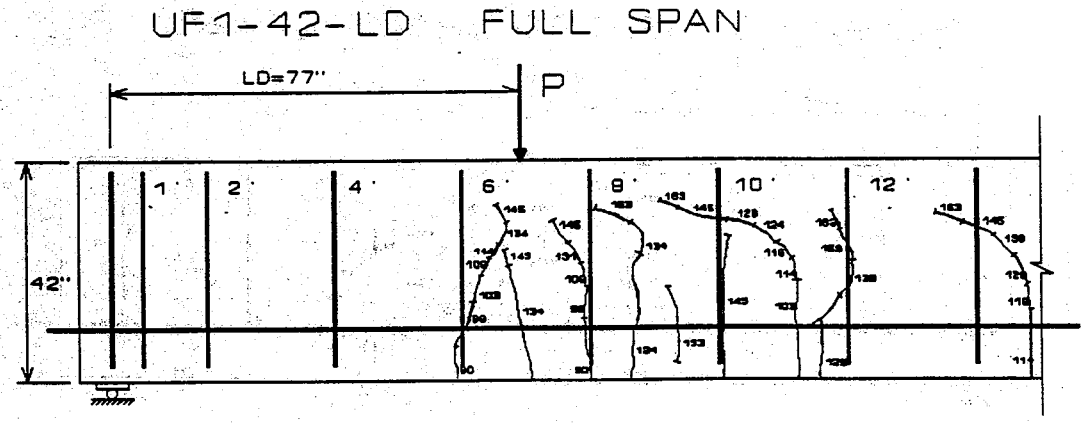

A-10. Cracking Pattern, UF1-42-LD

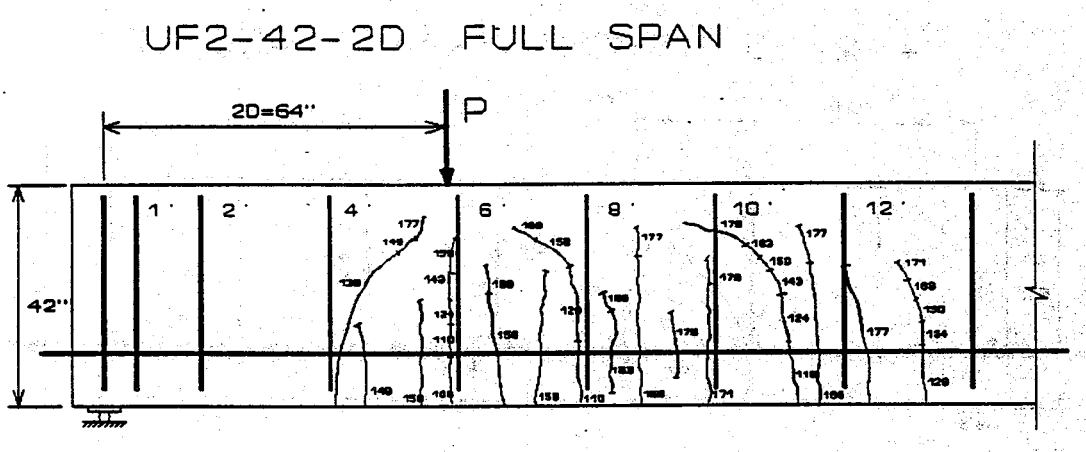

A-11. Cracking Pattern, UF2-42-2D

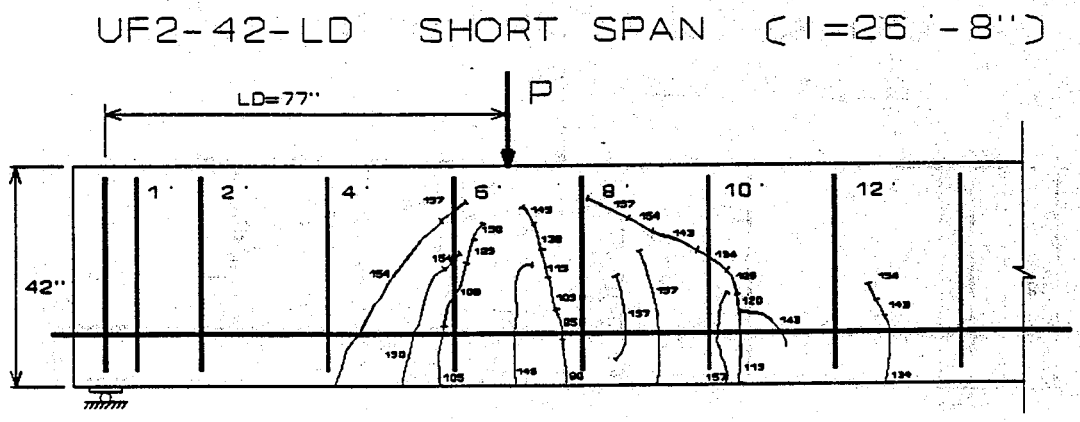

A-12. Cracking Pattern, UF2-42-LD

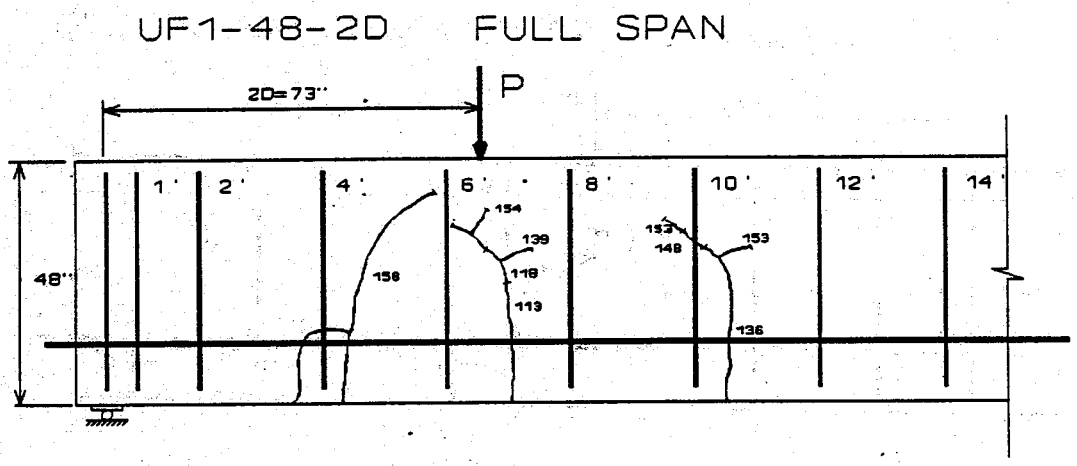

A-13. Cracking Pattern, UF1-48-2D

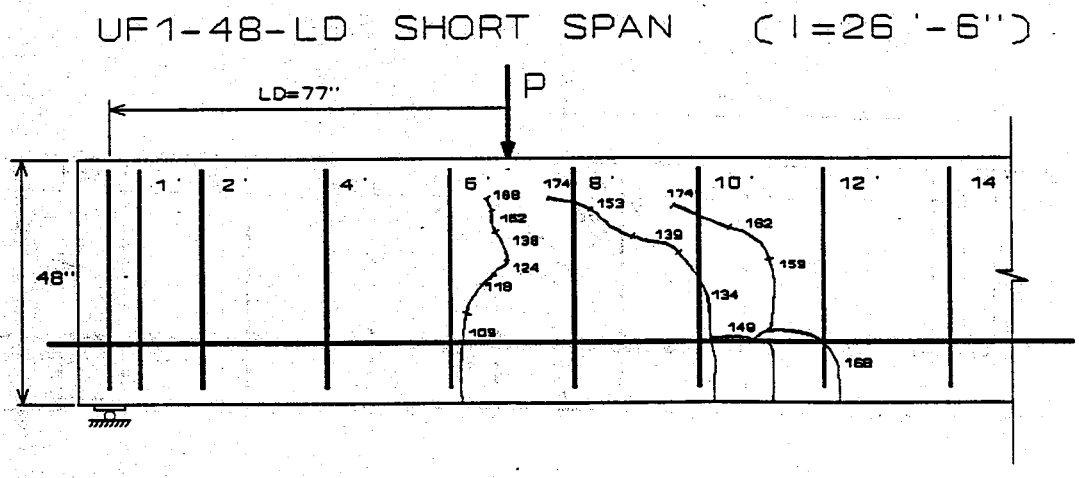

A-14. Cracking Pattern, UF1-48-LD

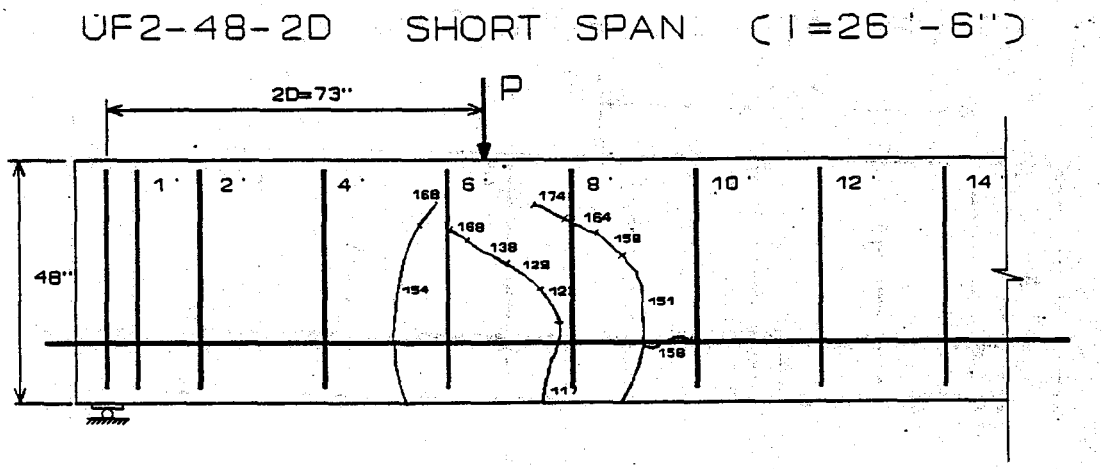

A-15. Cracking Pattern, UF2-48-2D

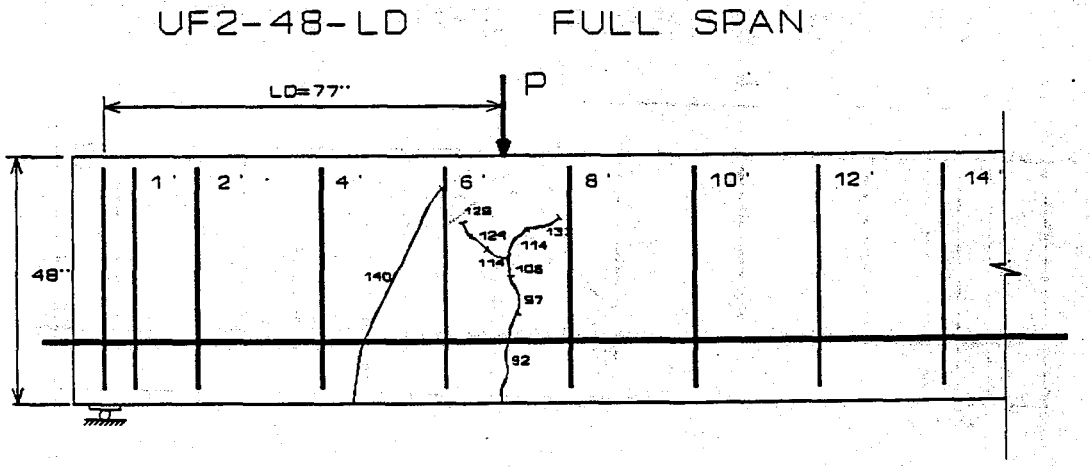

A-16. Cracking Pattern, UF2-48-LD

APPENDIX B
CONCRETE MIX DESIGN

The concrete that was used to construct these test beams was provided by Gate Concrete Products Company located in Jacksonville, Florida. The concrete used for each beam was a Class III 5000 psi mix.

SOURCES OF MATERIALS

Coarse aggregate:	Tarmac Florida, Inc.	Grade 67
Fine aggregate:	Florida Rock Industries	
Pit no. (coarse):	87-145	Type: Limestone
Pit no. (fine):	71-132	Type: Silica-Sand
Cement:	Tarmac Type I	Spec: AASHTO-M22
lst Admixture:	Master Builders 100-XR	Spec: ASTM C-494

QUANTITIES OF MATERIALS

Cement (1bs.):	611
Coarse aggregate (1bs.):	2013
Fine aggregate (1bs.):	1078
1st Admixture (oz.):	17
Water (gal.):	27.9
Water (1bs.):	232
Slump range (in.):	1-4
Unit weight (wet):	145.7 pcf
Water cement ratio (1bs./1bs.):	0.38
Maximum allowable w/c (field):	0.38
Theoretical yield (cu. ft.):	27

APPENDIX C
GRAPHICAL REPRESENTATION OF DEFLECTED SHAPES

The deflected shapes for every test are presented in Figures C-1 through C-16. The deflected shapes for the load at initial cracking, the failure load and an intermediate load are shown in each graph. The graphs were developed based on the analysis presented in Chapter 5.

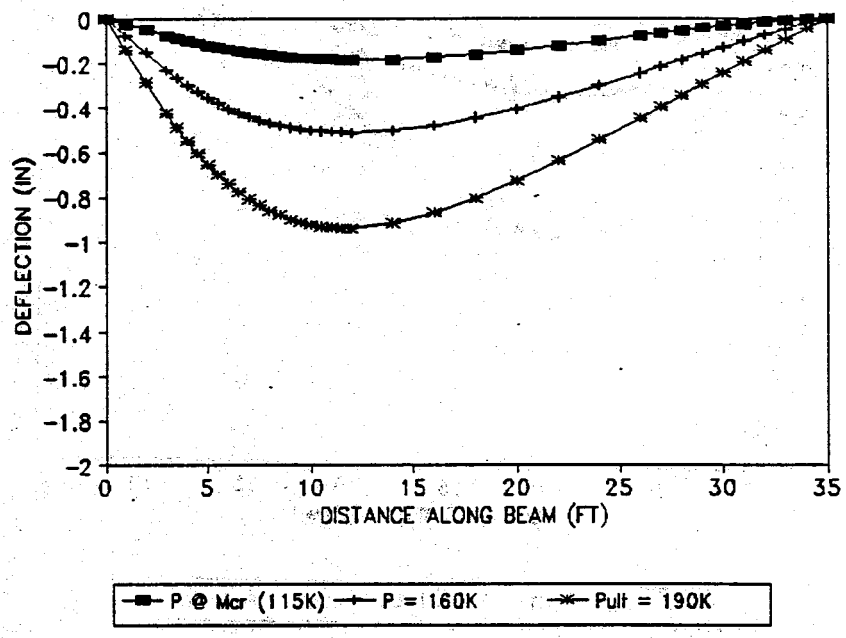

C-1. Deflected Shape (UF1-30-2D)

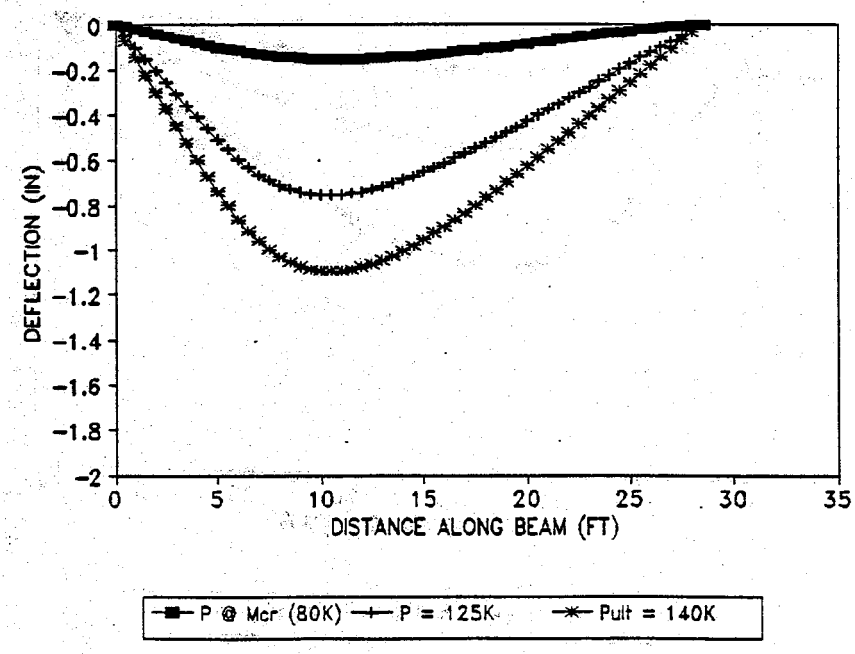

C-2. Deflected Shape (UF1-30-LD)

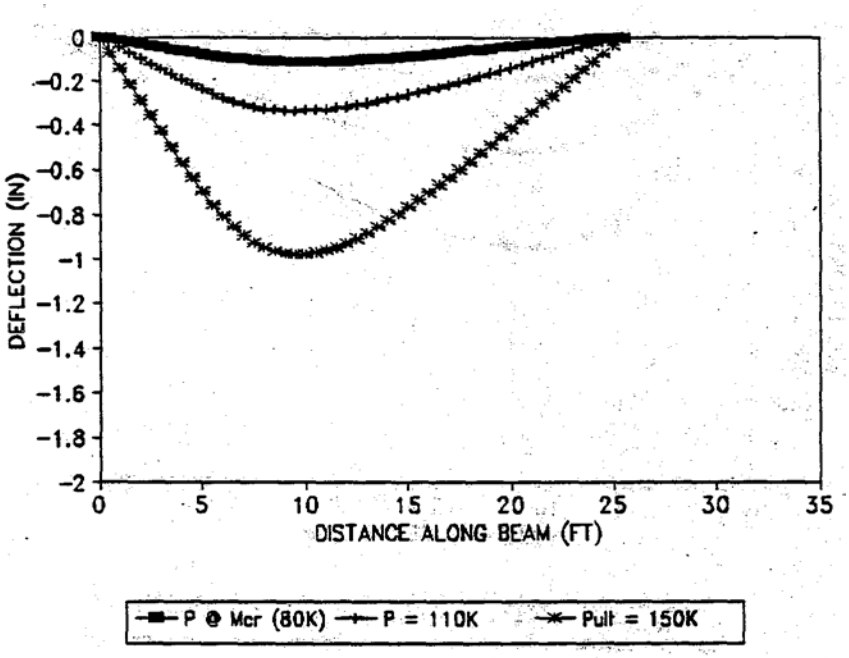

C-3. Deflected Shape (UF2-30-2D)

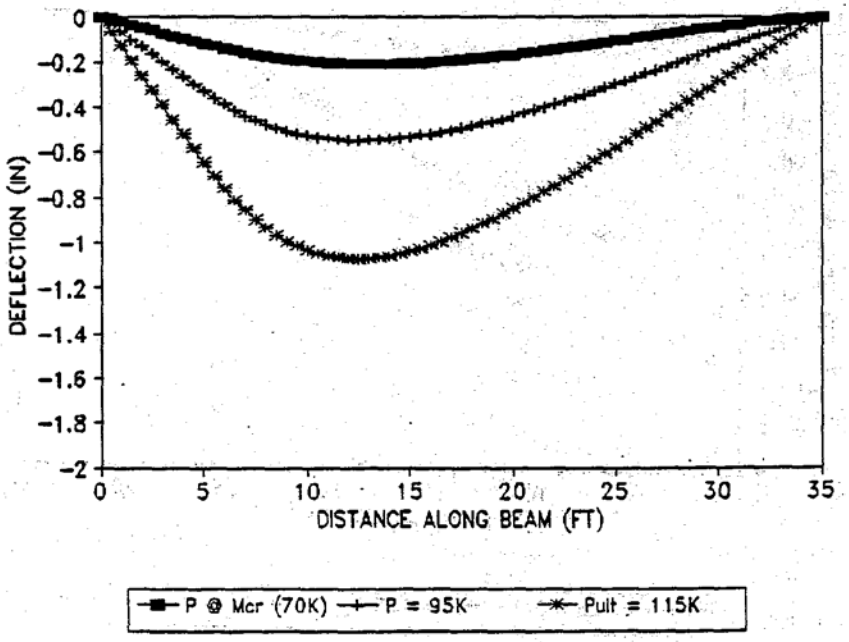

C-4. Deflected Shape (UF2-30-LD)

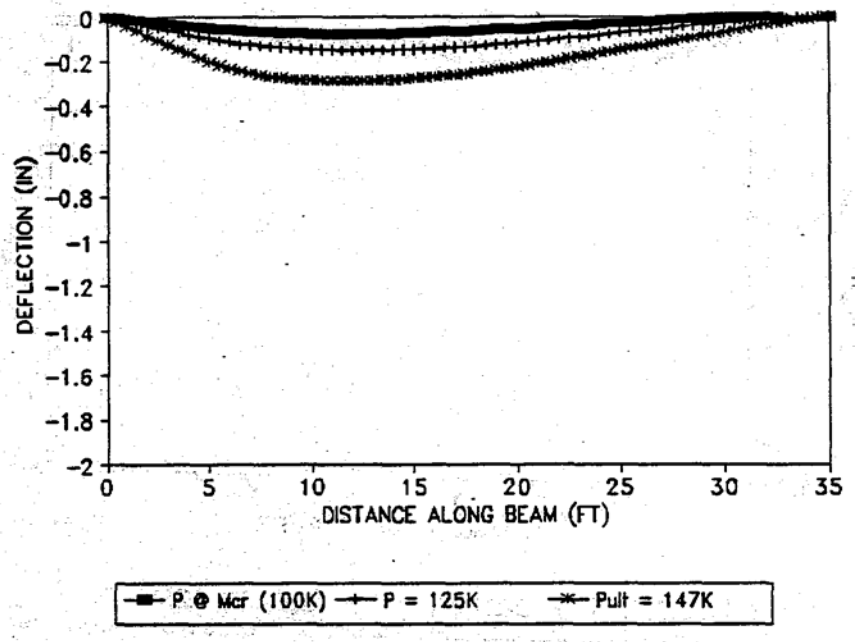

C-5. Deflected Shape (UF1-36-2D)

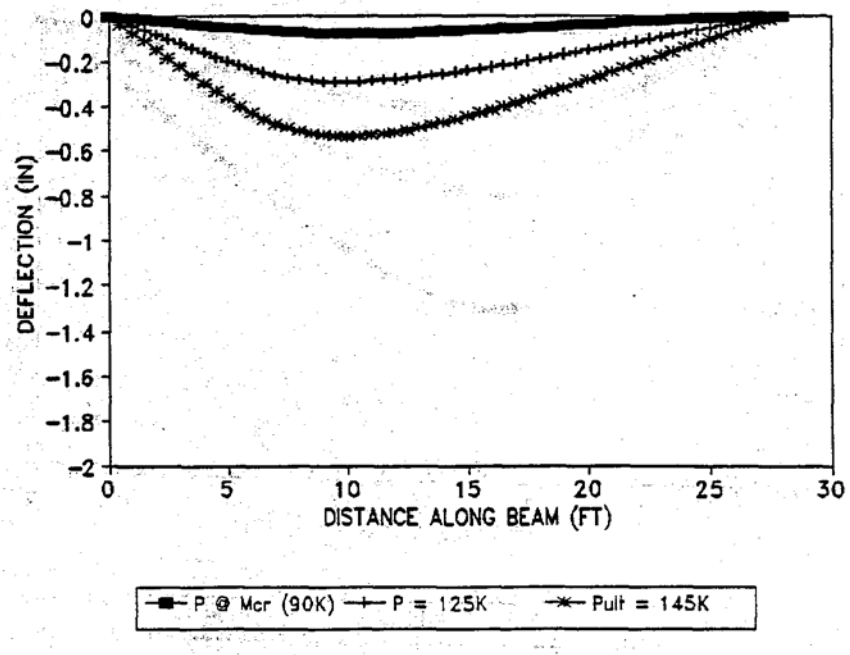

C-6. Deflected Shape (UF1-36-LD)

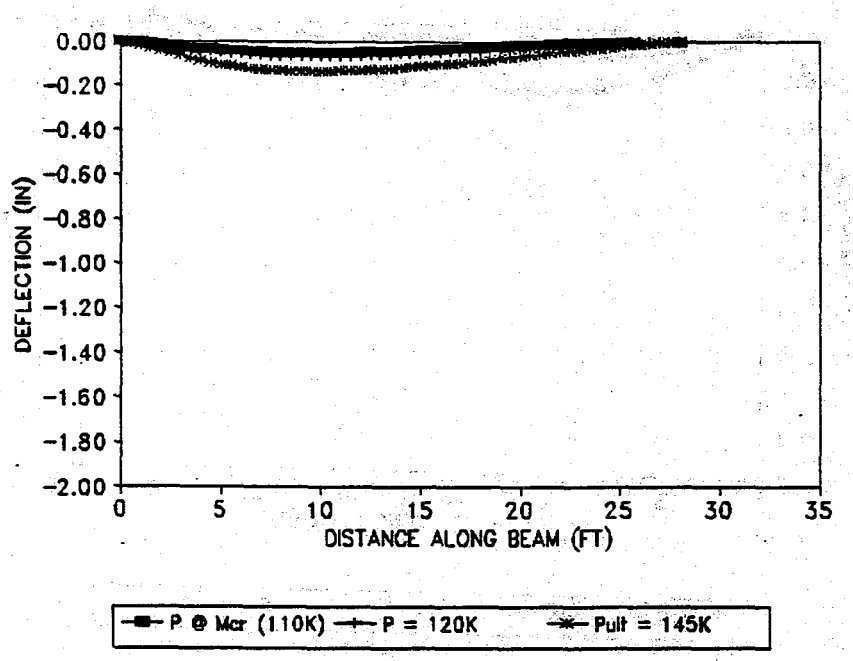

C-7. Deflected Shape (UF2-36-2D)

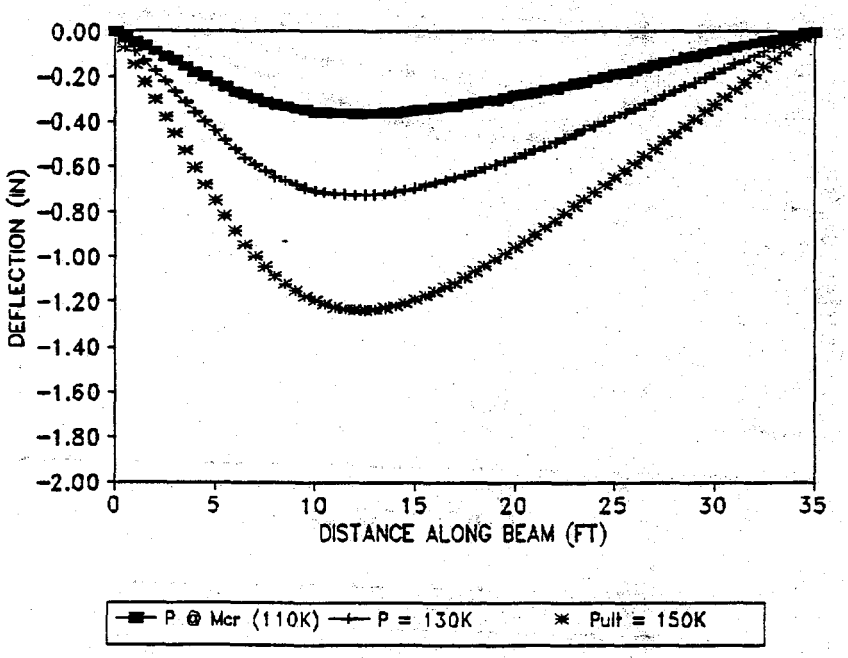

C-8. Deflected Shape (UF2-36-LD)

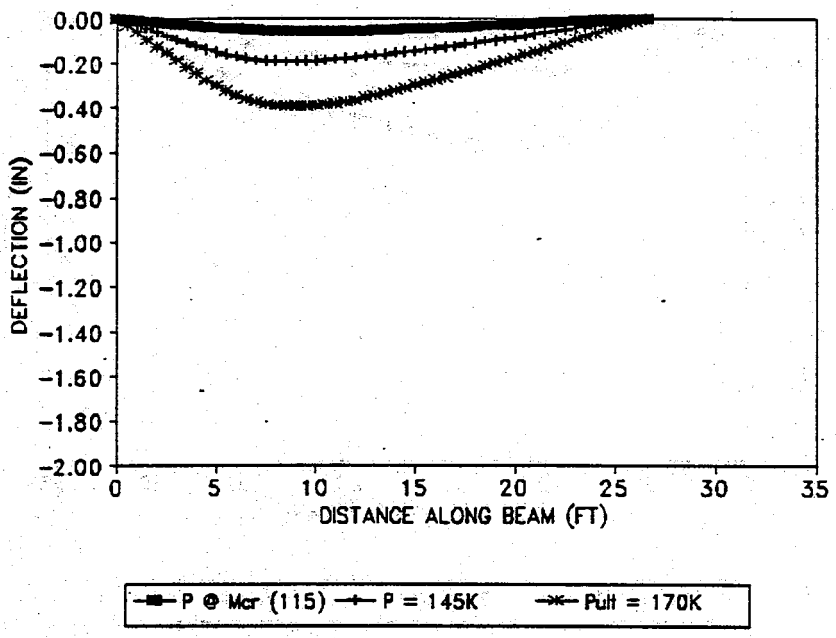

C-9. Deflected Shape (UF1-42-2D)

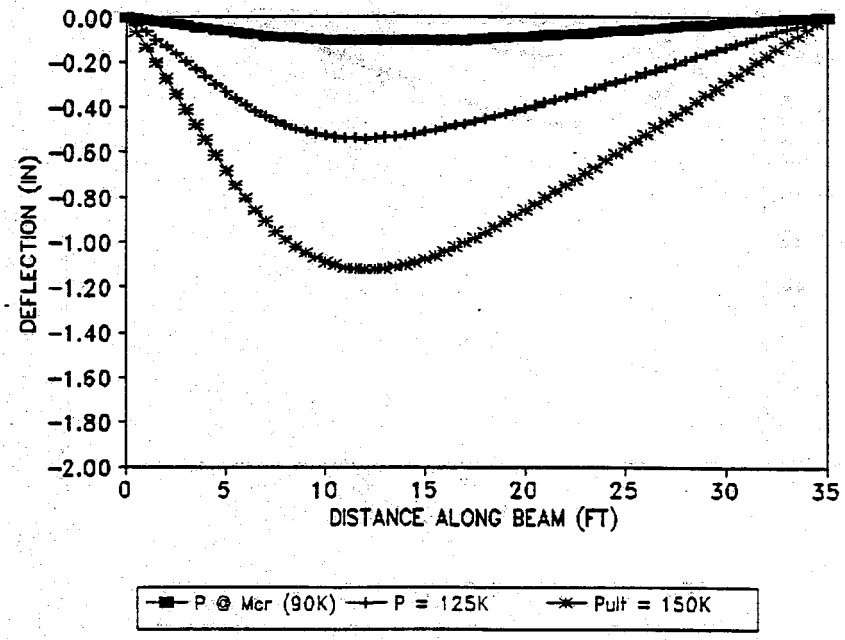

C-10. Deflected Shape (UF1-42-LD)

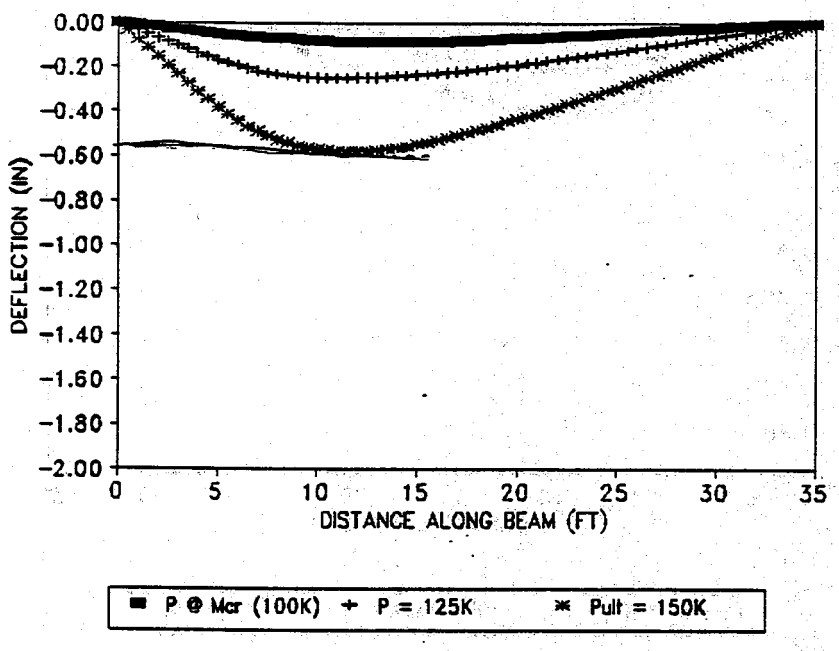

C-11. Deflected Shape (UF2-42-2D)

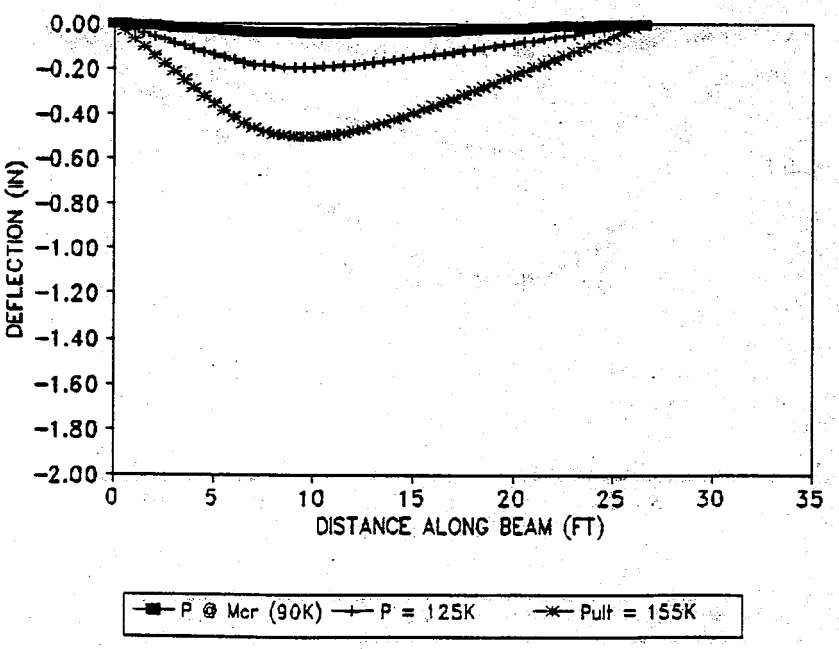

C-12. Deflected Shape (UF2-42-LD)

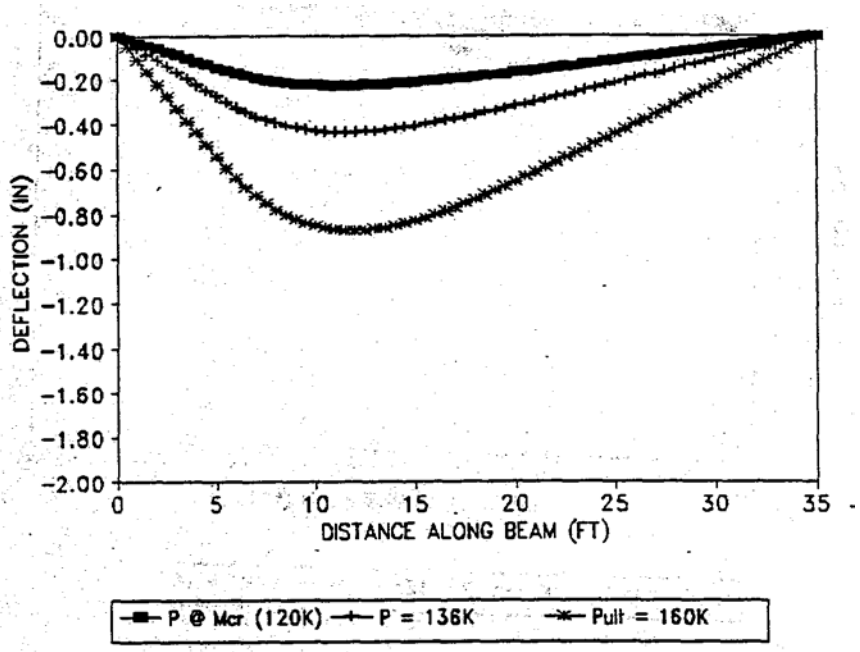

C-13. Deflected Shape (UF1-48-2D)

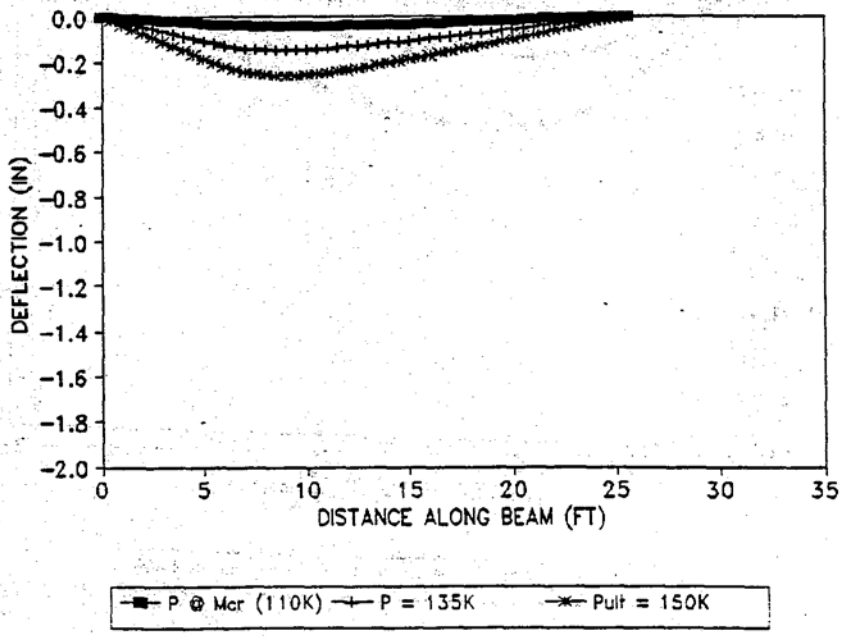

C-14. Deflected Shape (UF1-48-LD)

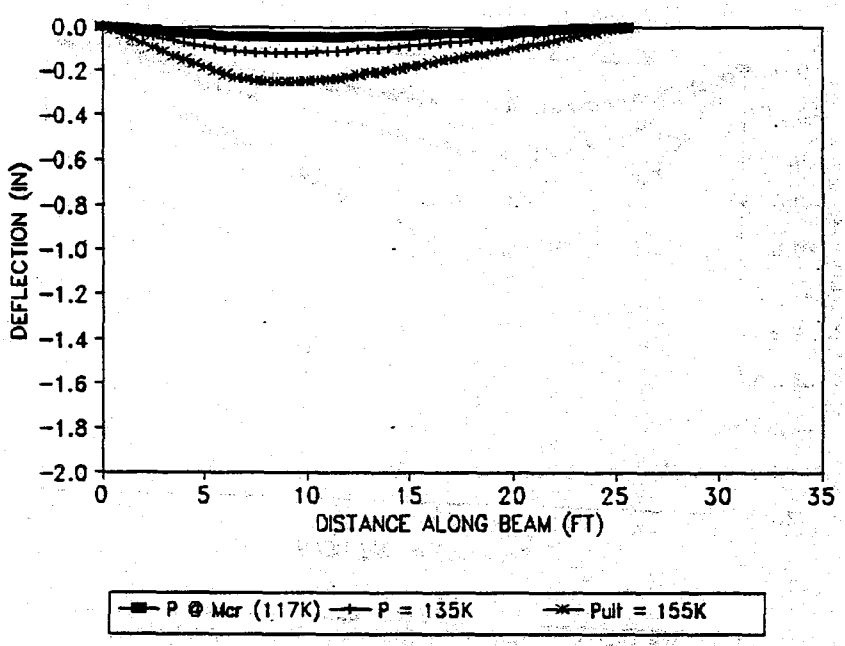

C-15. Deflected Shape (UF2-48-2D)

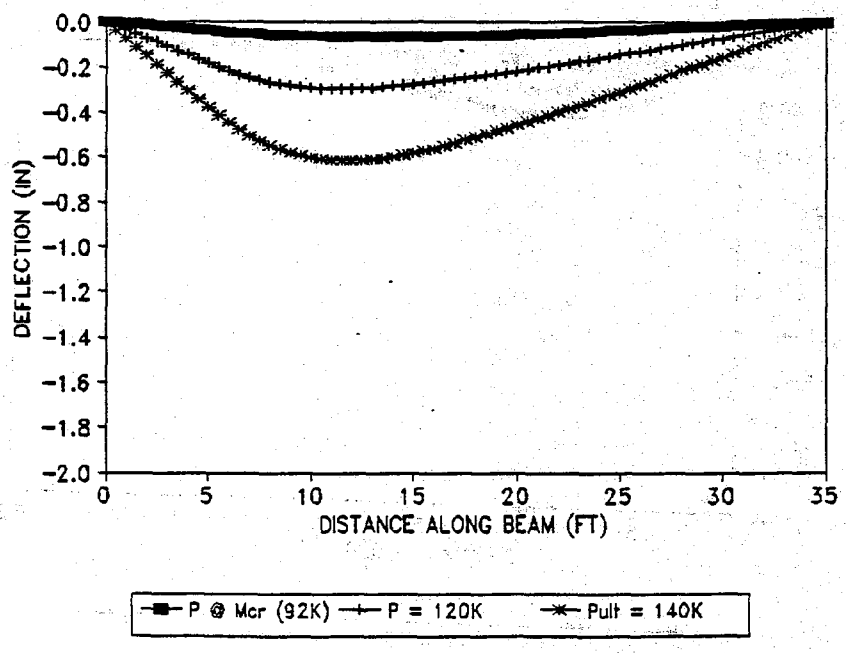

C-16. Deflected Shape (UF2-48-LD)

APPENDIX D
P-DELTA COMPARISON

The experimental and predicted P-Delta curves are compared in Figures D-1 through D-16. These values are compared at a point offset 1 foot towards midspan from the point where the load was applied.

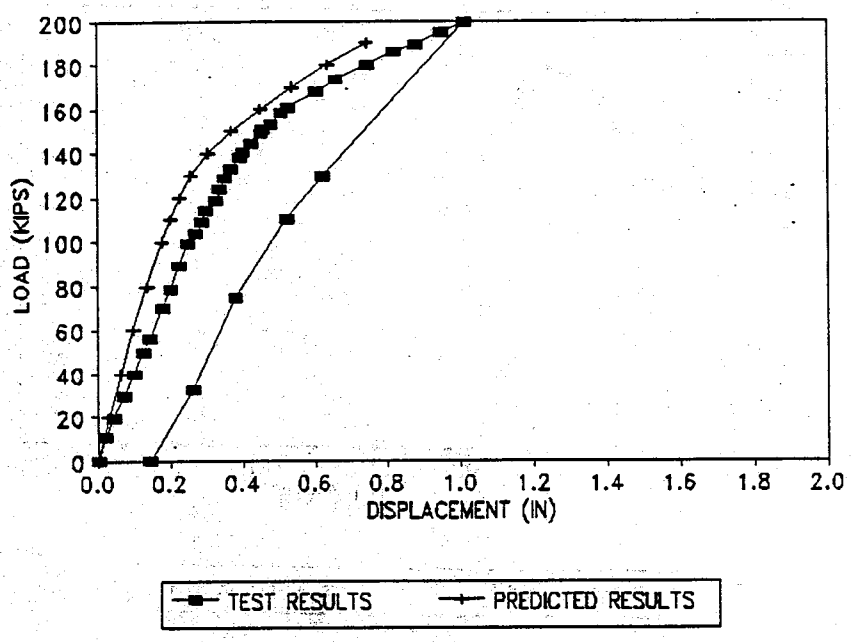

D-1. P-Delta Comparison (UF1-30-2D)

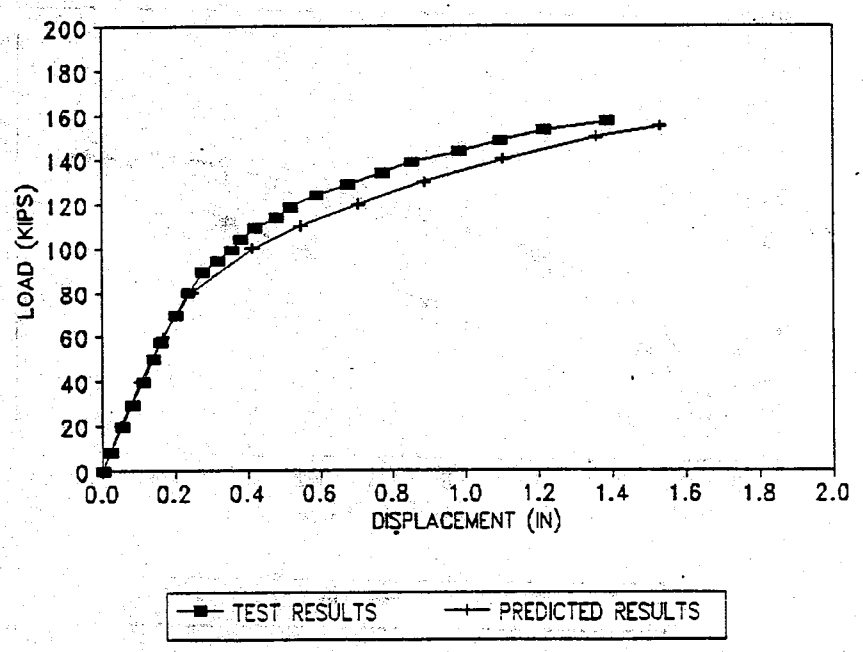

D-2. P-Delta Comparison (UF1-30-LD)

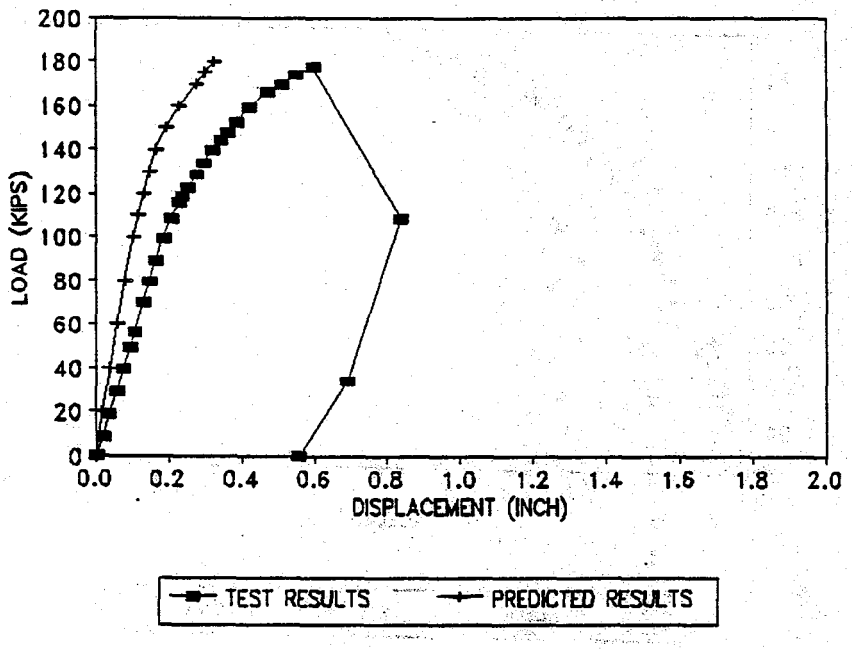

D-3. P-Delta Comparison (UF2-30-2D)

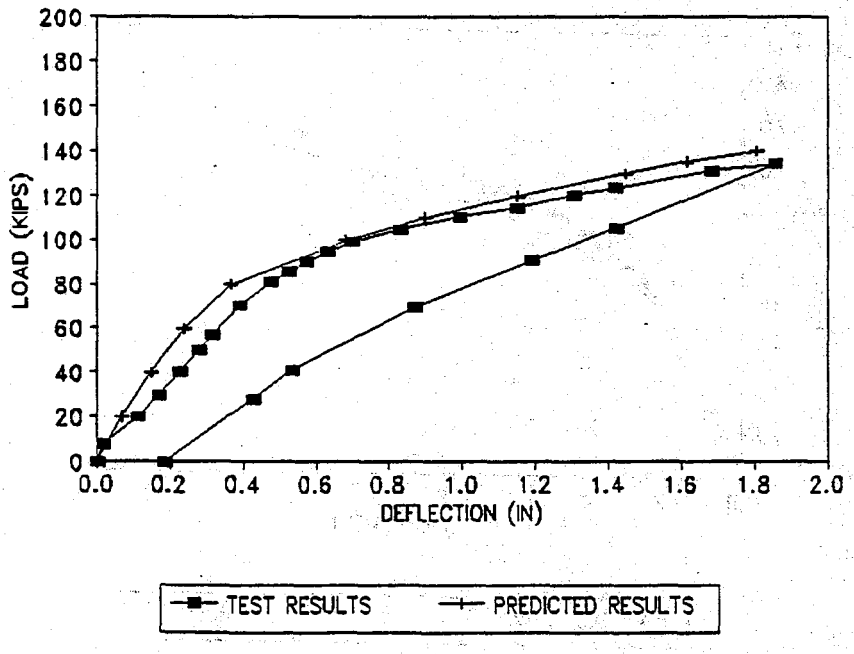

D-4. P-Delta Comparison (UF2-30-LD)

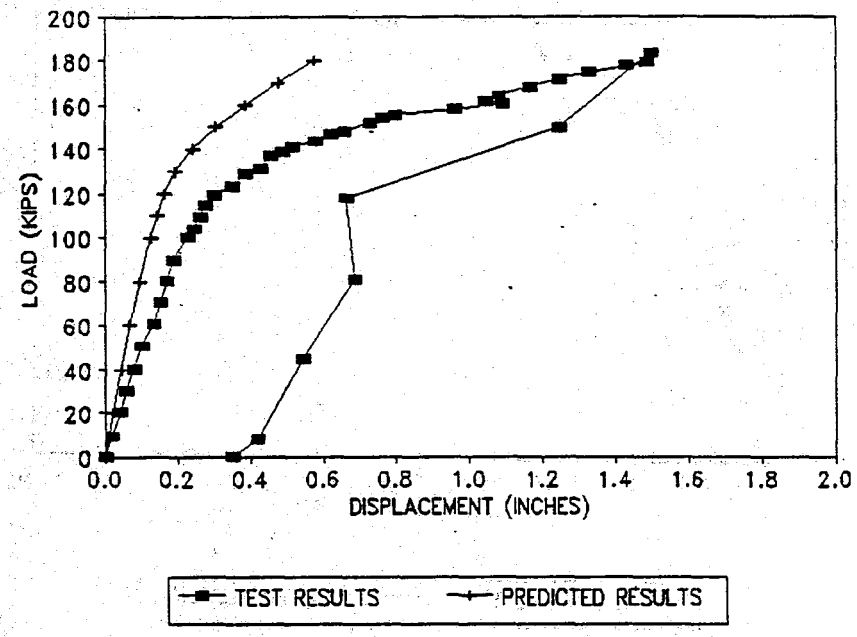

D-5. P-Delta Comparison (UF1-36-2D)

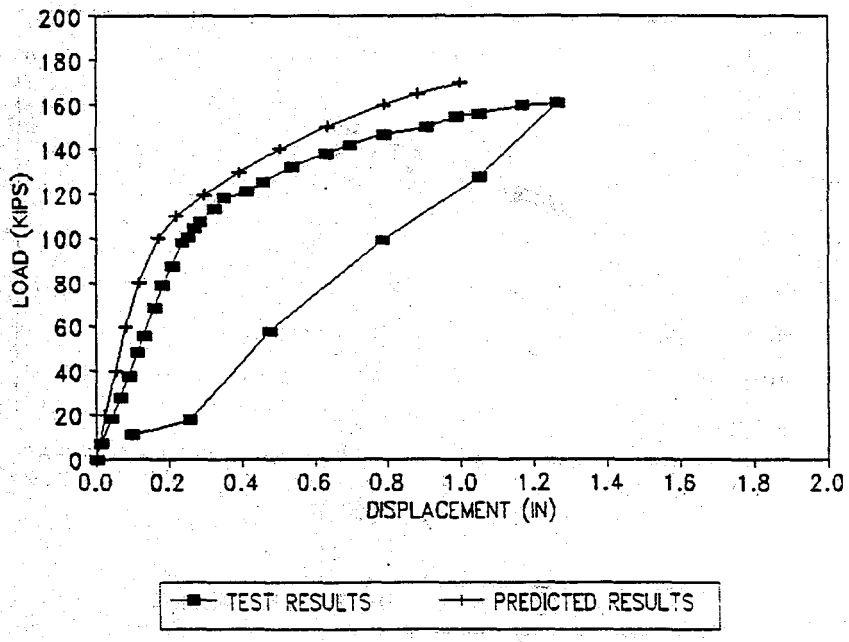

D-6. P-Delta Comparison (UF1-36-LD)

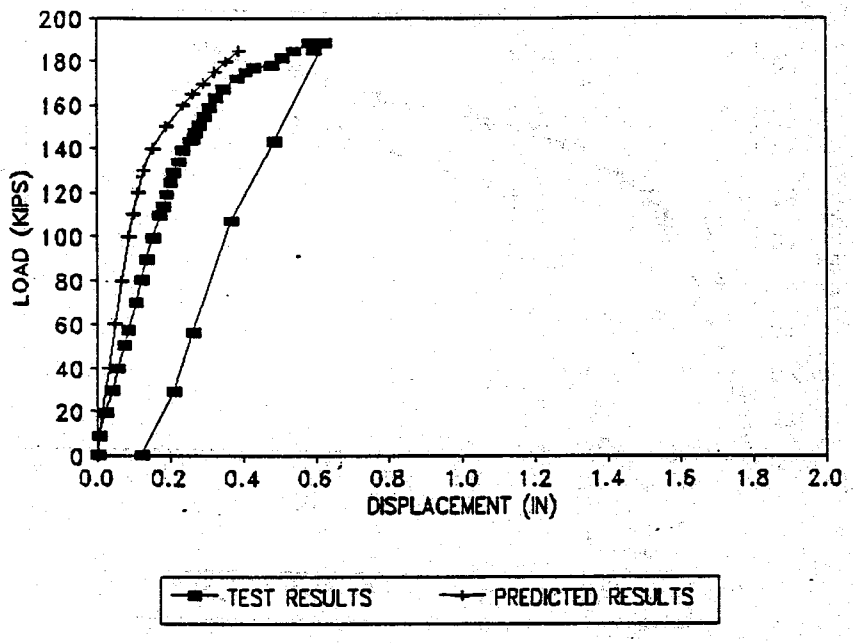

D-7. P-Delta Comparison (UF2-36-2D)

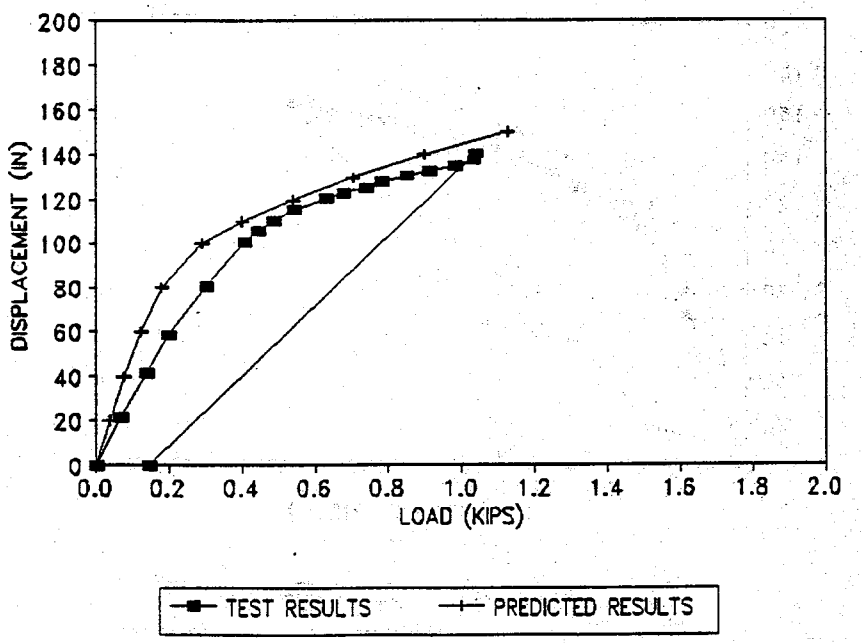

D-8. P-Delta Comparison (UF2-36-LD)

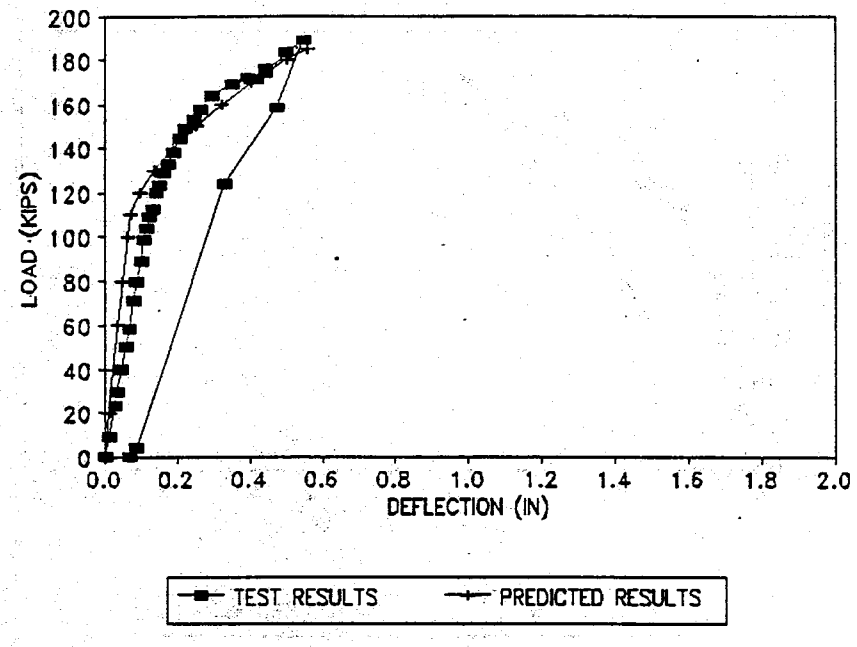

D-9. P-Delta Comparison (UF1-42-2D)

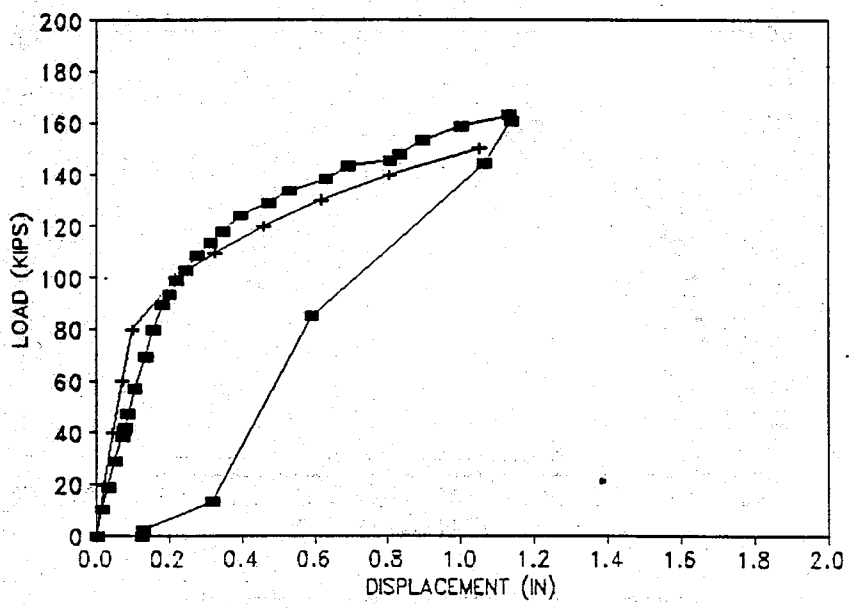

D-10. P-Delta Comparison (UF1-42-LD)

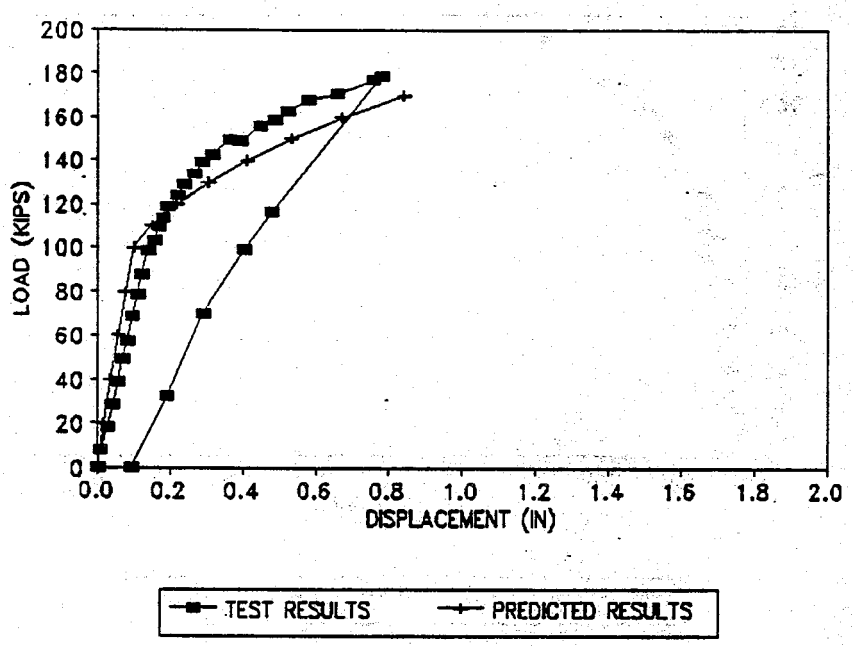

D-11. P-Delta Comparison (UF2-42-2D)

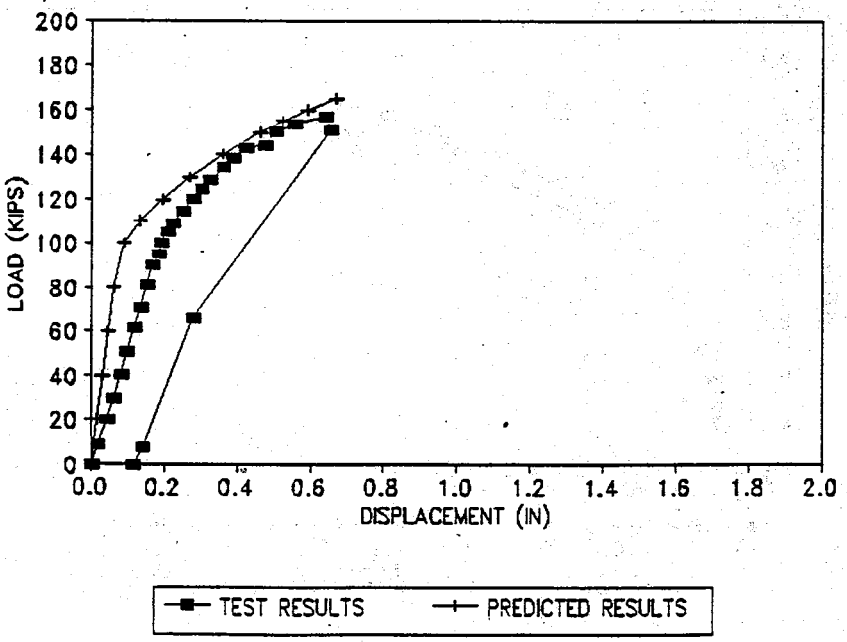

D-12. P-Delta Comparison (UF2-42-LD)

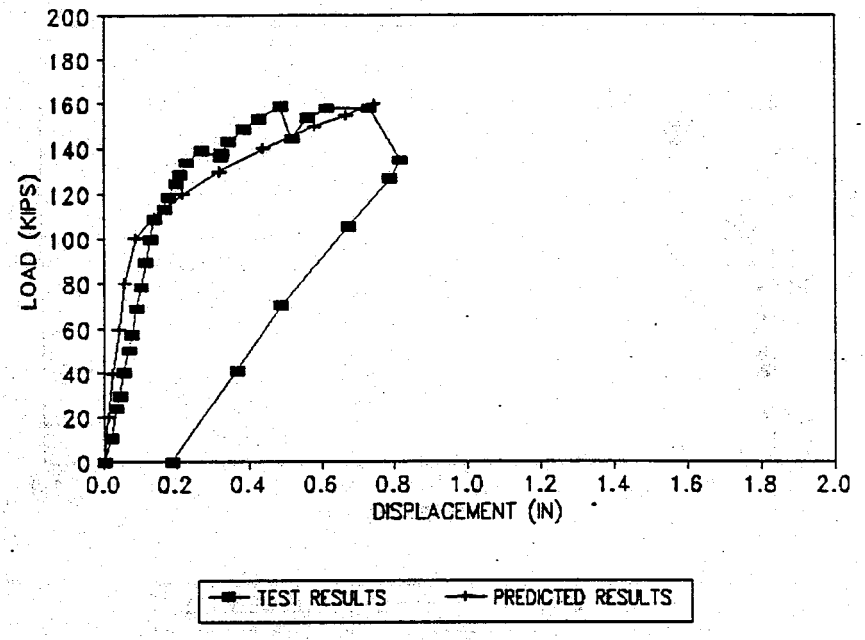

D-13. P-Delta Comparison (UF1-48-2D)

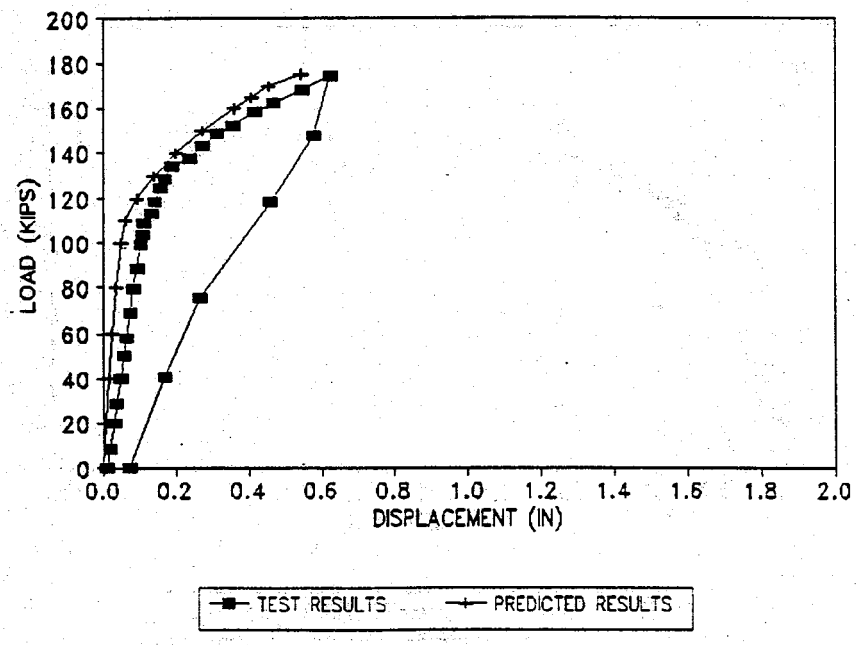

D-14. P-Delta Comparison (UF1-48-LD)

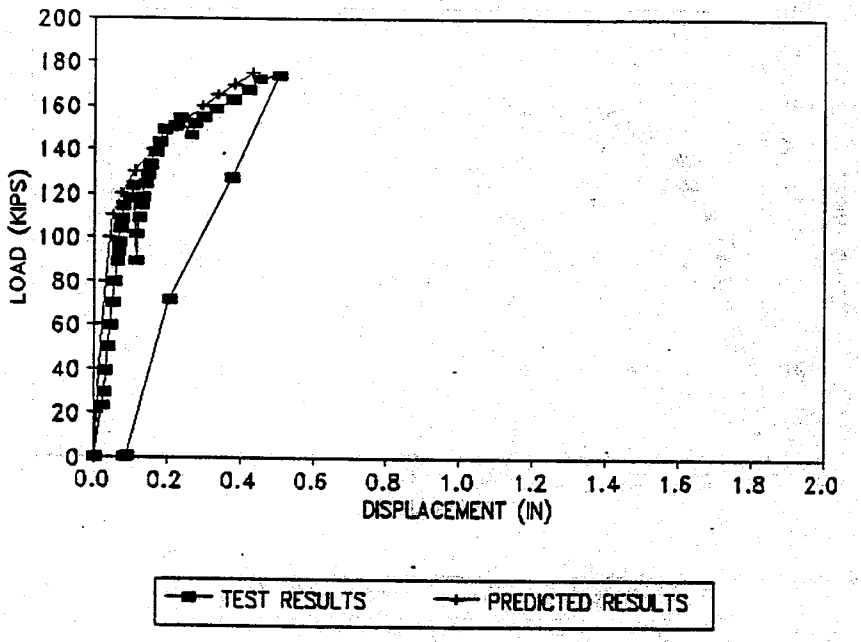

D-15. P-Delta Comparison (UF2-48-2D)

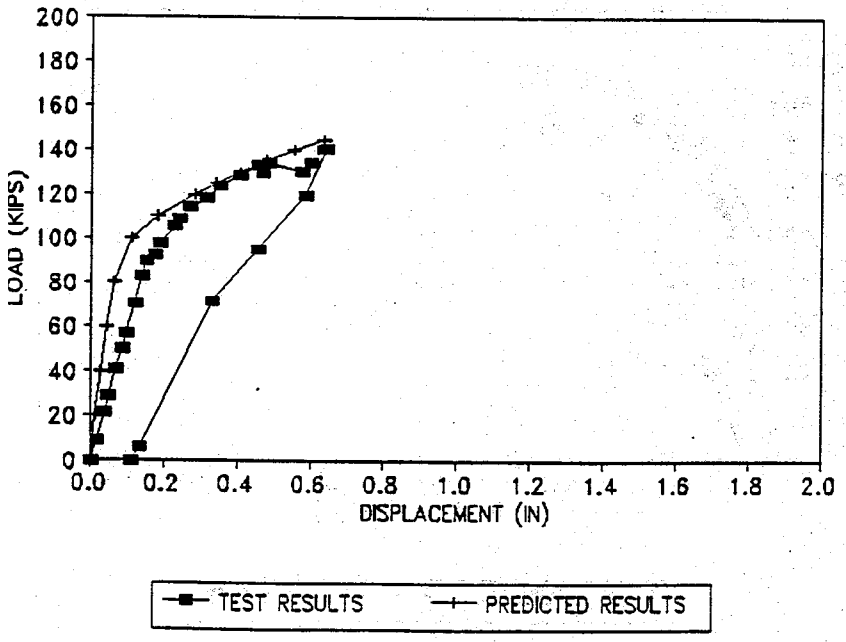

D-16. P-Delta Comparison (UF2-48-LD)

APPENDIX E
COMPUTATION OF PRESTRESS LOSSES

Sheet no. 1 of 4
Computed by: AB Checked by: Date: 11 / 20 / 95
Subject : Prestressed Concrete Design
Design-Example # UF1-30-2D

Compute Prestress Losses (LRFD Refined Method): (AASHTO 9.16.2.1)
H = Relative Humidity = 77 (figure 9.16.2.1.1)

Delta(f(p)(SH)) = Loss in P/S Steel Stress Due to Shrinkage = (17.0 - 0.150*H), (Equn. 9-4)
where: H = 77
Therefore, Delta(f(p)(SH)) = 545 ksi

Eci = 33000* w(c)^1.5 * sgrt(f'ci), (Equn. 9-8)
where: w(c) = Unit Weight of Concrete = 146 pcf
f'ci = Spec. Comp. Strength at Initial Loading = 6.30 ksi
Therefore, Eci = 4606.53 ksi

Use Low Relaxation Strands.

rho = Aps/Abeam,
where: Aps = Area of Prestressing Steel = 2.142 Inches^2
Abeam = Area of Beam 360.00 Inches^2
Therefore, rho = 0.0060

n(i) = Es/Eci,
where: Es = Modulus of Elasticity of Prestressing Tendons = 28000 ksi
Eci = Modulus of Elasticity of Concrete at Transfer = 4606.53 ksi
Therefore, n(i) = 6.08

f(s2) - f(pj) - Delta(f(p)(FR)),
where: f(pl) = 136.99 ksi
Delta(f(p)(FR)) = 0.00 ksi
Therefore, f(s2) = 136.99 ksi

Sheet no. 2 of 4
Computed by: AB Checked by: Date: 11/20/95
Subject: Prestressed Concrete Design
Design Example # UF1-30-2D

Compute Prestress Losses (LRFD Refined Method) (Continued): (AASHTO 9.16.2.1)

f(cir) = Sum of Concrete Stresses at the Center of Gravity of P/S Tendons Due to the P/S Force at Transfer and the Self-Weight of the Member at the Sections of Maximum Moment =

{rho*f(s2)*(1+(e^2 *Abeam/Ig)) - M(DLb)*e/Ig) / {1 + rho*n(i)*(1+(e^2 * Abeam/ig))}

where: rho = 0.0060
f(s2) = 136.99 ksi
e = 6.50 Inches
Abeam = 360.00 Inches^2
Ig = 27000 Inches^4
M(DLb) = 55.78 K-feet = 669.31 K-inches
n(i) = 6.08
Therefore, f(cir) = 1.05 ksi

Delta(f(p)(ES)) = Loss in P/S Steel Stress Due to Elastic Shortening= (Ep/Eci) * f(cir), (Equn. 9-6)

where: Ep = 28000 ksi
Eci = 4606.53 ksi
f(cir) = 1.05 ksi
Therefore, Delta(f(p)(ES)) = 6.40 ksi

For noncomposite girder,
Delta(f(cds)) = M(Deck) * e / I,

where: M(Deck) = Moment Due to Deck Slab =
0.00 K-feet = 0.00 K-inches
e = 6.50 Inch
I = 27000 Inch^4
Therefore, Delta(f(cds)) = 0.00 ksi

Delta(f(p)(CRC)) = 12.0*f(cir) - 7.0*Delta(f(cds)) >= 0 (Equn. 9-9)

where: f(cir) = 1.05 ksi
Delta(f(cds)) = 0.00 ksi
12.0*f(cir) - 7.0*Delta(f(cds)) = 12.64 ksi
Therefore, Delta(f(p)(CRC)) = 12.64 ksi

Sheet no. 3 of 4
Computed by : AB Checked by: Date: 11 / 20/95
Subject: Prestressed Concrete Design
Design Example # UF1-30-2D

Compute Prestress Losses (LRFD Refined Method) (Continued): (AASHTO 9.16.2.1)

Delta(f(p)(CRS)) = Loss in P/S Steel Stress Due to Relaxation of Steel After Transfer = 5.0 - 0.1 *Delta(f(p)(ES)) - 0.05*(Delta(f(p)(SH))+Delta(f(p)(CRC))), (Equn. 9-10A)

where: Delta(f(p)(ES)) = 6.40 ksi
Delta(f(p)(SH)) = 5.45 ksi
Delta(f(p)(CRC)) = 12.64 ksi
Therefore, Delta(f(p)(CRS)) = 3.45 ksi

Delta(f(p)(T)) = Total Loss in Prestressing Steel Stress = (Equn. 9-3)
Delta(f(p)(ES) + Delta(f(p)(SH)) + Delta(f(p)(CRC)) + Delta(f(p)(FR)) + Delta(f(p)(CRS)),

where: Delta(f(p)(ES)) = 6.40 ksi
Delta(f(p)(SH)) = 5.45 ksi
Delta(f(p)(CRC)) = 12.64 ksi
Delta(f(p)(FR)) = 0.00 ksi
Delta(f(p)(CRS)) = 3.45 ksi
Therefore, Delta(f(p)(T)) = 27.95 ksi

f(pl) = f(p) - Delta(f(p)(ES)) - Delta(f(p)(FR)),

where: f(pi) = 136.99 ksi
Delta(f(p)(ES)) = 6.40 ksi
Delta(f(p)(FR)) = 0.00 ksi
Therefore, f(pi) = 130.59 ksi

f(pf) = f(pj) - Delta(f(p)(T)),

where: f(pj) = 136.99 ksi
Delta(f(p)(D) = 27.95 ksi
Therefore, f(pf) = 109.04: ksi

Initial Prestressing Force = P(i) = f(pi)*Aps,

where: Aps = 2.142 Inches^2
f(pi) = 130.59 ksi
Therefore, P(i) = 279.72 Kips

Final Prestressing Force = P = P(e) = f(pf) * Aps = f(pe) * Aps,

where: Aps = 2.142 Inches^2
f(p) = f(pe) = 109.04 ksi
Therefore, P = P(e) = 233.57 Kips

Notes:
In the report f(pi) = 135.39 ksi
In the report f(pe) = 108.30 ksi

Sheet no. 4 of 4
Computed by: AB Checked by : Date: 11 / 20 / 95
Subject : Prestressed Concrete Design
Design Example # UFl-30-2D

Compute Prestress Losses (LRFD Refined Method) (Continued): (AASHTO 9.1.6.2.1)

LOSS = 1 - (f(Pf)/f(PD),

where:	f(pf) = f(pe) =	109.04 ksi
	f(pj) =	136.99 ksi
Therefore,	LOSS =	0.204

LLOSS = 1 - (f(pf) / f(pi)),

where:	f(pf) = f(pe) =	109.04 ksi
	f(pi) =	130.59 ksi
Therefore,	LLOSS =	0.165

LIST OF REFERENCES

1. American Concrete Institute, Building Code Requirement for Reinforced Concrete (ACI 318-89). Authors, Detroit, Michigan, 1989.

2. Hoyer, E. and Friedrich, E., "Contribution towards the Question of Bond Strength in Reinforced Concrete Members;" *Bentonoud Eisen,* Berlin, Vol. 38, No. 6, 1939, pp., 107-110.

3. American Associations of State Highway and Transportation Officials, Standard Specifications for Highway Bridges: Interim Specification Bridges 1990, Fourteenth Edition, Authors, Washington D. C., 1990.

4. Zia, P. and Mostafa, S. E., "Development Length of Prestressing Strands," PCI Jour*nal,* Vol. 22, No. 5, Sept.-Oct. 1977, pp. 54-65.

5. Shahawy, Mohsen A., "Strand Transfer Lengths in Full Scale AASTHO Prestressed Concrete Girders," PCI Journal, Vol. 37, No. 3, May-June 1992, pp. 84-96.

6. Morsch, E., *Concrete-Steel Construction,* McGraw-Hill Book Company, New York, 1909, pp. 368 (English translation by E. P. Goodrich of 3rd ed. of Der Eisenbentonbau, 1st ed., 1902).

7. Mitchell, D. and Collins, M., "Design of Disturbed Regions," *Prestressed Concrete Structures,* Prentice Hall, Englewood Cliffs, New Jersey, 1991.

8. MacGregor, J. G., "Shear in Beams," *Reinforced Concrete Mechanics & Design,* Prentice Hall, Englewood Cliffs, New Jersey, 1992.

9. Marti, P., "Basic Tools of Reinforced Concrete Beam-Design," ACI Journal, Vol. 82, No. 1, Jan.-Feb. 1985, pp. 46-56.

10. Vecchio, F.J. and Collins, M., "The Modified Compression Field Theory for Reinforced Concrete Elements Subjected to Shear," ACI Journal, Vol. 83, No. 2, March-April 1986, pp. 219-231.

11. Hognestad, E., Hanson, N. W. and McHenry D., "Concrete Stress Distribution in Ultimate Strength Design," AC[Journal, Vol. 52, No. 6, December 1955, pp. 455-479.

12. Mattock, Alan H, "Flexural Strength of Prestressed Concrete sections by Programmable Calculator," PCI Journal; Vol. 24, No. 1, Jan.-Feb. 1979, pp. 32-54.